# Scattering of Electromagnetic Waves by Two Parallel Chiral Circular Cylinders

Shafiqur Rahman

A Thesis

in

The Department

of

**Electrical and Computer Engineering**

Presented in Partial Fulfillment of the Requirements

for the Degree of Master of Applied Science at

**Concordia University**

Montreal, Quebec, Canada

April 2005

*Your file Votre référence*
*ISBN: 0-494-10247-0*
*Our file Notre référence*
*ISBN: 0-494-10247-0*

# Abstract

## Scattering of Electromagnetic Waves by Two Parallel Chiral Circular Cylinders

**Shafiqur Rahman**

The electromagnetic scattering from two parallel chiral circular cylinders is analyzed using a boundary value problem approach. Both cylinders are assumed to be illuminated by either a transverse electric (TE) or transverse magnetic (TM) wave. The separation of variable technique and proper transformation theorems are used to formulate the solution. The incident fields, scattered fields, and transmitted fields are expanded in terms of the cylindrical vector wave functions. Drude-Born-Fedorov (DBF) constitutive relations and Bohren decomposition formula are used to express the electromagnetic fields inside the chiral cylinders. The boundary conditions are imposed in conjunction with the addition theorem of the Hankel function on the boundary surface of each cylinder. The boundary conditions yield a system of linear equations for each type of polarization which can be numerically solved to obtain the unknown expansion coefficients by a proper truncation of the infinite sums into finite sums.

Numerical results are given to show the effects on co- and cross-polarized echo widths for some selected parameters and geometries. The effects on the back and forward scattering co- and cross-polarized echo widths are also given with respect to the

separation distance between two cylinders and angle of incidence. From the numerical results, it can be evident that chirality parameter plays an important role controlling the echo width. The validity and accuracy of the results are compared with available published results for special and limiting cases. Several numerical results are also given for the scattering of electromagnetic waves by single chiral cylinder for both the TM and TE cases and validated with existing published results.

# Acknowledgement

First and foremost, I would like to extend my deep and sincere gratitude to my respected advisor Dr. A. Sebak for providing his personal guidance, suggestions and critical review of this thesis draft. His logical ways of thinking, encouraging and invaluable information have provided a good foundation for the thesis. I also like to acknowledge the financial support that he provided me during my research work.

I am also grateful to the members of my examining committee, Dr. L. Lopes, Dr. M. Medraj, and Dr. R. Paknys, for providing necessary suggestion for overall improvement of the thesis work.

I would like to express my appreciation to my parents, uncle, brothers, and sisters for their continuous support and encouragement. Finally, I express my solemn gratitude to all mighty Allah, most glorious and most merciful.

# Table of Contents

# List of Figures

# Chapter 1

# Introduction

Chiral media has drawn much attention in the scattering problems because it responds with both electric and magnetic polarization to either electric or magnetic excitation. The electromagnetic scattering of chiral objects is relatively complicated and different from conducting and dielectric objects since chiral objects generate both co- and cross-polarized scattered fields. Bohren [1] analyzed the problem of electromagnetic wave scattering by an optically active cylinder using the cylindrical vector wave functions. He has also analyzed the scattering of electromagnetic waves by an optically active sphere [2] and an optically active spherical shell [3]. The problem of scattering from single chiral cylinder of arbitrary cross section has been treated by several numerical methods. Several researchers [4]-[6] used an integral equation approach combined with the Method of Moments (MOM) to solve the scattering problem for a chiral cylinder of arbitrary cross section. Kluskens and Newman [7] investigated an efficient recursive eigenfunction solution for the problem of scattering by a multilayer chiral circular cylinder.

Multiple scattering of electromagnetic waves by conducting or dielectric cylinders has been analyzed by various researchers using different techniques such as an integral equation formulation, partial differential equations, and hybrid techniques combining the partial differential equations with an eigenfunction expansion method. Twersky [8] analyzed the multiple scattering of electromagnetic waves by parallel conducting cylinders where the total field is considered as the sum of the incident field and different

orders of scattered fields. Olaofe [9] investigated the problem of scattering by two dielectric cylinders using a boundary value problem. Young and Bertrand [10] investigated the backscattering of a plane acoustic wave by two parallel conducting circular cylinders using the boundary value problem. Ragheb and Hamid [11] analyzed the scattering problem by N parallel conducting cylinders. Elsherbeni and Kishk [12] analyzed the plane wave scattering from an array of parallel conducting and dielectric circular cylinders using the boundary value problem. Sebak investigated electromagnetic scattering for both parallel conducting elliptic cylinders [13] and two parallel dielectric elliptic cylinders [14] using the separation of variable technique in conjunction with the addition theorem for Mathieu functions.

Recently researchers have become interested in analyzing the scattering of electromagnetic waves by multiple chiral objects. Elsherbeni and Sharkawy [15] analyzed the electromagnetic scattering from parallel chiral circular cylinders using an iterative procedure. Yin, Lee, and Leong [16] investigated the electromagnetic scattering of plane wave by multiple eccentrical cylinders in bianisotropic media. In this thesis, multiple scattering of electromagnetic waves by two parallel chiral circular cylinders is analyzed using a boundary value problem approach and computed for both the TM and TE polarizations. The incident fields, scattered fields, and transmitted fields are expanded in terms of the cylindrical vector wave functions. Drude-Born-Fedorov (DBF) constitutive relations [17] and the Bohren decomposition formula [3] are used to express the electromagnetic fields inside the chiral cylinders. The separation of variable technique and proper transformation theorems are used to formulate the multiple scattering from

two chiral circular cylinders. The scattered field from each cylinder is considered to be the incident field for the other cylinder. The addition theorem for Hankel functions [18] is then used to enforce the boundary conditions on the surface of each cylinder which permits the field expansions for both cylinders to be referenced to a common co-ordinate. Boundary conditions yield a set of linear equations which is solved numerically. After evaluating the unknown expansion coefficients, scattered far fields and echo widths can be computed. Several numerical results are presented to show the effects on the co- and cross-polarized echo widths with respect to different chirality parameters, frequencies, radii, incident angles, and separation distances between two cylinders. The numerical results are validated with existing scattering results for the special cases of two dielectric cylinders and single chiral cylinder. The effects on the back and forward scattering co- and cross-polarized echo widths are also given with respect to the separation distance between two cylinders and angle of incidence. In addition to, some numerical results are given for the scattering of electromagnetic waves by single chiral cylinder for both the TM and TE polarizations and validated with existing published results.

## 1.1 Literature Review

### 1.1.1 Chiral Media

The electromagnetic characteristics of chiral media are different from other dielectric and magnetic media and became the topic of interest at the beginning of the nineteenth century. Chirality is a property of a molecule that results from its structure. A material that is not superimposible on its mirror image by translation and rotation is called chiral and this phenomenon is called chirality or handedness. A material that is superimposible

on its mirror image is said to be achiral. The term chiral comes from the Greek name *kheir* meaning "hand" and apparently was invented by Lord Kelvin [17] in 1904. Many of naturally occurring and man-made objects fall into category of chiral objects. DNA, amino acids, proteins, hormones, and sugar solutions are examples of some natural chiral objects while wire helices, hand gloves, irregular tetrahedron, and stringed instruments are considered man made chiral objects. Fig. 1 shows some examples of chiral objects.

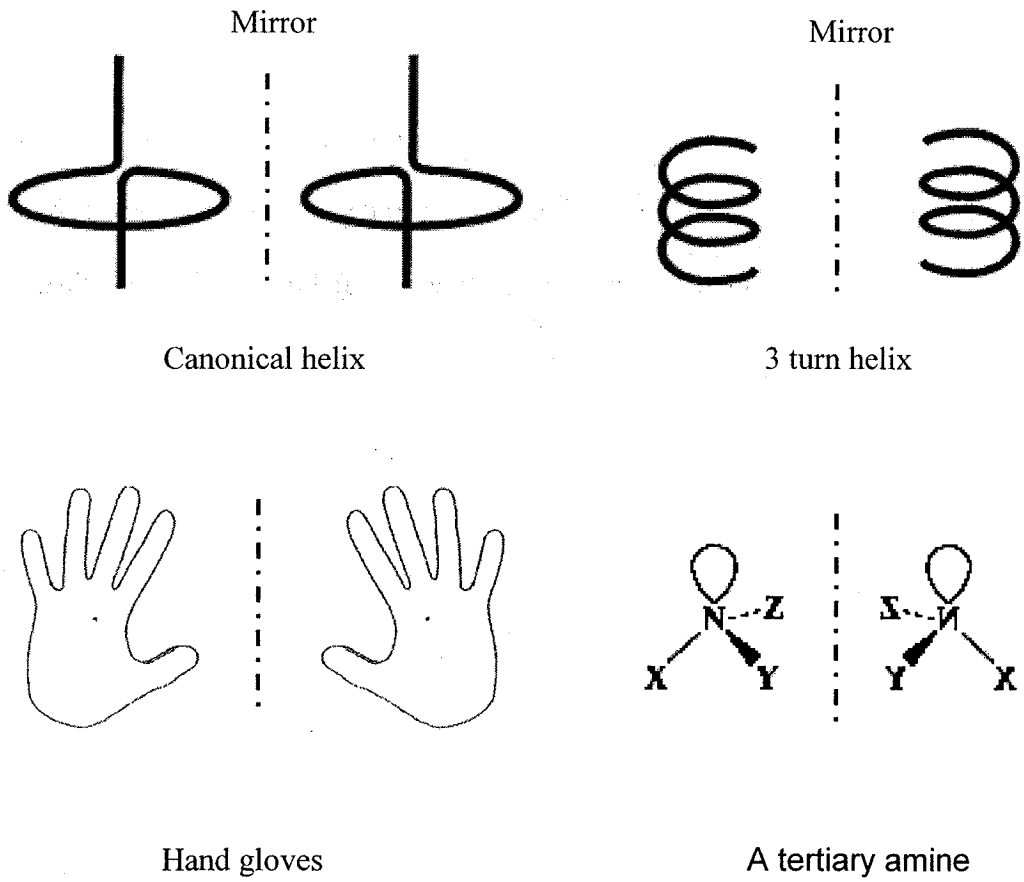


Fig. 1: Some chiral objects.

Chirality supports the property of optical activity and circular dichroism. A material which rotates the plane of incident linearly polarized light is said to be optically active. Circular dichroism indicates the property (as of an optically active medium) of unequal absorption of right and left plane-polarized light so that the emergent light is elliptically polarized. Some substances that rotate the plane clockwise (to the right) are said to be dextrorotatory (from the Latin *dexter*, "right") [19]. Those that rotate the plane counterclockwise (to the left) are called levorotatory (from the Latin *laevus*, "left"). The property was discovered in quartz in 1811 by Arago [20]. He found that crystals of quartz rotate the plane of polarization of linearly polarized light and two different crystalline structures of quartz produce dextrorotatory and levorotatory. A year later, Jean Baptiste Biot [17] noticed that plane-polarized light was rotated either to the right or the left when it passed through single crystals of quartz. He found that optical activity depends upon the thickness of the plates of crystal and on the light wavelength. He also discovered that optical activity appears in certain liquids such as solution of tartaric acid and oils of turpentine. In 1822 Fresnel [17] discovered that when a linearly polarized ray of light is traveling along the axis of crystal quartz, it is divided into two circularly polarized rays of opposite handedness and different velocities.

Pasteur [17] was the first to postulate that optical activity is caused by the chirality of molecules in 1847. He noted that sodium ammonium tartrate forms two different kinds of crystals that are mirror images of each other, much as the right hand is a mirror image of the left hand. By separating one type of crystal from the other with a pair of tweezers he was able to prepare two samples of this compound. One was dextrorotatory when

dissolved in aqueous solution, the other was levorotatory. The optical activity remained after the compound had been dissolved in water. Pasteur therefore concluded that there must be some asymmetry in the structure of this compound that allowed it to exist in two forms. In 1920, Lindman [17] introduced a novel approach to study chirality by using small helices and man made chiral objects instead of chiral molecules. He demonstrated the phenomenon of optical activity using microwaves instead of light. A number of useful literature reviews of the chiral media are provided by the references [17] [19] - [21].

Chiral material is characterized by either left-handedness or right-handedness. Hence left circularly polarized (LCP) and right circularly polarized (RCP) fields propagate with different phase velocity in a chiral media. Normally chiral material is specified by the parameters of permittivity, permeability, and chirality parameter. The third chirality parameter of the chiral material gives more flexibility to control the scattering properties.

Chiral medium has focused considerable attention in recent years due to its potential applications in the fields of antennas, waveguide propagation, optics, radar absorbing materials (RAM), and scattering. Several researchers have investigated radiation from antenna arrays in chiral media. Jaggard and Sun [22] examined the radiation of electromagnetic waves from a set of canonical arrays. Mahmoud [23] has studied the radiation characteristics of a chiral-coated slotted cylindrical antenna. Pozar [24] analyzed the radiation of electromagnetic waves from microstrip antennas and arrays on a chiral substrate.

Pelet and Engheta [25] introduced a new type of waveguide structures, called chirowaveguides. They analyzed the propagation properties of electromagnetic waves for cylindrical and parallel plate chirowaveguides in chiral medium. They suggested that these types of chirowaveguides can be used in integrated optical devices, telecommunications electronic systems, and printed-circuit elements.

Chiral materials have an extra degree of freedom for scattering problems because the chirality parameter plays a vital role to control the echo width for scattering objects. Bohren has analyzed the scattering of a plane wave incidence by an optically active cylinder [1] and sphere [2] as well as spherical shell [3]. Several researchers [4]-[6] investigated the scattering problem of a chiral cylinder of arbitrary cross section. The electromagnetic scattering from parallel chiral circular cylinders [15] and bianisotropic circular cylinders [16] has also been investigated in recent years.

Chiral materials have also played vital role in the design of microwave devices such as reciprocal phase shifters, directional couplers, and antireflection coatings since these materials have the property of rotating the plane of polarization of the electromagnetic waves propagating through them. Magnetized ferrite materials have also same property of rotating the plane of polarization but they are nonreciprocal. Chiral materials have been used as coatings for reducing the radar cross section (RCS) because chiral material which is invisible to incident electromagnetic energy by virtue of zero reflectance makes it invisible to radar [26]. Recently researchers motivated to work in the fields of remote

sensing, radiation through plasma [27], and radomes [28] because of birefringence and circular dichroism properties of chiral materials.

### 1.1.2 Multiple Scattering

The scattering of electromagnetic waves from many objects has been investigated by several researchers in recent years and drawn much attention in many practical applications such as modeling of complex structures and controlling of echo width of different objects. For this reason, researchers have chosen two-dimensional objects such as circular cylinders, strips, and elliptic cylinders to study the multiple scattering characteristics. The formulation of scattering of electromagnetic waves by multiple scatterers is different from single scatterer since coupling effects are taken into consideration to solve this type of problem. The theoretical solutions of multiple scattering from conducting and dielectric cylinders have been analyzed by several researchers using an integral equation formulation, partial differential equations, and hybrid techniques combining the partial differential equations with an eigenfunction expansion method. Twersky [8] first analyzed the multiple scattering of electromagnetic waves by parallel conducting cylinders. In his analysis, the total field is considered as the sum of the incident field and different orders of scattered fields. The required expansion coefficients were generated by an iterative procedure. Olaofe [9] investigated the problem of scattering by two dielectric cylinders using a boundary value problem. He solved a system of simultaneous linear equations for the multiple scattering unknown expansion coefficients in terms of the known single particle scattering expansion coefficients.

Young and Bertrand [10] investigated the backscattering of a plane acoustic wave by two parallel conducting circular cylinders. Their analysis was carried out using the boundary value problem. Ragheb and Hamid [11] developed Twersky's technique in a matrix form to analyse the scattering problem by N parallel conducting cylinders. Elsherbeni and Kishk [12] analyzed the plane wave scattering from an array of parallel conducting and dielectric circular cylinders using the boundary value problem. Sebak investigated electromagnetic scattering for both parallel conducting elliptic cylinders [13] and two parallel dielectric elliptic cylinders [14] using the separation of variable technique in conjunction with the addition theorem for Mathieu functions.

The electromagnetic scattering from chiral cylinders is much more complicated than from achiral cylinders because the scattered field has both co- and cross-polarized fields. Hence, the number of unknown expansions coefficients to be solved here doubles compared to dielectric cylinders. Elsherbeni and Sharkawy [15] analyzed the electromagnetic scattering from parallel chiral circular cylinders using an iterative procedure. In their analysis, the boundary conditions are applied on the surface of each cylinder in an iterative procedure in order to solve for the unknown expansion coefficients and showed that it is possible to reduce the Radar Cross Section (RCS) in forward or backward scattering by proper choice of the chirality parameter of the chiral media. Yin, Lee, and Leong [16] analyzed the electromagnetic scattering of a plane wave from a planar array of eccentric bianisotropic cylinders. They also investigated the multiple scattering characteristics of two-dimensional bianisotropic objects of arbitrary cross section.

In this thesis, scattering of electromagnetic waves by two parallel chiral circular cylinders is analyzed using a boundary value problem approach and computed for both the TM and TE polarizations. The separation of variable technique and proper transformation theorems are used to formulate the multiple scattering from two chiral circular cylinders. The scattered field from each cylinder is considered to be the incident field for the other cylinder. The addition theorem for Hankel functions [18] is then used to enforce the boundary conditions which permits the field expansions for both cylinders to be referenced to a common co-ordinate. The unknown expansion coefficients can be solved for numerically by enforcing the boundary conditions on the surface of each cylinder. After evaluating the unknown expansion coefficients, scattered far fields and both co- and cross-polarized echo widths can be computed.

## 1.2 Overview

The remainder of the thesis is organized as follows:

**Chapter 2** reviews Maxwell's equations, constitutive relations, and electromagnetic field equations in the chiral medium. Cylindrical co-ordinate systems and vector wave functions for cylindrical structure are also described for review. Both TM and TE scattering of electromagnetic waves by single chiral cylinder are briefly analyzed. The incident, scattered, and transmitted fields inside the cylinder are expanded using the cylindrical vector wave functions. DBF constitutive relations and the Bohren decomposition formula are used to express the electromagnetic fields inside the chiral

cylinder. Then the boundary conditions are applied on the surface of the cylinder to obtain the unknown expansion coefficients. The boundary conditions yield four linear equations for four unknown expansion coefficients for each type of polarization which can be solved numerically. After evaluating the unknown expansion coefficients, scattered far fields and both co- and cross-polarized echo widths are computed. Several numerical results are given to show the effect of different parameters on the co- and cross-polarized echo widths which compare well with existing published results.

**Chapter 3** presents the complete analysis of the scattering of electromagnetic waves by two parallel chiral circular cylinders. The excitation type for this scattering problem is transverse magnetic (TM). The incident fields, scattered fields, and transmitted fields are expanded using the cylindrical vector wave functions. DBF constitutive relations and the Bohren decomposition formula are used to express the electromagnetic fields inside the chiral cylinders. Boundary conditions are applied in conjunction with the addition theorem for Hankel functions for solving the unknown expansion coefficients. Several numerical results are given to show the co- and cross- polarized echo widths for selected geometries and parameters. The effects on the back and forward scattering co- and cross-polarized echo widths are also given with respect to the separation distance between two cylinders and angle of incidence. The validity and accuracy of the results are compared with available published results for special and limiting cases.

**Chapter 4** presents the analysis of the transverse electric (TE) scattering of electromagnetic waves by two parallel chiral circular cylinders. The incident fields,

scattered fields, and transmitted fields are expanded using the cylindrical vector wave functions. DBF constitutive relations and the Bohren decomposition formula are used to express the electromagnetic fields inside the chiral cylinders. Boundary conditions are applied in conjunction with the addition theorem for Hankel functions for solving the unknown expansion coefficients. Finally several numerical results are given to show the co- and cross-polarized echo widths for selected geometries and parameters. The effects on the back and forward scattering co- and cross-polarized echo widths are also given as a function of separation distance between two cylinders and angle of incidence. The validity and accuracy of the results are compared with available published results for special and limiting cases.

**Chapter 5** summarizes the results and outcome of the thesis.

# Chapter 2

# Chiral Media-Electromagnetic Field Equations and Single Scatterer

## 2.1 Maxwell's Equations and Constitutive Relations

The electromagnetic fields are governed by the time harmonic Maxwell's equation. If time dependence $e^{-j\omega t}$ is assumed then Maxwell's equations [20] for a linear, isotropic, and homogeneous media are

$$\nabla \times \vec{E} - j\omega\vec{B} = 0 \tag{2.1}$$

$$\nabla \times \vec{H} + j\omega\vec{D} = 0 \tag{2.2}$$

$$\nabla \cdot \vec{D} = 0 \tag{2.3}$$

$$\nabla \cdot \vec{E} = 0 \tag{2.4}$$

where $\vec{E}, \vec{H}, \vec{D}$, and $\vec{B}$ denote the electric field, magnetic field, electric flux density, and magnetic flux density, respectively. $\omega$ is the angular frequency.

The electric and magnetic fields [18] can be expressed as

$$\vec{E} = \frac{j\omega\mu}{k^2}\left(\nabla \times \vec{H}\right) \tag{2.5}$$

$$\vec{H} = \frac{1}{j\omega\mu}\left(\nabla \times \vec{E}\right) \tag{2.6}$$

where $k = \omega\sqrt{\mu\varepsilon}$, is the wave number , $\mu$ is the permeability, and $\varepsilon$ is the permittivity of the medium.

The usual constitutive relations for the electromagnetic fields can be expressed as

$$\vec{D} = \varepsilon \vec{E} \tag{2.7}$$

$$\vec{B} = \mu \vec{H} \tag{2.8}$$

These constitutive equations are merely inadequate for chiral medium because they admit a single phase velocity that is generally frequency dependent. The chiral medium has two different phase velocities for right circularly polarized (RCP) and left circularly polarized (LCP) waves. Several sets of constitutive relations have been proposed to illustrate the electromagnetic characteristics of chiral media. One of the sets is called Lindell-Sihvola constitutive relations [17] and can be expressed as

$$\vec{D} = \varepsilon \vec{E} + (\chi - j\kappa)\sqrt{\mu_0 \varepsilon_0}\, \vec{H} \tag{2.9}$$

$$\vec{B} = \mu \vec{H} + (\chi + j\kappa)\sqrt{\mu_0 \varepsilon_0}\, \vec{E} \tag{2.10}$$

where $\kappa$ measures the chirality of the material and $\chi$ measures the non reciprocity of the material. A material is said to chiral when $\kappa \neq 0$ and called reciprocal when $\chi = 0$. It is nonreciprocal when $\chi \neq 0$. Material with $\kappa = 0$ is called achiral.

Another set of constitutive relations named after Post [17], can be expressed as

$$\vec{D} = \varepsilon \vec{E} - j\xi_c \vec{B} + \psi_n \vec{B} \tag{2.11}$$

$$\vec{H} = \frac{1}{\mu}\vec{B} - j\xi_c \vec{E} - \psi_n \vec{E} \tag{2.12}$$

where $\xi_c$ is the chirality admittance and $\psi_n$ is the non-reciprocity susceptance. For reciprocal chiral media, $\psi_n = 0$.

The other constitutive relations are called Drude-Born-Fedorov (DBF) relations [17]. Generally DBF constitutive relations are used in the analysis of reciprocal chiral media and can be expressed as

$$\vec{D} = \varepsilon\vec{E} + \gamma\varepsilon\nabla\times\vec{E} \tag{2.13}$$

$$\vec{B} = \mu\vec{H} + \beta\mu\nabla\times\vec{H} \tag{2.14}$$

where $\gamma$ and $\beta$ are the chirality parameters of the medium in terms of length. $\varepsilon$ and $\mu$ are the permittivity and permeability of the chiral medium. In an isotropic media, permeability, permittivity and chirality parameter are scalar. DBF constitutive relations are used in this thesis.

It should be noticed that the permittivity, permeability and chirality parameter are not equivalent in these different forms of constitutive relations. The relations between the parameters of different constitutive relations exist and have been given in [17]. In reciprocal chiral media, the chirality admittance $\xi_c$ of (2.11, 2.12) and chirality parameter $\gamma$ of (2.13, 2.14) can be written as following relation

$$\gamma = \frac{\xi_c}{\omega\varepsilon} \tag{2.15}$$

To develop the Helmholtz wave equation in chiral media, substituting equation (2.14) into equation (2.1), we obtain

$$\nabla\times\vec{E} = j\omega\left(\mu\vec{H} + \beta\mu\nabla\times\vec{H}\right) \tag{2.16}$$

Using equation (2.13) into equation (2.2)

$$\nabla\times\vec{H} = -j\omega\left(\varepsilon\vec{E} + \gamma\varepsilon\nabla\times\vec{E}\right) \tag{2.17}$$

From equation (2.16) and equation (2.17), $\vec{E}$ and $\vec{H}$ can be written as

$$\vec{E} = -\frac{j}{\omega\varepsilon}\left[k^2\gamma\vec{H} - \left(1 - k^2\gamma\beta\right)\nabla\times\vec{H}\right] \tag{2.18}$$

$$\vec{H} = \frac{j}{\omega\mu}\left[k^2\beta\vec{E} - \left(1 - k^2\gamma\beta\right)\nabla\times\vec{E}\right] \tag{2.19}$$

Taking the curl of equation (2.19) and placing $\nabla\times\vec{H}$ from equation (2.17), then the following chiral Helmholtz equation can be obtained for $\vec{E}$

$$\left(1 - k^2\gamma\beta\right)\nabla\times\nabla\times\vec{E} - k^2(\gamma+\beta)\nabla\times\vec{E} - k^2\vec{E} = 0 \tag{2.20}$$

Let a left circularly polarized (LCP) plane wave propagates in a chiral medium with

$$\overline{E} = \left(\hat{u}_x - j\hat{u}_y\right)e^{-jk_L x} \tag{2.21}$$

where $k_L$ is the LCP wave number for left circularly polarized wave.

Using equation (2.21) in equation (2.20), the LCP wave number $k_L$ can be written as

$$k_L = \omega\sqrt{\mu\varepsilon}\,\frac{\sqrt{1+(\gamma-\beta)^2\mu\varepsilon\omega^2/4} + (\gamma+\beta)\omega\sqrt{\mu\varepsilon}/2}{1-\mu\varepsilon\gamma\beta\omega^2} \tag{2.22}$$

Similarly for a right circularly polarized (RCP) plane wave, the RCP wave number $k_R$ can be written as

$$k_R = \omega\sqrt{\mu\varepsilon}\,\frac{\sqrt{1+(\gamma-\beta)^2\mu\varepsilon\omega^2/4} - (\gamma+\beta)\omega\sqrt{\mu\varepsilon}/2}{1+\mu\varepsilon\gamma\beta\omega^2} \tag{2.23}$$

If $\gamma = \beta$ and both are scalar, then the chiral medium is reciprocal. Hence left and right circularly polarized wave numbers $k_L$ and $k_R$ can be simplified as

$$k_L = \frac{\omega\sqrt{\mu\varepsilon}}{1-\gamma\omega\sqrt{\mu\varepsilon}} \tag{2.24}$$

$$k_R = \frac{\omega\sqrt{\mu\varepsilon}}{1+\gamma\omega\sqrt{\mu\varepsilon}} \tag{2.25}$$

The chirality parameter $\gamma$ can be written in terms of $k_L$ and $k_R$ as

$$\gamma = \frac{1}{2}\left(\frac{1}{k_R} - \frac{1}{k_L}\right) \tag{2.26}$$

## 2.2 Electromagnetic Fields in Chiral Medium

Chiral media support LCP and RCP fields and are represented as $\vec{Q}_L$ and $\vec{Q}_R$, respectively. These fields propagate with wave numbers $k_L$ and $k_R$ respectively. A linear transformation [3] of the electromagnetic fields inside the chiral media in terms of LCP and RCP fields are given by following relations

$$\vec{E} = \vec{Q}_L + a_R\vec{Q}_R \tag{2.27}$$

$$\vec{H} = a_L\vec{Q}_L + \vec{Q}_R \tag{2.28}$$

where $a_R$ and $a_L$ carry the unit of an impedance and an admittance, respectively and are denoted [3] by

$$a_R = -i\left[\frac{k_R\left(1-\gamma\beta\omega^2\varepsilon\mu\right)+\gamma\omega^2\varepsilon\mu}{\omega\varepsilon}\right] \tag{2.29}$$

$$a_L = -i\left[\frac{k_L\left(1-\gamma\beta\omega^2\varepsilon\mu\right)-\beta\omega^2\varepsilon\mu}{\omega\mu}\right] \tag{2.30}$$

For left and right circularly polarized waves ($\gamma = \beta$), $a_L$ and $a_R$ can be simplified by

$$a_L = -i\sqrt{\frac{\varepsilon}{\mu}} \qquad \text{and} \qquad a_R = -i\sqrt{\frac{\mu}{\varepsilon}} \tag{2.31}$$

The internal LCP and RCP fields ($\vec{Q}_L$ and $\vec{Q}_R$) independently satisfy the wave equations and can be expressed in the following forms

$$\nabla^2\vec{Q}_L + k_L^2\vec{Q}_L = 0 \qquad \nabla\times\vec{Q}_L = k_L\vec{Q}_L \qquad \nabla\cdot\vec{Q}_L = 0 \tag{2.32}$$

$$\nabla^2\vec{Q}_R + k_R^2\vec{Q}_R = 0 \qquad \nabla\times\vec{Q}_R = -k_R\vec{Q}_R \qquad \nabla\cdot\vec{Q}_R = 0 \tag{2.33}$$

## 2.3 Wave Equation in Cylindrical Co-ordinate System

The problem of a cylindrical configuration is solved by using the cylindrical co-ordinate system. The geometry of the cylindrical coordinate system is shown in Fig 2.1.

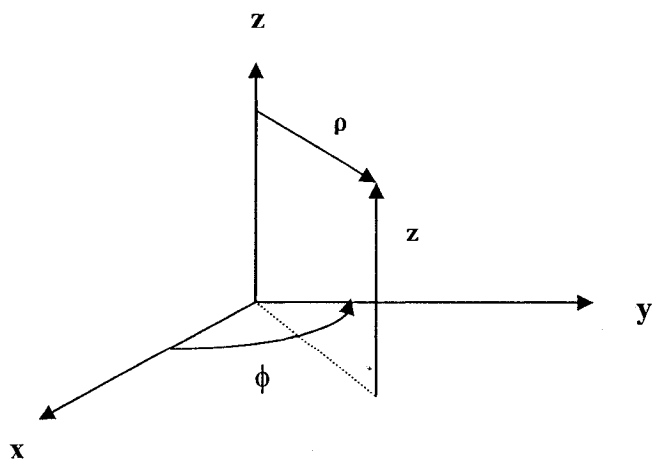


Fig. 2.1: Cylindrical co-ordinate system.

For a lossless and source free medium, the scalar Helmholtz equation in cylindrical co-ordinates [29] is

$$\frac{\partial^2\psi_n}{\partial\rho^2}+\frac{1}{\rho}\frac{\partial\psi_n}{\partial\rho}+\frac{1}{\rho^2}\frac{\partial^2\psi_n}{\partial\phi^2}+\frac{\partial^2\psi_n}{\partial z^2}+k^2\psi_n=0 \tag{2.34}$$

where $\psi_n$ is the solution of the scalar Helmholtz equation.

The solution $\psi_n$ of the wave equation can be written using the separation of variables as

$$\psi_n(\rho,\phi,z)=f(\rho)\,g(\phi)\,h(z) \tag{2.35}$$

Substitution equation (2.35) into equation (2.34) yields

$$\frac{1}{\rho f}\frac{d}{d\rho}\left(\rho\frac{df}{d\rho}\right)+\frac{1}{\rho^2 g}\frac{d^2g}{d\phi^2}+\frac{1}{h}\frac{d^2h}{dz^2}+k^2=0 \tag{2.36}$$

The third term on the left side of equation (2.36) is independent of $\rho$ and $\phi$, is a function of z only, can be written as

$$\frac{1}{h}\frac{d^2h}{dz^2}+k_z^2=0 \tag{2.37}$$

where $k_z$ is a constant. Substituting equation (2.37) into equation (2.36) and multiplying by $\rho^2$, simplifies it to

$$\frac{\rho}{f}\frac{d}{d\rho}\left(\rho\frac{df}{d\rho}\right)+\frac{1}{g}\frac{d^2g}{d\phi^2}+\left(k^2-k_z^2\right)\rho^2=0 \tag{2.38}$$

The second term of equation (2.38) is independent of ρ and z, the other terms are independent of $\phi$. Therefore second term can be written as

$$\frac{1}{g}\frac{d^2g}{d\phi^2}+n^2=0 \tag{2.39}$$

where n is a constant.

Substituting equation (2.39) into equation (2.38), gives an equation in ρ only

$$\frac{\rho}{f}\frac{d}{d\rho}\left(\rho\frac{df}{d\rho}\right)+\left(k^2-k_z^2\right)\rho^2-n^2=0 \tag{2.40}$$

If $k^2-k_z^2=k_\rho^2$, the separated equations (2.40),(2.39), and (2.37) can be written as

$$\rho\frac{d}{d\rho}\left(\rho\frac{df}{d\rho}\right)+\left[\left(k_\rho\rho\right)^2-n^2\right]f=0 \tag{2.41}$$

$$\frac{d^2g}{d\phi^2}+n^2g=0 \tag{2.42}$$

$$\frac{d^2h}{dz^2}+k_z^2h=0 \tag{2.43}$$

The solutions of equations (2.41), (2.42), and (2.43) can be written in one of the following forms depending on the region of interest respectively.

$$f_1(\rho)=A_1J_n\left(k_\rho\rho\right)+B_1Y_m\left(k_\rho\rho\right),\ f_2(\rho)=C_1H_n^1\left(k_\rho\rho\right)+D_1H_n^2\left(k_\rho\rho\right) \tag{2.44}$$

$$g_1(\phi)=A_2e^{-jn\phi}+B_2e^{jn\phi},\quad g_2(\phi)=C_2\cos\left(n\phi\right)+D_2\sin\left(n\phi\right) \tag{2.45}$$

$$h_1(z) = A_3 e^{-jk_z z} + B_3 e^{jk_z z}, \quad h_2(z) = C_3 \cos(k_z z) + D_3 \sin(k_z z) \tag{2.46}$$

where $J_n(k_\rho \rho)$ is the Bessel function of first kind, $Y_n(k_\rho \rho)$ is the Bessel function of second kind, $H_n^{(1)}(k_\rho \rho)$ is the Hankel function of first kind, and $H_n^{(2)}(k_\rho \rho)$ is the Hankel function of second kind. The choosing of the appropriate solutions for $f(\rho), g(\phi)$, and $h(z)$ depend upon the cylindrical problems. The Bessel and Hankel functions are used to represent the standing and traveling wave, respectively for equation (2.44). The exponentials of (2.45) and (2.46) represent traveling wave while sines and cosines represent standing waves.

## 2.4 Vector Wave Functions

If $\psi_n$ is the solution of the scalar wave equation

$$\nabla^2 \psi_n + k_0^2 \psi_n = 0 \tag{2.47}$$

where $k_0$ is the free space wave number, then three independent vector solutions of the vector wave equation [18] are given by

$$\vec{M}_n = \nabla \times (\hat{u}_z \psi_n) \quad \vec{N}_n = \frac{1}{k_0}(\nabla \times \vec{M}_n) \quad \vec{L}_n = \nabla \psi_n \tag{2.48}$$

where $\hat{u}_z$ is a unit vector in the z direction. $\vec{M}_n$ can be also expressed as

$$\vec{M}_n = \frac{1}{k_0}(\nabla \times \vec{N}_n) \tag{2.49}$$

The solutions of the vector wave equation in cylindrical co-coordinate system can be written using the separation of variables as

$$\psi_n^p(k_0\rho) = e^{jn\phi} Z_n^p(k_0\rho), \qquad n = 0, \pm 1, \pm 2... \tag{2.50}$$

where superscript p could be 1 or 3, and stands for incoming and outgoing waves, respectively. The term $Z_n^p(k_0\rho)$ can be written in terms of superscript 1 and 3 as

$$Z_n^1(k_0\rho) = J_n(k_0\rho) \qquad Z_n^3(k_0\rho) = H_n^{(1)}(k_0\rho) \tag{2.51}$$

where $J_n(k_0\rho)$ is the Bessel function of the first kind of order n with argument $k_0\rho$ and $H_n^{(1)}(k_0\rho)$ is the Hankel function of the first kind of order n with argument $k_0\rho$.

In general, the cylindrical vector wave functions $\vec{N}_n$ and $\vec{M}_n$ can be written as

$$\vec{N}_n^p(k_0\rho) = \hat{u}_z k_0 Z_n^p(k_0\rho) e^{jn\phi} \tag{2.52}$$

$$\vec{M}_n^p(k_0\rho) = \hat{u}_\rho \frac{jn}{\rho} Z_n^p(k_0\rho) e^{jn\phi} - \hat{u}_\phi e^{jn\phi} \frac{\partial}{\partial\rho}\{Z_n^p(k_0\rho)\} \tag{2.53}$$

The entire analyses of multiple scattering from two chiral circular cylinders and single chiral cylinder have been carried out by using above mentioned vector wave functions.

## 2.5 Scattering by Single Chiral Circular Cylinder

### 2.5.1 Description of the Problem

The scattering of electromagnetic waves by single chiral circular cylinder for both TM and TE polarizations has been introduced briefly before going to the two chiral circular

cylinders scattering analysis. The problem of scattering from a single chiral circular cylinder has been investigated by several methods. Bohren [1] has analyzed the scattering of electromagnetic waves from infinitely long optically active cylinder using a boundary value problem approach. Several researchers used an integral equation approach combined with the Method of Moments (MOM) to solve the scattering problem for a chiral cylinder of arbitrary cross section. In this section, the incident, scattered, and transmitted fields inside the cylinder are expanded using the cylindrical vector wave functions. DBF constitutive relations [17] and the Bohren decomposition formula [3] are used to express the electromagnetic fields inside the chiral cylinder. The unknown expansion coefficients can be solved numerically by enforcing the boundary conditions on the surface of the cylinder. After evaluating the unknown expansion coefficients, far scattered fields and both co- and cross-polarized echo widths can be computed.

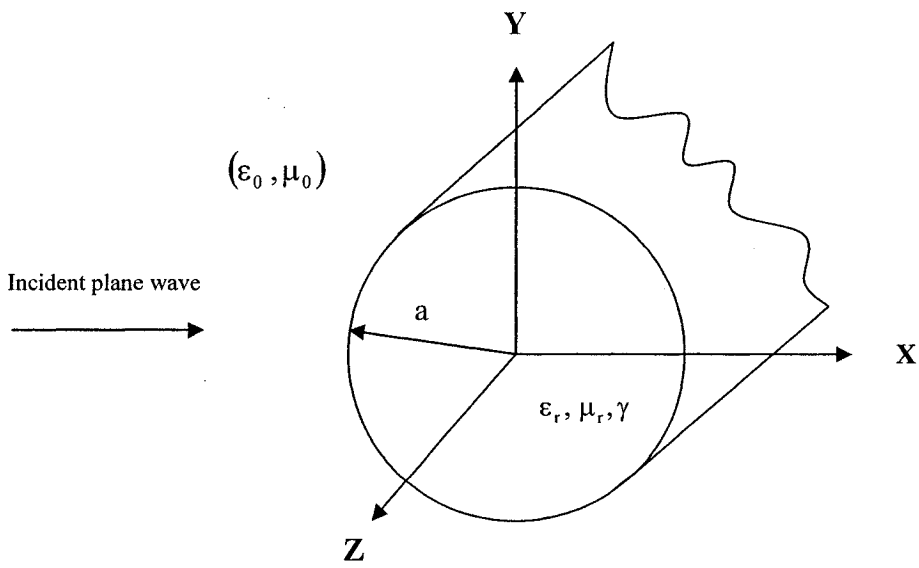


Fig. 2.2: The scattering geometry of a chiral circular cylinder.

Assume that a plane wave is normally incident upon a chiral circular cylinder as shown in Fig. 2.2. The radius, relative permittivity, relative permeability, and chirality parameter of the cylinder are $a, \varepsilon_r, \mu_r$, and $\gamma$, respectively. The medium of the surrounding cylinder is free space with permeability $\mu_0$ and permittivity $\varepsilon_0$.

### 2.5.2 TM Polarization

For a TM polarized incident plane wave, the incident electric field vector is parallel to the cylinder axis (z axis). The incident electric and magnetic fields with $e^{-j\omega t}$ time dependence can be expressed in terms of the cylindrical vectors wave functions as

$$\vec{E}^{inc} = \frac{1}{k_0} \sum_{n=-\infty}^{+\infty} j^n \vec{N}_n^1(k_0\rho) \tag{2.54}$$

$$\vec{H}^{inc} = \frac{1}{j\omega\mu_0} \sum_{n=-\infty}^{+\infty} j^n \vec{M}_n^1(k_0\rho) \tag{2.55}$$

where

$$\vec{N}_n^1(k_0\rho) = \hat{u}_z k_0 J_n(k_0\rho) e^{jn\phi} \tag{2.56}$$

$$\vec{M}_n^1(k_0\rho) = \hat{u}_\rho \frac{jn}{\rho} J_n(k_0\rho) e^{jn\phi} - \hat{u}_\varphi k_0 J_n'(k_0\rho) e^{jn\phi} \tag{2.57}$$

The scattered field of the chiral cylinder embraces both $TM^z$ and $TE^z$ fields due to the property of chiral media. The scattered electric and magnetic fields can be expressed as

$$\vec{E}^s = -\frac{1}{k_0} \sum_{n=-\infty}^{+\infty} j^n \left[ b_n \vec{N}_n^3(k_0\rho) + jc_n \vec{M}_n^3(k_0\rho) \right] \tag{2.58}$$

$$\vec{H}^s = -\frac{1}{j\omega\mu_0}\sum_{n=-\infty}^{+\infty} j^n\left[b_n\vec{M}_n^3(k_0\rho) + jc_n\vec{N}_n^3(k_0\rho)\right] \tag{2.59}$$

where $b_n$ and $c_n$ are the unknown scattering expansion coefficients of the chiral circular cylinder for TM polarization. The cylindrical vector wave functions $\vec{N}_n^3(k_0\rho)$ and $\vec{M}_n^3(k_0\rho)$ can be expressed as

$$\vec{N}_n^3(k_0\rho) = \hat{u}_z k_0 H_n^{(1)}(k_0\rho)e^{jn\phi} \tag{2.60}$$

$$\vec{M}_n^3(k_0\rho) = \hat{u}_\rho \frac{jn}{\rho} H_n^{(1)}(k_0\rho)e^{jn\phi} - \hat{u}_\phi k_0 H_n^{(1)'}(k_0\rho)e^{jn\phi} \tag{2.61}$$

The chiral medium has two internal fields, LCP and RCP fields, and are represented as $\vec{Q}_L$ and $\vec{Q}_R$, respectively. LCP and RCP fields propagate with wave numbers $k_L$ and $k_R$ respectively. The LCP field $(\vec{Q}_L)$ and RCP field $(\vec{Q}_R)$ [1] can be expressed as

$$\vec{Q}_L = \frac{1}{k_0}\sum_{n=-\infty}^{+\infty} j^n g_n\left[\vec{M}_n^1(k_L\rho) + \vec{N}_n^1(k_L\rho)\right] \tag{2.62}$$

$$\vec{Q}_R = \frac{1}{k_0}\sum_{n=-\infty}^{+\infty} j^n f_n\left[\vec{M}_n^1(k_R\rho) - \vec{N}_n^1(k_R\rho)\right] \tag{2.63}$$

where $g_n$ and $f_n$ are the unknown expansion coefficients of the internal fields inside the chiral cylinder for TM polarization.

Electric and magnetic fields inside the chiral cylinder are written by following relations

$$\vec{E}^c = \vec{Q}_L + a_R\vec{Q}_R \tag{2.64}$$

$$\vec{H}^c = \vec{Q}_R + a_L\vec{Q}_L \tag{2.65}$$

The unknown expansion coefficients can be determined by enforcing the boundary conditions on the surface of the cylinder. The boundary conditions of the electromagnetic scattering state that the tangential components of the electric and magnetic fields must be continuous across the boundary.

The boundary conditions on the surface of the cylinder i.e., $\rho = a$ , are given by

$$\left(\vec{E}^{inc} + \vec{E}^{s} - \vec{E}^{c}\right) \times \hat{u}_{\rho} = 0 \tag{2.66}$$

$$\left(\vec{H}^{inc} + \vec{H}^{s} - \vec{H}^{c}\right) \times \hat{u}_{\rho} = 0 \tag{2.67}$$

where $\hat{u}_{\rho}$ is the outward unit vector normal to the cylinder.

The boundary conditions yield the following four linear equations after doing some mathematical calculations.

$$c_n j H_n^{(1)'}(k_0 a) + g_n \frac{k_L}{k_0}\left[J_n'(k_L a)\right] + f_n \frac{a_R k_R}{k_0}\left[J_n'(k_R a)\right] = 0 \tag{2.68}$$

$$b_n H_n^{1}(k_0 a) + g_n \frac{k_L}{k_0}\left[J_n(k_L a)\right] - f_n \frac{a_R k_R}{k_0}\left[J_n(k_R a)\right] = J_n(k_0 a) \tag{2.69}$$

$$b_n H_n^{(1)'}(k_0 a) + g_n \frac{a_L k_L j\omega\mu_0}{k_0^{\,2}}\left[J_n'(k_L a)\right] + f_n \frac{k_R j\omega\mu_0}{k_0^{\,2}}\left[J_n'(k_R a)\right] = J_n'(k_0 a) \tag{2.70}$$

$$c_n j H_n^{1}(k_0 a) + g_n \frac{a_L k_L j\omega\mu_0}{k_0^{\,2}}\left[J_n(k_L a)\right] - f_n \frac{k_R j\omega\mu_0}{k_0^{\,2}}\left[J_n(k_R a)\right] = 0 \tag{2.71}$$

These four linear equations (2.68 to 2.71) can be solved numerically to obtain the unknown expansion coefficients, $b_n$ , $c_n$ , of the scattered field.

After evaluating the unknown scattering coefficients, the far scattered field can be computed. The scattered electric field $\left(\vec{E}^{s}\right)$ carries both co- and cross-polarized fields. The asymptotic expansion for the Hankel function [30] for large arguments is applied to achieve the far scattered field.

The echo width can be obtained by knowing the scattered field in the far zone. The echo width $(\sigma)$ or radar cross section (RCS) is defined as "the area intercepting the amount of power that, when scattered isotropically, produces at the receiver a density that is equal to the density scattered by the actual target" [30].

The co- and cross-polarized echo widths [30] can be expressed for TM polarization as

$$\sigma_{co}^{TM} = \lim_{\rho\to\infty} 2\pi\rho \frac{\left|\vec{E}_{co}^{s}\right|^2}{\left|\vec{E}^{inc}\right|^2} \tag{2.72}$$

$$\sigma_{cross}^{TM} = \lim_{\rho\to\infty} 2\pi\rho \frac{\left|\vec{E}_{cross}^{s}\right|^2}{\left|\vec{E}^{inc}\right|^2} \tag{2.73}$$

where $\vec{E}_{co}^{s}$ and $\vec{E}_{cross}^{s}$ are the co- and cross- polarized scattered electric fields.

The final expression of co- and cross-polarized echo widths can be written as

$$\sigma_{co}^{TM} = \frac{2\lambda}{\pi}\left|\sum_{n=-\infty}^{+\infty} b_n e^{jn\phi}\right|^2 \tag{2.74}$$

$$\sigma_{cross}^{TM} = \frac{2\lambda}{\pi}\left|\sum_{n=-\infty}^{+\infty} c_n e^{jn\phi}\right|^2 \tag{2.75}$$

### 2.5.3 TE Polarization

For a TE polarized incident plane wave, the incident magnetic field vector is parallel to the cylinder axis (z axis). The incident electric and magnetic fields can be expressed as

$$\vec{H}^{inc} = \frac{1}{\omega\mu_0} \sum_{n=-\infty}^{\infty} j^n \vec{N}_n^1(k_0\rho) \tag{2.76}$$

$$\vec{E}^{inc} = \frac{j}{k_0} \sum_{n=-\infty}^{+\infty} j^n \vec{M}_n^1(k_0\rho) \tag{2.77}$$

The scattered electric and magnetic fields can be expressed as

$$\vec{E}^{s} = -\frac{1}{k_0} \sum_{n=-\infty}^{+\infty} j^n \left[ B_n \vec{N}_n^3(k_0\rho) + jC_n \vec{M}_n^3(k_0\rho) \right] \tag{2.78}$$

$$\vec{H}^{s} = -\frac{1}{j\omega\mu_0} \sum_{n=-\infty}^{+\infty} j^n \left[ B_n \vec{M}_n^3(k_0\rho) + jC_n \vec{N}_n^3(k_0\rho) \right] \tag{2.79}$$

where $B_n$ and $C_n$ are the unknown scattering coefficients of the chiral cylinder for TE polarization.

A similar procedure of TM polarization is followed to express the electromagnetic fields inside the chiral cylinder. The unknown expansion coefficients can be solved for numerically by enforcing the boundary conditions on the surface of the cylinder. The co- and cross-polarized echo widths [30] can be expressed for TE polarization as

$$\sigma_{co}^{TE} = \lim_{\rho\to\infty} 2\pi\rho \frac{\left|\vec{H}_{co}^{s}\right|^2}{\left|\vec{H}^{inc}\right|^2} \tag{2.80}$$

$$\sigma_{cross}^{TE} = \lim_{\rho\to\infty} 2\pi\rho \frac{\left|\vec{H}_{cross}^{s}\right|^2}{\left|\vec{H}^{inc}\right|^2} \tag{2.81}$$

where $\vec{H}_{co}^{s}$ and $\vec{H}_{cross}^{s}$ are the co- and cross-polarized scattered magnetic fields.

The final expression of co- and cross- polarized echo widths can be written as

$$\sigma_{co}^{TE} = \frac{2\lambda}{\pi}\left|\sum_{n=-\infty}^{+\infty} C_n\, e^{jn\phi}\right|^2 \tag{2.82}$$

$$\sigma_{cross}^{TM} = \frac{2\lambda}{\pi}\left|\sum_{n=-\infty}^{+\infty} B_n\, e^{jn\phi}\right|^2 \tag{2.83}$$

### 2.5.4 Numerical Results

Numerical results are presented for both TM and TE polarized incident waves using the formulation described in the earlier section. The unknown expansion coefficients are numerically solved by a proper truncation of the infinite sums into finite sums. In order to generate numerical results, a truncation number N is used and it depends upon the degree of accuracy required and the electrical size of the cylinder. For large value of ka, N should be 2ka+2. When ka $\approx$1 or less, N should be 2ka+5 to 2ka+10 for required accuracy.

Fig. 2.3 shows the bistatic co- and cross-polarized echo widths from a single chiral circular cylinder for TM polarized incident wave. The result is in excellent agreement with the results obtained by Rojas [5]. For reference, the result for scattering by a single

achiral cylinder is also shown. It is seen that bistatic echo width of the chiral cylinder is relatively lower than the achiral cylinder.

Fig. 2.4 shows the co- and cross-polarized echo widths from a single chiral circular cylinder for two different chiral parameters $k_0\gamma = 0.10$ and $k_0\gamma = 0.15$, respectively. The result is shown for TM polarization. The results illustrate that echo width of the chiral cylinder can be controlled by changing the chirality parameter. It is seen that both back and forward scattering echo widths reduce for higher chirality parameter.

Fig. 2.5 shows the co- and cross-polarized echo widths from a single chiral circular cylinder for two different radii $a = 0.08\lambda$ and $a = 0.20\lambda$, respectively for TM polarization. The results illustrate that both echo widths are dependent upon the size of the cylinder. It is seen that the echo width increases with size for electrically large cylinder.

Fig. 2.6 shows the co- and cross-polarized backscattering ($\phi = 180^0$) echo widths versus the cylinder radius from a single chiral circular cylinder for TM polarization. Both echo widths increase very quickly with size for electrically small cylinder ($a << \lambda$). When electrical size of the cylinder is on the order of a wavelength, both echo widths are oscillating with frequency due to phase addition and cancellation of various scattered field components.

Fig. 2.7 shows the co- and cross-polarized forward scattering ( $\phi = 0^0$ ) echo widths versus the cylinder radius from a single chiral circular cylinder for TM polarized incident wave. Both echo widths increase sharply for electrically small cylinder ($a << \lambda$) and are oscillating with frequency when electrical size of the cylinder is on the order of a wavelength.

Fig. 2.8 shows the bistatic co- and cross-polarized echo widths patterns from single chiral circular cylinder for TE polarized incident wave. The result is in excellent agreement with the results obtained by Rojas [5]. For comparison, the numerical result for the echo width pattern for single achiral cylinder is also given.

Fig. 2.9 shows the co- and cross-polarized echo widths from single chiral circular cylinder for two different chiral parameters $k_0\gamma = 0.10$ and $k_0\gamma = 0.15$, respectively for TE polarization. The results illustrate that backscattering echo widths reduce for large chirality parameter while forward scattering echo widths decrease for small chirality parameter.

Fig. 2.10 shows the co- and cross-polarized echo widths from single chiral circular cylinder for two different radii $a = 0.08\lambda$ and $a = 0.20\lambda$, respectively for TE polarized incident wave. The results illustrate that both echo widths are dependent upon the size of the cylinder. It is seen that the echo width increases with size for electrically large cylinder.

Fig. 2.11 shows the co- and cross-polarized backscattering ($\phi = 180^0$) echo widths versus the cylinder radius from a single chiral circular cylinder for TE polarized incident wave. Both echo widths increase sharply for electrically small cylinder ($a << \lambda$) and are oscillating with frequency when electrical size of the cylinder is on the order of a wavelength.

Fig. 2.12 shows the co- and cross-polarized forward scattering ($\phi = 0^0$) echo widths versus the cylinder radius from a single chiral circular cylinder for TE polarization. Both echo widths increase sharply for electrically small cylinder ($a << \lambda$) and are oscillating with frequency when electrical size of the cylinder is on the order of a wavelength.

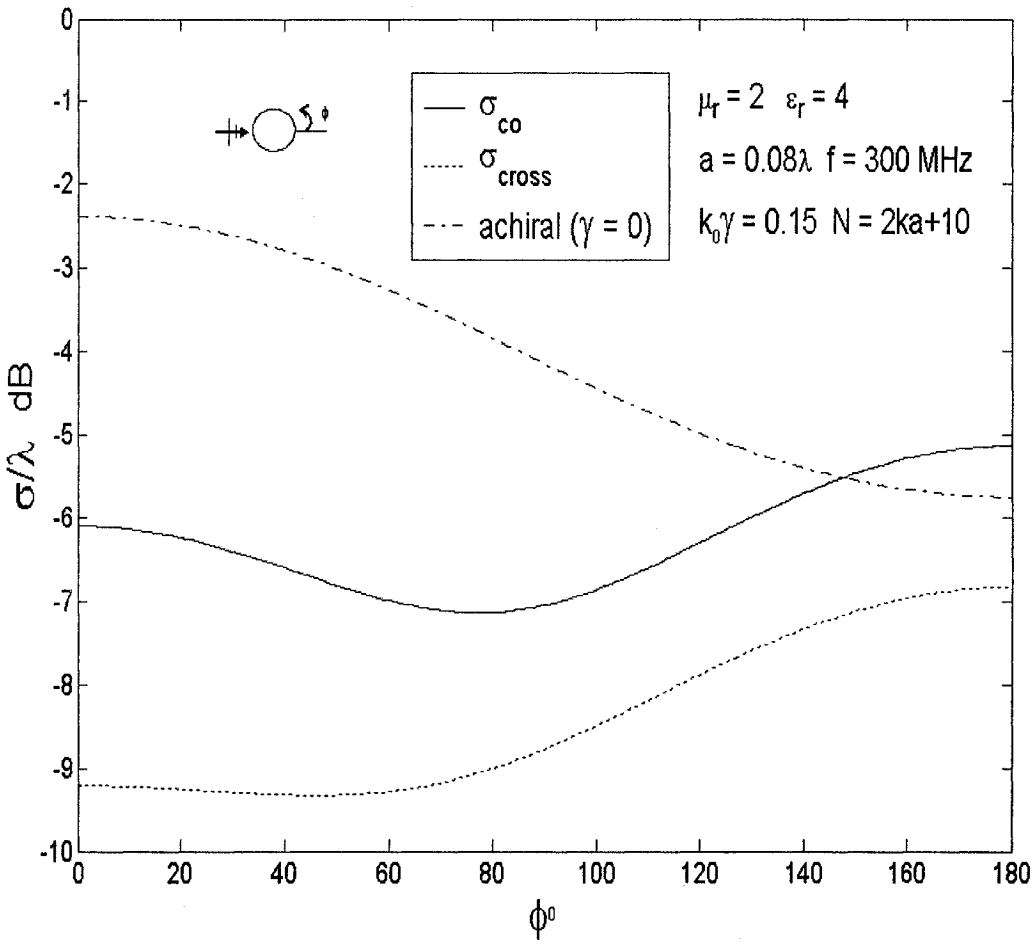


Fig. 2.3: The co- and cross-polarized echo width patterns for single chiral circular cylinder, TM case.

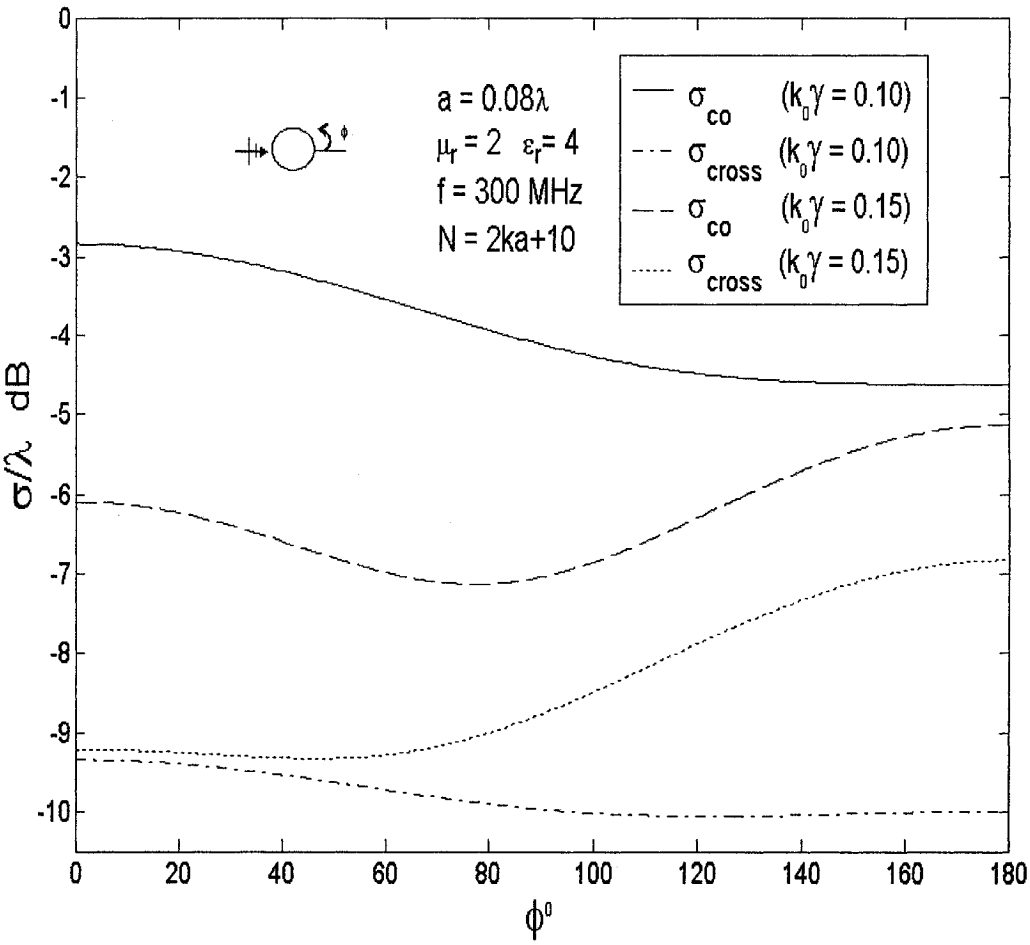


Fig. 2.4: The co- and cross-polarized echo width patterns from single chiral circular cylinder for two different chiral parameters, TM case.

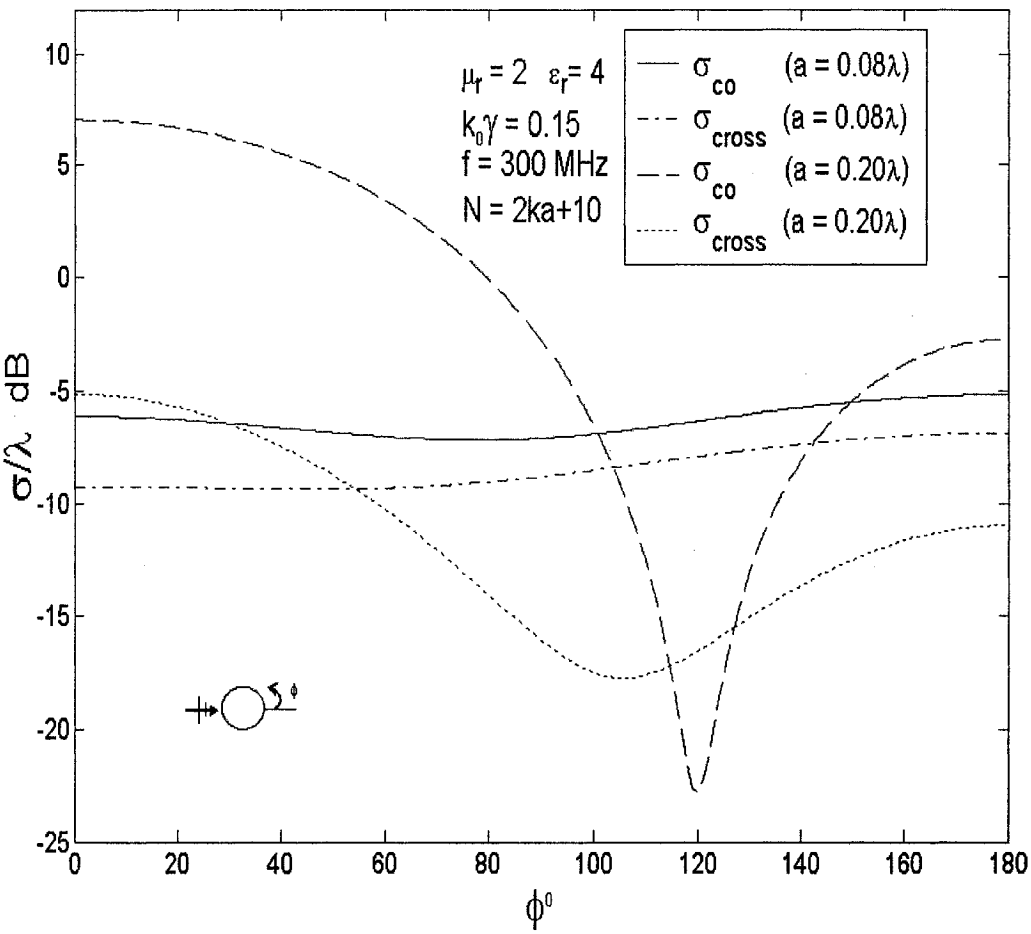


Fig. 2.5: The co- and cross-polarized echo width patterns from single chiral circular cylinder for two different radii, TM case.

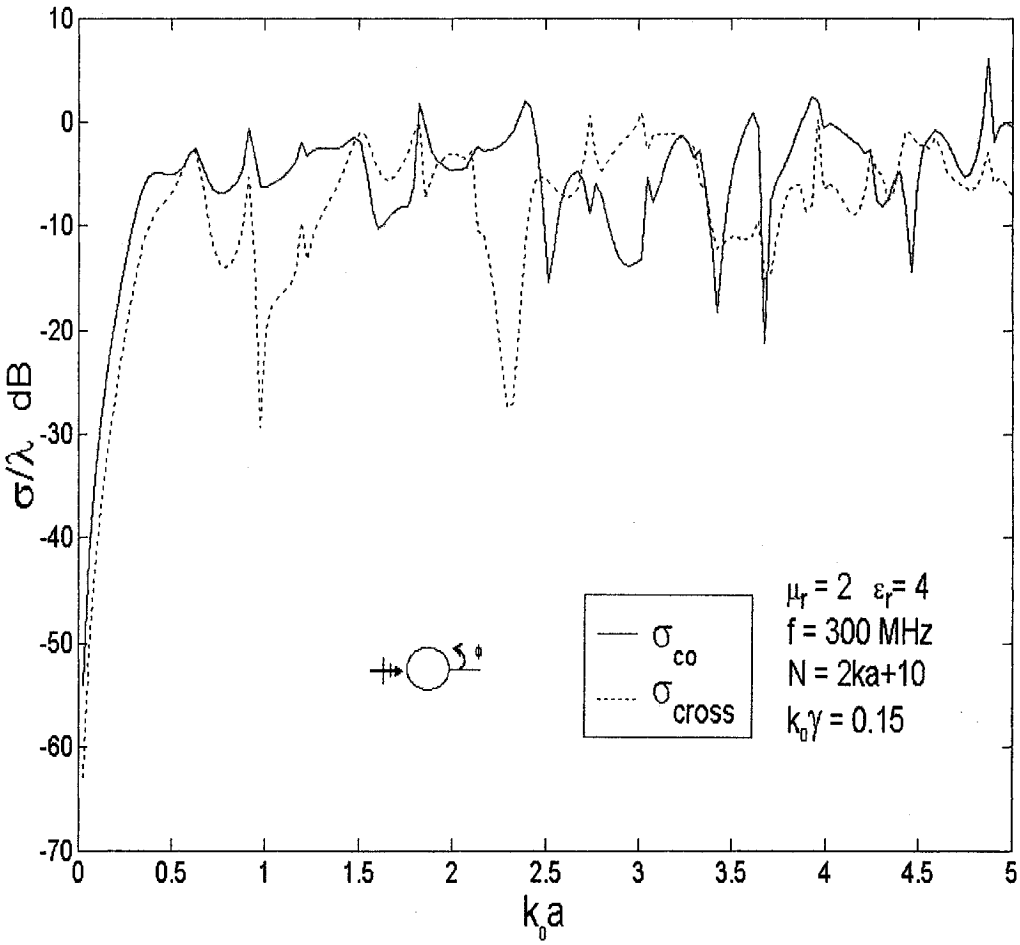


Fig. 2.6: The co- and cross-polarized backscattering echo widths for a chiral circular cylinder as a function of cylinder radius, TM case.

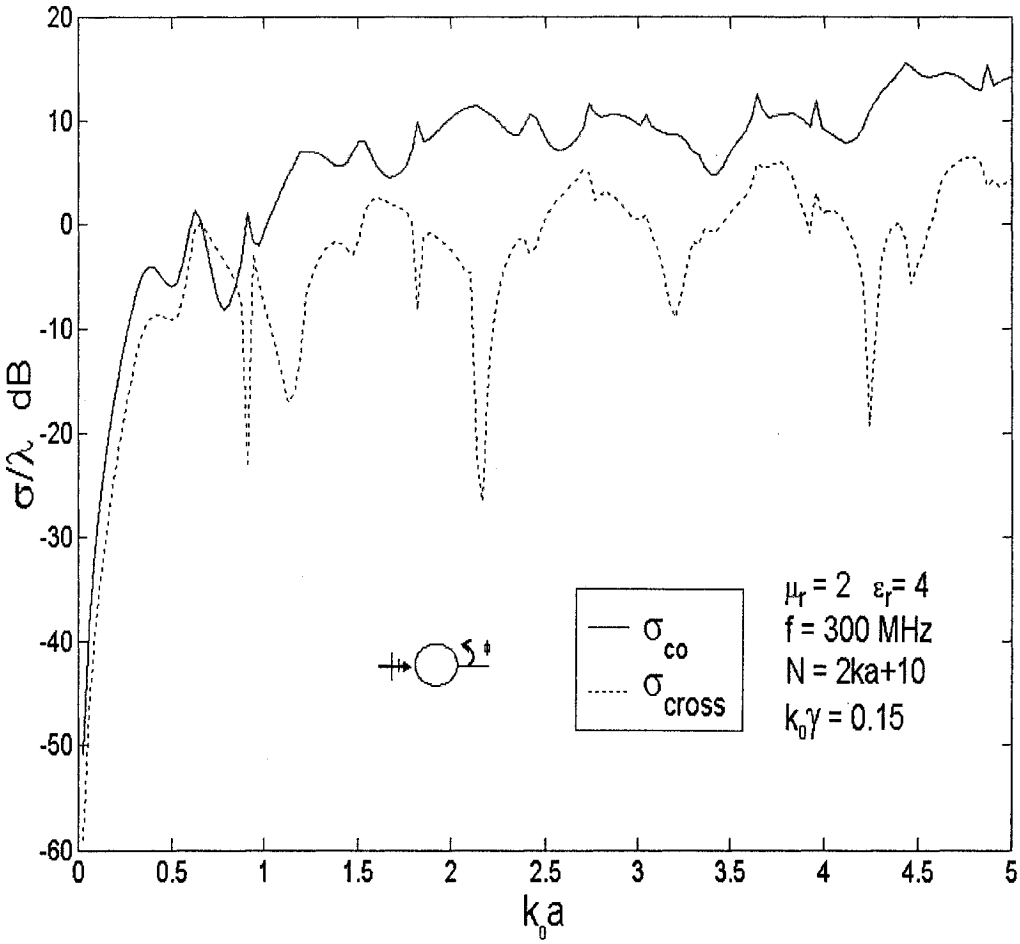


Fig. 2.7: The co- and cross-polarized forward scattering echo widths for a chiral circular cylinder as a function of cylinder radius, TM case.

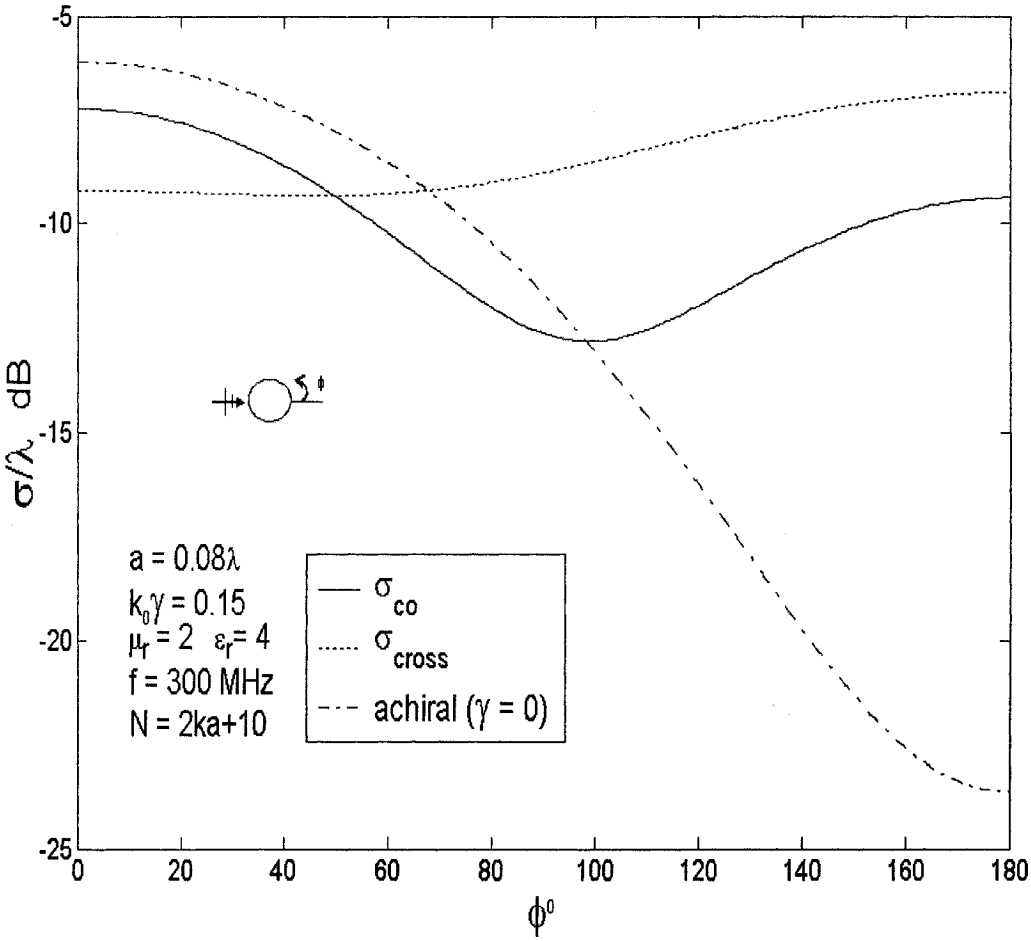


Fig. 2.8: The co- and cross-polarized echo width patterns from single chiral circular cylinder, TE case.

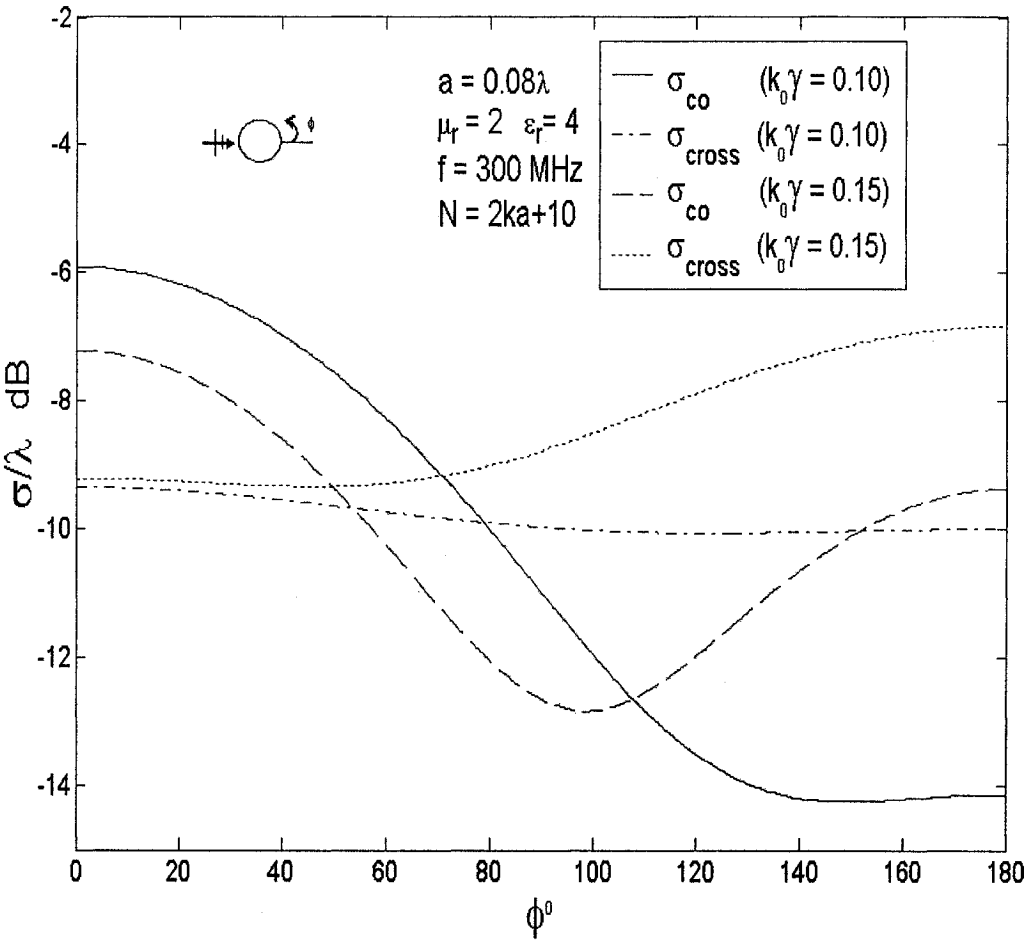


Fig. 2.9: The co- and cross-polarized echo width patterns from single chiral circular cylinder for two different chiral parameters, TE case.

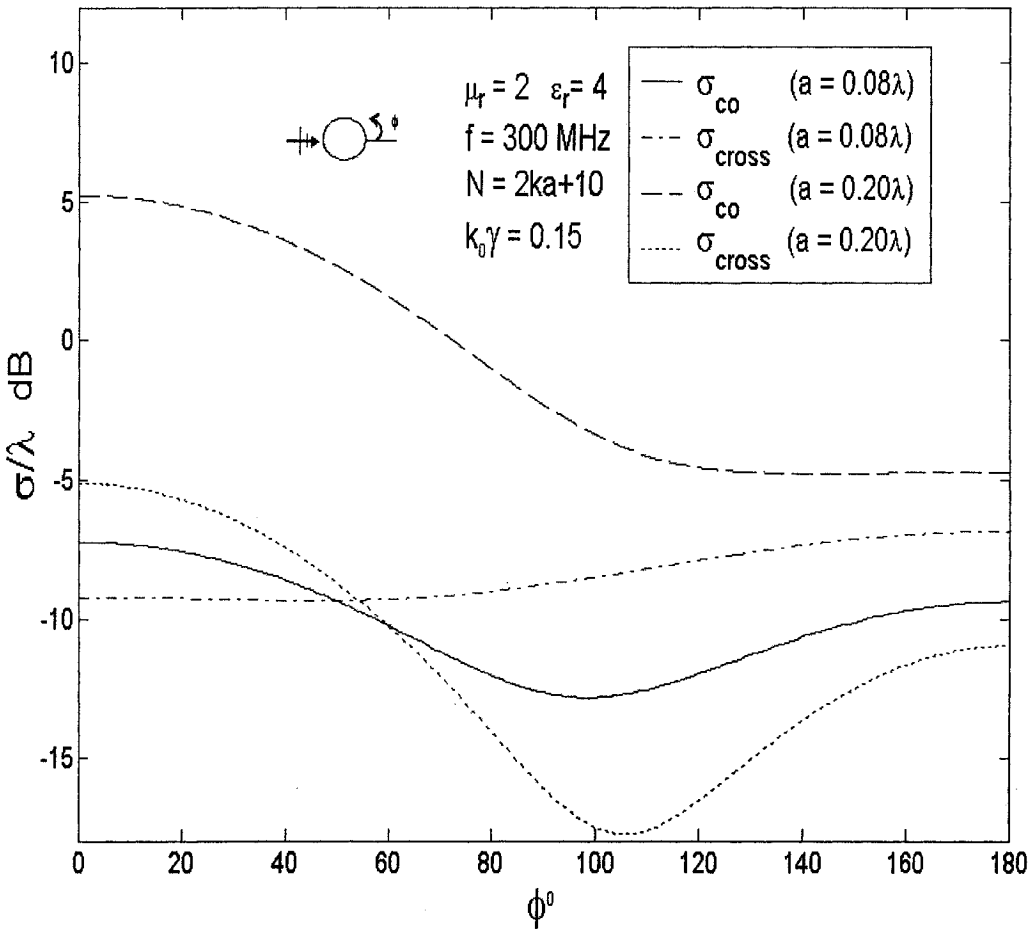


Fig. 2.10: The co- and cross-polarized echo width patterns from single chiral circular cylinder for two different radii, TE case.

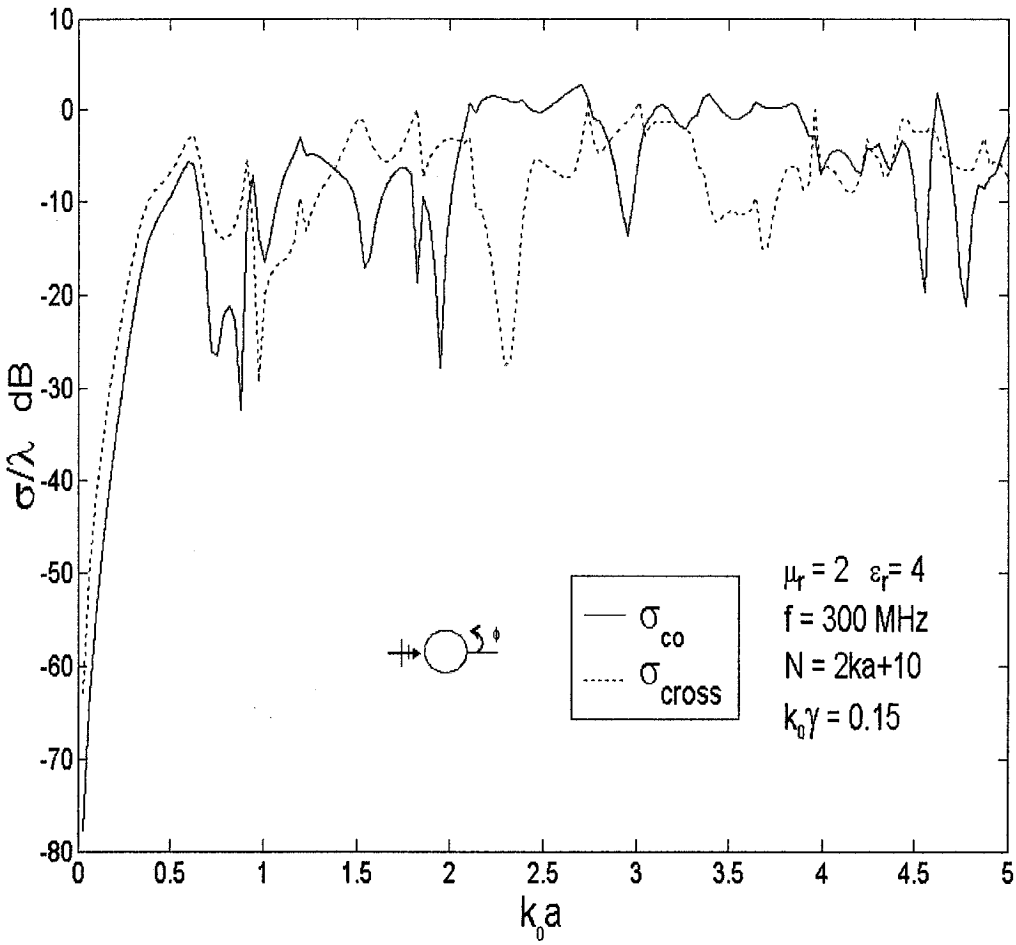


Fig. 2.11: The co- and cross-polarized backscattering echo widths for a chiral circular cylinder as a function of cylinder radius, TE case.

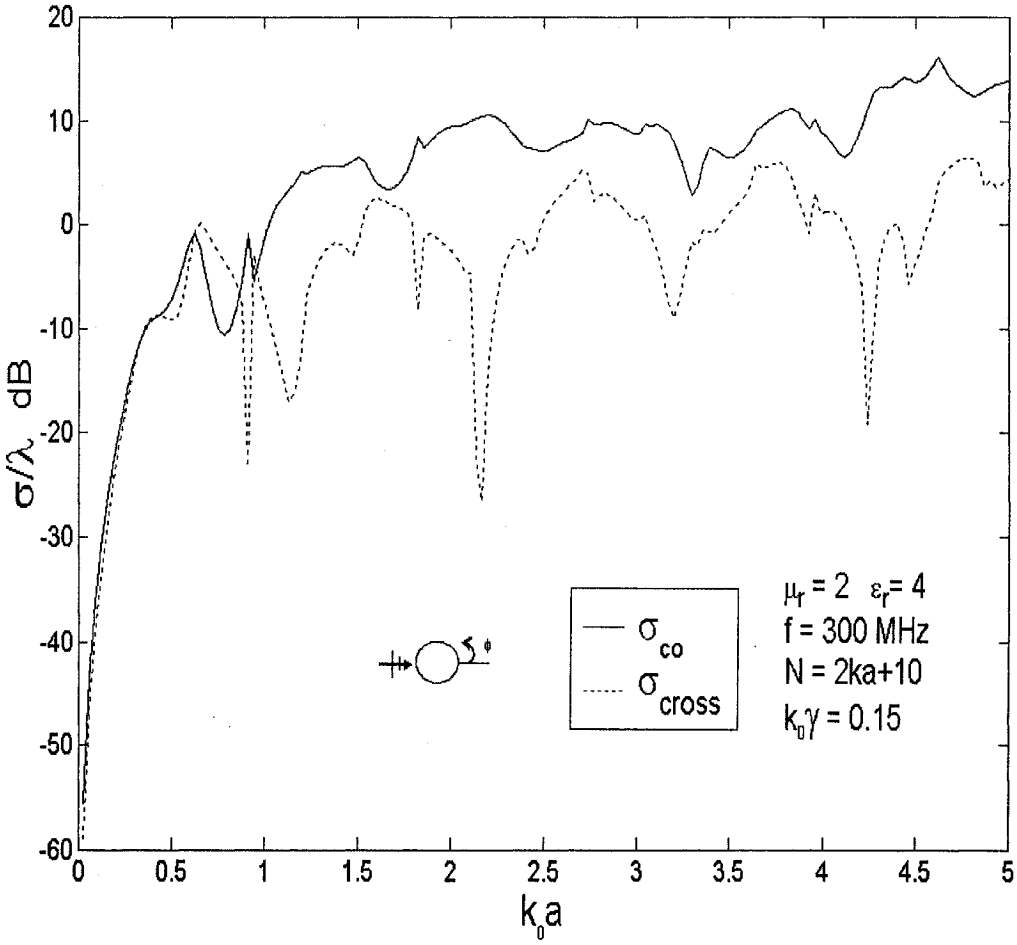


Fig. 2.12: The co- and cross-polarized forward scattering echo widths for a chiral circular cylinder as a function of cylinder radius, TE case.

# Chapter 3

# Scattering by Two Chiral Cylinders, TM case

## 3.1 Description of the Problem

The geometry of the scattering problem consists of two infinitely long parallel chiral circular cylinders Q and L as shown in Fig. 3.1. The axes of two cylinders are parallel to the z axis of the cylindrical co-ordinate system. The centre of the $r^{th}$ cylinder, $r = Q, L$, is located at $(d_r, \psi_r)$ with respect to the origin O. The radius, relative permittivity, relative permeability, and chiral parameter of the $r^{th}$ cylinder are $a_r, \mu_r, \varepsilon_r$, and $\gamma_r$, respectively. The centers of two cylinders are separated by $d_{LQ}$ or d, where $d > a_L + a_Q$ and the line connecting the two centers makes an angle $\psi_{LQ}$ with respect to the x axis.

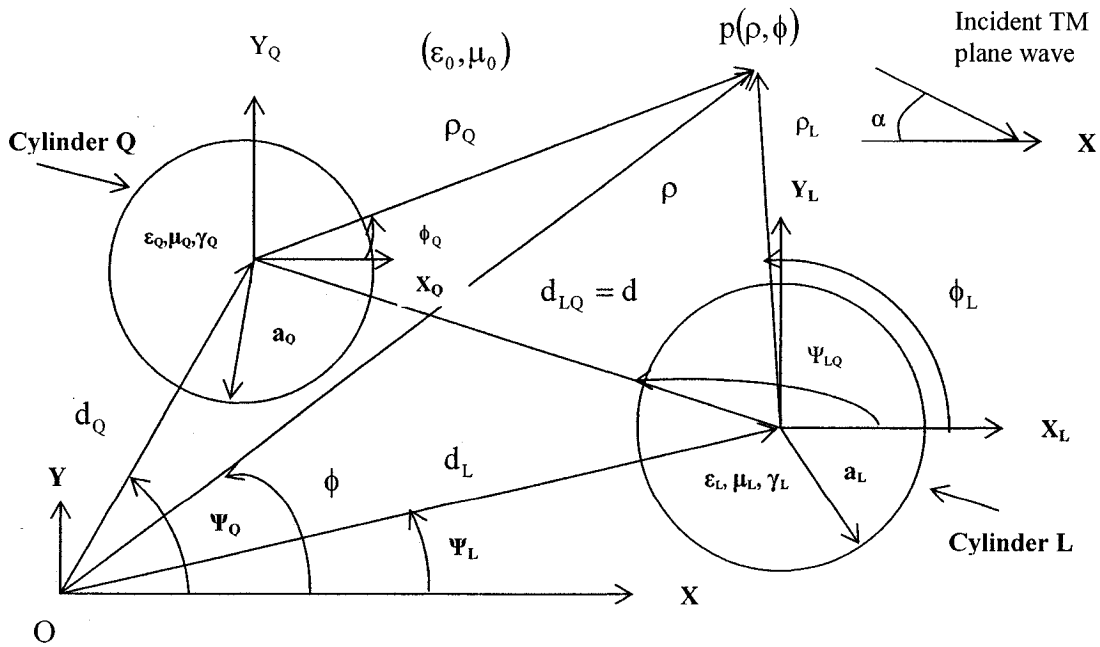


Fig. 3.1: The scattering geometry of two chiral circular cylinders, TM case

The medium of the surrounding cylinders is free space with permeability $\mu_0$ and permittivity $\varepsilon_0$. The excitation is provided by a TM polarized incident plane wave where the electric field vector is parallel to the z axis. We consider a TM polarized plane wave incident upon the cylindrical structures at an angle $\alpha$ with respect to the x axis. The time dependence of the fields is assumed to be $e^{-j\omega t}$ and suppressed throughout.

## 3.2 Expressions for Electromagnetic Fields

### 3.2.1 Expressions for Incident Fields

The incident electric field can be expressed with respect to the co-ordinate system of the $r^{th}$ cylinder as

$$\vec{E}_r^{inc} = e^{jk_0 d_r \cos(\psi_r+\alpha)} \sum_{n=-\infty}^{+\infty} \frac{j^n}{k_0} \vec{N}_n^1(k_0\rho_r) \tag{3.1}$$

where $k_0 = \omega\sqrt{\mu_0\varepsilon_0}$, is the wave number of the region surrounding the cylinders and $\vec{N}_n^1(k_0\rho_r)$ is the cylindrical vector wave function, can be denoted by

$$\vec{N}_n^1(k_0\rho_r) = \hat{u}_z k_0 J_n(k_0\rho_r) e^{jn(\phi_r+\alpha)} \tag{3.2}$$

In an isotropic, homogeneous, and linear media with time dependence $e^{-j\omega t}$, the magnetic field can be written as

$$\vec{H} = \frac{1}{j\omega\mu}(\nabla \times \vec{E}) \tag{3.3}$$

Therefore, the corresponding incident magnetic field of the $r^{th}$ cylinder is given by

$$\vec{H}_r^{inc} = \frac{1}{j\omega\mu_0} e^{jk_0 d_r \cos(\psi_r+\alpha)} \sum_{n=-\infty}^{+\infty} j^n \vec{M}_n^1(k_0\rho_r) \tag{3.4}$$

where the cylindrical vector wave function $\vec{M}_n^1(k_0\rho_r)$ can be defined by

$$\vec{M}_n^1(k_0\rho_r) = \hat{u}_\rho \frac{jn}{\rho_r} J_n(k_0\rho_r) e^{jn(\phi_r+\alpha)} - \hat{u}_\phi k_0 J_n'(k_0\rho_r) e^{jn(\phi_r+\alpha)} \tag{3.5}$$

### 3.2.2 Expressions for Scattered Fields

The scattered field of the chiral cylinder embraces both TM and TE fields since chiral scatterers generate both co- and cross-polarized scattered fields. The scattered electric field of the $r^{th}$ cylinder can be written in terms of vector wave functions as

$$\vec{E}_r^s = -\frac{1}{k_0} \sum_{n=-\infty}^{+\infty} j^n \left[ b_n^r \vec{N}_n^3(k_0\rho_r) + jc_n^r \vec{M}_n^3(k_0\rho_r) \right] \tag{3.6}$$

where $b_n^r$ and $c_n^r$ are the unknown scattering expansion coefficients of the $r^{th}$ cylinder. The cylindrical vector wave functions $\vec{N}_n^3(k_0\rho_r)$ and $\vec{M}_n^3(k_0\rho_r)$ can be written as

$$\vec{N}_n^3(k_0\rho_r) = \hat{u}_z k_0 H_n^{(1)}(k_0\rho_r) e^{jn\phi_r} \tag{3.7}$$

$$\vec{M}_n^3(k_0\rho_r) = \hat{u}_\rho \frac{jn}{\rho_r} H_n^{(1)}(k_0\rho_r) e^{jn\phi_r} - \hat{u}_\phi k_0 H_n^{(1)'}(k_0\rho_r) e^{jn\phi_r} \tag{3.8}$$

The corresponding scattered magnetic field of the $r^{th}$ cylinder can be expressed as

$$\vec{H}_r^s = -\frac{1}{j\omega\mu_0} \sum_{n=-\infty}^{+\infty} j^n \left[ b_n^r \vec{M}_n^3(k_0\rho_r) + jc_n^r \vec{N}_n^3(k_0\rho_r) \right] \tag{3.9}$$

### 3.2.3 Expressions for Internal Fields

Generally two types of internal fields (LCP and RCP) exist in a chiral medium. These fields propagate with two different wave numbers and each of these satisfies the wave equation. The internal LCP field $\left(\vec{Q}_L^r\right)$ and RCP field $\left(\vec{Q}_R^r\right)$ of the $r^{th}$ cylinder can be expressed as

$$\vec{Q}_L^r = \frac{1}{k_0}\sum_{n=-\infty}^{+\infty} j^n\, g_n^r\left[\vec{M}_n^1\left(k_L^r\rho_r\right)+\vec{N}_n^1\left(k_L^r\rho_r\right)\right] \tag{3.10}$$

$$\vec{Q}_R^r = \frac{1}{k_0}\sum_{n=-\infty}^{+\infty} j^n\, f_n^r\left[\vec{M}_n^1\left(k_R^r\rho_r\right)-\vec{N}_n^1\left(k_R^r\rho_r\right)\right] \tag{3.11}$$

where ($g_n^r$ and $f_n^r$), are the unknown expansion coefficients of the internal fields and ($k_L^r$ and $k_R^r$), are the LCP and RCP wave numbers of the $r^{th}$ cylinder, respectively.

The LCP and RCP wave numbers of the $r^{th}$ chiral cylinder can be expressed as

$$K_L^r = \frac{k_r}{1-\gamma_r k_r} \qquad K_R^r = \frac{k_r}{1+\gamma_r k_r} \tag{3.12}$$

where $k_r = \omega\sqrt{\mu_0\mu_r\varepsilon_0\varepsilon_r}$, the wave number and $\gamma_r$ is the chirality parameter of the $r^{th}$ chiral cylinder.

The Bohren linear transformation is used here to express the electromagnetic fields inside the chiral cylinders. Electric and magnetic fields inside the $r^{th}$ chiral cylinder are written as following relations in terms of left and right circularly polarized fields

$$\vec{E}_r^c = \vec{Q}_L^r + a_R^r\vec{Q}_R^r \tag{3.13}$$

$$\vec{H}_r^c = \vec{Q}_R^r + a_L^r \vec{Q}_L^r \tag{3.14}$$

where $a_R^r$ and $a_L^r$ have the unit of an impedance and an admittance of the $r^{th}$ chiral cylinder and can be denoted by

$$a_R^r = -i\sqrt{\frac{\mu_0\mu_r}{\varepsilon_0\varepsilon_r}} \qquad a_L^r = -i\sqrt{\frac{\varepsilon_0\varepsilon_r}{\mu_0\mu_r}} \tag{3.15}$$

The expression of the internal electric field (3.13) can be expanded as

$$\vec{E}_r^c = \frac{1}{k_0}\sum_{n=-\infty}^{+\infty} j^n g_n^r\left[\vec{M}_n^1\left(k_L^r\rho_r\right) + \vec{N}_n^1\left(k_L^r\rho_r\right)\right] + a_R^r\frac{1}{k_0}\sum_{n=-\infty}^{+\infty} j^n f_n^r\left[\vec{M}_n^1\left(k_R^r\rho_r\right) - \vec{N}_n^1\left(k_R^r\rho_r\right)\right] \tag{3.16}$$

The expression of the internal magnetic field (3.14) can be expanded as

$$\vec{H}_r^c = \frac{1}{k_0}\sum_{n=-\infty}^{+\infty} j^n f_n^r\left[\vec{M}_n^1\left(k_R^r\rho_r\right) - \vec{N}_n^1\left(k_R^r\rho_r\right)\right] + a_L^r\frac{1}{k_0}\sum_{n=-\infty}^{+\infty} j^n g_n^r\left[\vec{M}_n^1\left(k_L^r\rho_r\right) + \vec{N}_n^1\left(k_L^r\rho_r\right)\right] \tag{3.17}$$

## 3.3 Evaluation of the Unknown Expansion Coefficients

### 3.3.1 Transformation of Co-ordinate Systems

The unknown expansion coefficients of scattered and internal fields can be determined by applying the boundary condition on the surface of each cylinder. For this reason, it is necessary to transform the scattered field from one cylinder in terms of the local co-ordinate of another cylinder. The addition theorem for Hankel functions [17] is then used which permits the field expansions for both cylinders to be referenced to a common co-ordinate.

The addition theorem for Hankel functions is valid for all $\rho_r = a_r < d$. When $|\rho_L| < |d_{QL}\cos(\phi_L - \psi_{QL})|$ or $|\rho_Q| < |d_{LQ}\cos(\phi_Q - \psi_{LQ})|$, then the transformation from the $Q^{th}$ co-ordinate to the $L^{th}$ co-ordinate can be expressed as

$$H_n^{(1)}(k_0\rho_Q)e^{jn\phi_Q} = \sum_{m=-\infty}^{+\infty} J_m(k_0\rho_L)H_{m-n}^{(1)}(k_0 d_{LQ})e^{jm\phi_L}\, e^{-j(m-n)\psi_{LQ}} \tag{3.18}$$

Similarly, the transformation from the $L^{th}$ co-ordinate to the $Q^{th}$ co-ordinate can be expressed as

$$H_n^{(1)}(k_0\rho_L)e^{jn\phi_L} = \sum_{m=-\infty}^{+\infty} J_m(k_0\rho_Q)H_{m-n}^{(1)}(k_0 d_{QL})e^{jm\phi_Q}\, e^{-j(m-n)\psi_{QL}} \tag{3.19}$$

where

$$d_{LQ} = \sqrt{d_L^2 + d_Q^2 - 2d_L d_Q \cos(\psi_L - \psi_Q)} \tag{3.20}$$

$$\psi_{LQ} = \cos^{-1}\left[\frac{d_Q\cos\psi_Q - d_L\cos\psi_L}{d_{LQ}}\right] \tag{3.21}$$

### 3.3.2 Boundary Conditions

The unknown expansion coefficients can be determined by enforcing boundary conditions in conjunction with the addition theorem for Hankel functions on the boundary surface of each cylinder. The boundary conditions of the electromagnetic scattering state that the tangential components of the electric and magnetic fields must be continuous across the boundary.

The boundary conditions on the surface of the $L^{th}$ cylinder i.e., $\rho_L = a_L$, are given by

$$\left(\vec{E}_L^{inc} + \vec{E}_L^{s} + \vec{E}^{s}_{QQ\to L} - \vec{E}_L^{c}\right) \times \hat{u}_\rho = 0 \tag{3.22}$$

$$\left(\vec{H}_L^{inc} + \vec{H}_L^{s} + \vec{H}^{s}_{QQ\to L} - \vec{H}_L^{c}\right) \times \hat{u}_\rho = 0 \tag{3.23}$$

where $\hat{u}_\rho$ is the outward unit vector normal to the cylinder surface. $\vec{E}_L^{inc}$ and $\vec{H}_L^{inc}$ are the incident electric and magnetic fields of the $L^{th}$ cylinder. $\vec{E}_L^{s}$ and $\vec{H}_L^{s}$ are the scattered electric and magnetic fields of the $L^{th}$ cylinder. $\vec{E}_L^{c}$ and $\vec{H}_L^{c}$ are the internal electric and magnetic fields of the $L^{th}$ cylinder. $\vec{E}^{s}_{QQ\to L}$ and $\vec{H}^{s}_{QQ\to L}$ are the transform of the $Q^{th}$ cylinder scattered electric and magnetic fields as incident fields for the $L^{th}$ cylinder.

The boundary conditions on the surface of the $Q^{th}$ cylinder i.e., $\rho_Q = a_Q$, are given by

$$\left(\vec{E}_Q^{inc} + \vec{E}_Q^{s} + \vec{E}^{s}_{LL\to Q} - \vec{E}_Q^{c}\right) \times \hat{u}_\rho = 0 \tag{3.24}$$

$$\left(\vec{H}_Q^{inc} + \vec{H}_Q^{s} + \vec{H}^{s}_{LL\to Q} - \vec{H}_Q^{c}\right) \times \hat{u}_\rho = 0 \tag{3.25}$$

where $\hat{u}_\rho$ is the outward unit vector normal to the cylinder surface. $\vec{E}_Q^{inc}$ and $\vec{H}_Q^{inc}$ are the incident electric and magnetic fields of the $Q^{th}$ cylinder. $\vec{E}_Q^{s}$ and $\vec{H}_Q^{s}$ are the scattered electric and magnetic fields of the $Q^{th}$ cylinder. $\vec{E}_Q^{c}$ and $\vec{H}_Q^{c}$ are the internal electric and magnetic fields of the $Q^{th}$ cylinder. $\vec{E}^{s}_{LL\to Q}$ and $\vec{H}^{s}_{LL\to Q}$ are the transform of the $L^{th}$ cylinder scattered electric and magnetic fields as incident fields for the $Q^{th}$ cylinder.

In order to solve the boundary condition (3.22), the expression of the $\vec{E}^{s}_{QQ\to L}$ can be expanded as follows:

From equation (3.6), the term $\vec{E}^{s}_{Q}\times\hat{u}_{\rho}$ can be written as

$$\vec{E}^{s}_{Q}\times\hat{u}_{\rho}=-\frac{1}{k_0}\sum_{n=-\infty}^{+\infty}j^{n}\left[\hat{u}_{\varphi}b_n^{Q}k_0H_n^{(1)}(k_0\rho_Q)e^{jn\phi_Q}+\hat{u}_z jc_n^{Q}k_0H_n^{(1)'}(k_0\rho_Q)e^{jn\phi_Q}\right] \tag{3.26}$$

Then the addition theorem for Hankel functions is applied to express the $H_n^{(1)}(k_0\rho_Q)e^{jn\phi_Q}$ and $H_n^{(1)'}(k_0\rho_Q)e^{jn\phi_Q}$ terms and can be written using (3.18) as

$$H_n^{(1)}(k_0\rho_Q)e^{jn\phi_Q}=\sum_{m=-\infty}^{+\infty}J_m(k_0\rho_L)H_{m-n}^{(1)}(k_0d_{LQ})e^{jm\phi_L}e^{-j(m-n)\psi_{LQ}} \tag{3.27}$$

$$H_n^{(1)'}(k_0\rho_Q)e^{jn\phi_Q}=\sum_{m=-\infty}^{+\infty}J_m'(k_0\rho_L)H_{m-n}^{(1)}(k_0d_{LQ})e^{jm\phi_L}e^{-j(m-n)\psi_{LQ}} \tag{3.28}$$

Then, the final expression for $\vec{E}^{s}_{QQ\to L}$ can be written as

$$\vec{E}^{s}_{QQ\to L}\times\hat{u}_{\rho}=-\sum_{n=-\infty}^{+\infty}j^{n}\left[\begin{array}{l}\hat{u}_{\phi}b_n^{Q}\sum_{m=-\infty}^{+\infty}J_m(k_0\rho_L)H_{m-n}^{(1)}(k_0d_{LQ})e^{jm\phi_L}e^{-j(m-n)\psi_{LQ}}\\ +\hat{u}_z jc_n^{Q}\sum_{m=-\infty}^{+\infty}J_m'(k_0\rho_L)H_{m-n}^{(1)}(k_0d_{LQ})e^{jm\phi_L}e^{-j(m-n)\psi_{LQ}}\end{array}\right] \tag{3.29}$$

Similarly the expression of the $\vec{E}^{s}_{LL\to Q}$ can be expanded to solve the equation (3.24) as

$$\vec{E}^{s}_{LL\to Q}\times\hat{u}_{\rho}=-\sum_{n=-\infty}^{+\infty}j^{n}\left[\begin{array}{l}\hat{u}_{\phi}b_{n}^{L}\sum\limits_{m=-\infty}^{+\infty}J_{m}(k_{0}\rho_{Q})H^{(1)}_{m-n}(k_{0}d_{QL})e^{jm\phi_{Q}}\,e^{-j(m-n)\psi_{QL}}\\ +\hat{u}_{z}jc_{n}^{L}\sum\limits_{m=-\infty}^{+\infty}J'_{m}(k_{0}\rho_{Q})H^{(1)}_{m-n}(k_{0}d_{QL})e^{jm\phi_{Q}}\,e^{-j(m-n)\psi_{QL}}\end{array}\right] \tag{3.30}$$

Similarly the expression $\vec{H}^{s}_{Q_{Q\to L}}$ can be expanded to solve the equation (3.23) as

$$\vec{H}^{s}_{Q_{Q\to L}}\times\hat{u}_{\rho}=-\frac{k_{0}}{j\omega\mu_{0}}\sum_{n=-\infty}^{+\infty}j^{n}\left[\begin{array}{l}\hat{u}_{z}b_{n}^{Q}\sum\limits_{m=-\infty}^{+\infty}J'_{m}(k_{0}\rho_{L})H^{(1)}_{m-n}(k_{0}d_{LQ})e^{jm\phi_{L}}\,e^{-j(m-n)\psi_{LQ}}\\ +\hat{u}_{\phi}c_{n}^{Q}\sum\limits_{m=-\infty}^{+\infty}J_{m}(k_{0}\rho_{L})H^{(1)}_{m-n}(k_{0}d_{LQ})e^{jm\phi_{L}}\,e^{-j(m-n)\psi_{LQ}}\end{array}\right] \tag{3.31}$$

Similarly the expression $\vec{H}^{s}_{L_{L\to Q}}$ can be expanded to solve the equation (3.25) as

$$\vec{H}^{s}_{L_{L\to Q}}\times\hat{u}_{\rho}=-\frac{k_{0}}{j\omega\mu_{0}}\sum_{n=-\infty}^{+\infty}j^{n}\left[\begin{array}{l}\hat{u}_{z}b_{n}^{L}\sum\limits_{m=-\infty}^{+\infty}J'_{m}(k_{0}\rho_{Q})H^{(1)}_{m-n}(k_{0}d_{QL})e^{jm\phi_{Q}}\,e^{-j(m-n)\psi_{QL}}\\ +\hat{u}_{\phi}jc_{n}^{L}\sum\limits_{m=-\infty}^{+\infty}J_{m}(k_{0}\rho_{Q})H^{(1)}_{m-n}(k_{0}d_{QL})e^{jm\phi_{Q}}\,e^{-j(m-n)\psi_{QL}}\end{array}\right] \tag{3.32}$$

where $(b_n^L, c_n^L)$ and $(b_n^Q, c_n^Q)$ are the unknown scattering expansion coefficients of the $L^{th}$ and $Q^{th}$ cylinders, respectively.

The boundary condition (3.22) can be written using equations (3.1), (3.6), (3.16), and (3.29) as

$$
\begin{aligned}
&\hat{u}_\phi e^{jk_0 d_L \cos(\psi_L+\alpha)} \sum_{n=-\infty}^{+\infty} j^n J_n(k_0 a_L)\, e^{jn(\phi_L+\alpha)} \\
&-\frac{1}{k_0}\sum_{n=-\infty}^{+\infty} j^n\left[\hat{u}_\phi b_n^L k_0 H_n^{(1)}(k_0 a_L) e^{jn\phi_L} + \hat{u}_z j c_n^L k_0 H_n^{(1)'}(k_0 a_L)\, e^{jn\phi_L}\right] \\
&-\sum_{n=-\infty}^{+\infty} j^n\left[\begin{array}{l}\hat{u}_\phi b_n^Q \sum_{m=-\infty}^{+\infty} J_m(k_0 a_L) H_{m-n}^{(1)}(k_0 d_{LQ})\, e^{jm\phi_L}\, e^{-j(m-n)\psi_{LQ}} \\ + \hat{u}_z j c_n^Q \sum_{m=-\infty}^{+\infty} J_m'(k_0 a_L) H_{m-n}^{(1)}(k_0 d_{LQ})\, e^{jm\phi_L}\, e^{-j(m-n)\psi_{LQ}}\end{array}\right] \\
&-\frac{1}{k_0}\sum_{n=-\infty}^{+\infty} j^n g_n^L\left[\hat{u}_z k_L^L J_n'(k_L^L a_L)\, e^{jn\phi_L} + \hat{u}_\phi k_L^L J_n(k_L^L a_L)\, e^{jn\phi_L}\right] \\
&-\frac{a_R^L}{k_0}\sum_{n=-\infty}^{+\infty} j^n f_n^L\left[\hat{u}_z k_R^L J_n'(k_R^L a_L)\, e^{jn\phi_L} - \hat{u}_\phi k_R^L J_n(k_R^L a_L)\, e^{jn\phi_L}\right] = 0
\end{aligned}
\tag{3.33}
$$

Equating $\hat{u}_\phi$ terms from equation (3.33)

$$
\begin{aligned}
&-\sum_{n=-\infty}^{+\infty}\left[b_n^L H_n^{(1)}(k_0 a_L)\right] - \sum_{n=-\infty}^{+\infty}\left[b_n^Q \sum_{m=-\infty}^{+\infty} J_m(k_0 a_L) H_{m-n}^{(1)}(k_0 d_{LQ})\, e^{-j(m-n)\psi_{LQ}}\right] \\
&-\frac{k_L^L}{k_0}\sum_{n=-\infty}^{+\infty} g_n^L\left[J_n(k_L^L a_L)\right] + \frac{a_R^L k_R^L}{k_0}\sum_{n=-\infty}^{+\infty} f_n^L\left[J_n(k_R^L a_L)\right] = -e^{jk_0 d_L \cos(\psi_L+\alpha)} \sum_{n=-\infty}^{n=\infty} J_n(k_0 a_L) e^{jn\alpha}
\end{aligned}
\tag{3.34}
$$

Equating $\hat{u}_z$ terms from equation (3.33)

$$
\begin{aligned}
&-\sum_{n=-\infty}^{+\infty}\left[j c_n^L H_n^{(1)'}(k_0 a_L)\right] - \sum_{n=-\infty}^{+\infty}\left[j c_n^Q \sum_{m=-\infty}^{+\infty} J_m'(k_0 a_L) H_{m-n}^{(1)}(k_0 d_{LQ})\, e^{-j(m-n)\psi_{LQ}}\right] \\
&-\frac{k_L^L}{k_0}\sum_{n=-\infty}^{+\infty} g_n^L\left[J_n'(k_L^L a_L)\right] - \frac{a_R^L k_R^L}{k_0}\sum_{n=-\infty}^{+\infty} f_n^L\left[J_n'(k_R^L a_L)\right] = 0
\end{aligned}
\tag{3.35}
$$

The boundary condition (3.24) can be written using equations (3.1), (3.6), (3.16), and (3.30) as

$$\begin{aligned}
&\hat{u}_\phi e^{jk_0 d_Q \cos(\psi_Q+\alpha)} \sum_{n=-\infty}^{+\infty} j^n J_n(k_0 a_Q) e^{jn(\phi_Q+\alpha)} \\
&-\frac{1}{k_0}\sum_{n=-\infty}^{+\infty} j^n \left[\hat{u}_\phi b_n^Q k_0 H_n^{(1)}(k_0 a_Q) e^{jn\phi_Q} + \hat{u}_z j c_n^Q k_0 H_n^{(1)'}(k_0 a_Q) e^{jn\phi_Q}\right] \\
&-\sum_{n=-\infty}^{+\infty} j^n \left[\begin{array}{l} \hat{u}_\phi b_n^L \sum_{m=-\infty}^{+\infty} J_m(k_0\rho_Q) H_{m-n}^{(1)}(k_0 d_{QL}) e^{jm\phi_Q} e^{-j(m-n)\psi_{QL}} \\ + \hat{u}_z j c_n^L \sum_{m=-\infty}^{+\infty} J_m'(k_0\rho_Q) H_{m-n}^{(1)}(k_0 d_{QL}) e^{jm\phi_Q} e^{-j(m-n)\psi_{QL}} \end{array}\right] \\
&-\frac{1}{k_0}\sum_{n=-\infty}^{+\infty} j^n g_n^Q \left[\hat{u}_z k_L^Q J_n'(k_L^Q a_Q) e^{jn\phi_L} + \hat{u}_\varphi k_L^Q J_n(k_L^Q a_Q) e^{jn\phi_Q}\right] \\
&-\frac{a_R^Q}{k_0}\sum_{n=-\infty}^{+\infty} j^n f_n^Q \left[\hat{u}_z k_R^Q J_n'(k_R^Q a_Q) e^{jn\phi_Q} - \hat{u}_\varphi k_R^Q J_n(k_R^Q a_Q) e^{jn\phi_Q}\right] = 0
\end{aligned} \tag{3.36}$$

Equating $\hat{u}_\phi$ terms from equation (3.36)

$$\begin{aligned}
&-b_n^Q \sum_{n=-\infty}^{+\infty} \left[H_n^{(1)}(k_0 a_Q)\right] - b_n^L \sum_{n=-\infty}^{+\infty} \left[\sum_{m=-\infty}^{+\infty} J_m(k_0 a_Q) H_{m-n}^{(1)}(k_0 d_{QL}) e^{-j(m-n)\psi_{QL}}\right] \\
&-g_n^Q \frac{k_L^Q}{k_0}\sum_{n=-\infty}^{+\infty} J_n(k_L^Q a_Q) + f_n^Q \frac{a_R^Q k_R^Q}{k_0}\sum_{n=-\infty}^{+\infty} J_n(k_R^Q a_Q) = -e^{jk_0 d_Q \cos(\psi_Q+\alpha)} \sum_{n=-\infty}^{n=\infty} J_n(k_0 a_Q) e^{jn\alpha}
\end{aligned} \tag{3.37}$$

Equating $\hat{u}_z$ terms from equation (3.36)

$$\begin{aligned}
&-c_n^Q \sum_{n=-\infty}^{+\infty} \left[jH_n^{(1)'}(k_0 a_Q)\right] - c_n^L \sum_{n=-\infty}^{+\infty} \left[j\sum_{m=-\infty}^{+\infty} J_m'(k_0 a_Q) H_{m-n}^{(1)}(k_0 d_{QL}) e^{-j(m-n)\psi_{QL}}\right] \\
&-g_n^Q \frac{k_L^Q}{k_0}\sum_{n=-\infty}^{+\infty} \left[J_n'(k_L^Q a_Q)\right] - f_n^Q \frac{a_R^Q k_R^Q}{k_0}\sum_{n=-\infty}^{+\infty} \left[J_n'(k_R^Q a_Q)\right] = 0
\end{aligned} \tag{3.38}$$

The boundary condition (3.23) can be written using equations (3.4), (3.9), (3.17), and (3.31) as

$$\begin{aligned}
&\hat{u}_z \frac{k_0}{j\omega\mu_0} e^{jk_0 d_L \cos(\psi_L+\alpha)} \sum_{n=-\infty}^{+\infty} j^n J_n'(k_0 a_L) e^{jn(\phi_L+\alpha)} \\
&- \frac{k_0}{j\omega\mu_0} \sum_{n=-\infty}^{+\infty} j^n \left[ \hat{u}_z b_n^L H_n^{(1)'}(k_0 a_L) e^{jn\phi_L} + \hat{u}_\varphi j c_L H_n^{(1)}(k_0 a_L) e^{jn\phi_L} \right] \\
&- \frac{k_0}{j\omega\mu_0} \sum_{n=-\infty}^{+\infty} j^n \left[ \begin{array}{l} \hat{u}_z b_n^Q \sum_{m=-\infty}^{+\infty} J_m'(k_0\rho_L) H_{m-n}^{(1)}(k_0 d_{LQ}) e^{jm\phi_L} e^{-j(m-n)\psi_{LQ}} \\ + \hat{u}_\phi j c_n^Q \sum_{m=-\infty}^{+\infty} J_m(k_0 a_L) H_{m-n}^{(1)}(k_0 d_{LQ}) e^{jm\phi_L} e^{-j(m-n)\psi_{LQ}} \end{array} \right] \\
&- \frac{1}{k_0} \sum_{n=-\infty}^{+\infty} j^n f_n^L \left[ \hat{u}_z k_R^L J_n'(k_R^L a_L) e^{jn\phi_L} - \hat{u}_\phi k_R^L J_n(k_R^L a_L) e^{jn\phi_L} \right] \\
&- a_L^L \frac{1}{k_0} \sum_{n=-\infty}^{+\infty} j^n g_n^L \left[ \hat{u}_z k_L^L J_n'(k_L^L a_L) e^{jn\phi_L} + \hat{u}_\phi k_L^L J_n(k_L^L a_L) e^{jn\phi_L} \right] = 0
\end{aligned} \tag{3.39}$$

Equating $\hat{u}_\varphi$ terms from equation (3.39)

$$\begin{aligned}
&- \frac{c_n^L k_0}{\omega\mu_0} \sum_{n=-\infty}^{+\infty} H_n^{(1)}(k_0 a_L) - \frac{c_n^Q k_0}{\omega\mu_0\mu_m} \sum_{n=-\infty}^{+\infty} \sum_{m=-\infty}^{+\infty} J_m(k_0 a_L) H_{m-n}^{(1)}(k_0 d_{LQ}) e^{-j(m-n)\psi_{LQ}} \\
&+ f_n^L \frac{k_R^L}{k_0} \sum_{n=-\infty}^{+\infty} J_n(k_R^L a_L) - g_n^L \frac{a_L^L k_L^L}{k_0} \sum_{n=-\infty}^{+\infty} J_n(k_L^L a_L) = 0
\end{aligned} \tag{3.40}$$

Equating $\hat{u}_z$ terms from equation (3.39)

$$\begin{aligned}
&- \frac{b_n^L k_0}{j\omega\mu_0} \sum_{n=-\infty}^{+\infty} H_n^{(1)'}(k_0 a_L) - \frac{b_n^Q k_0}{j\omega\mu_0} \sum_{n=-\infty}^{+\infty} \sum_{m=-\infty}^{+\infty} J_m'(k_0 a_L) H_{m-n}^{(1)}(k_0 d_{LQ}) e^{-j(m-n)\psi_{LQ}} \\
&- f_n^L \frac{k_R^L}{k_0} \sum_{n=-\infty}^{+\infty} J_n'(k_R^L a_L) - g_n^L \frac{a_L^L k_L^L}{k_0} \sum_{n=-\infty}^{+\infty} J_n'(k_L^L a_L) = - \frac{k_0 e^{jk_0 d_L \cos(\psi_L+\alpha)}}{j\omega\mu_0} \sum_{n=-\infty}^{+\infty} J_n'(k_0 a_L) e^{jn\alpha}
\end{aligned} \tag{3.41}$$

The boundary condition (3.25) can be written using equations (3.4), (3.9), (3.17), and (3.32) as

$$\begin{aligned}
&\hat{u}_z \frac{k_0}{j\omega\mu_0} e^{jk_0 d_Q \cos(\psi_Q+\alpha)} \sum_{n=-\infty}^{+\infty} j^n J_n'(k_0 a_Q) e^{jn(\phi_Q+\alpha)} \\
&-\frac{k_0}{j\omega\mu_0} \sum_{n=-\infty}^{+\infty} j^n \left[\hat{u}_z b_n^Q H_n^{(1)'}(k_0 a_Q) e^{jn\phi_Q} + \hat{u}_\varphi j c_n^Q H_n^{(1)}(k_0 a_Q) e^{jn\phi_Q}\right] \\
&-\frac{k_0}{j\omega\mu_0} \sum_{n=-\infty}^{+\infty} j^n \left[\begin{array}{l} \hat{u}_z b_n^L \sum_{m=-\infty}^{+\infty} J_m'(k_0 a_Q) H_{m-n}^{(1)}(k_0 d_{QL}) e^{jm\phi_Q} e^{-j(m-n)\psi_{QL}} \\ + \hat{u}_\phi j c_n^L \sum_{m=-\infty}^{+\infty} J_0(k_0 a_Q) H_{m-n}^{(1)}(k_0 d_{QL}) e^{jm\phi_Q} e^{-j(m-n)\psi_{QL}} \end{array}\right] \\
&-\frac{1}{k_0} \sum_{n=-\infty}^{+\infty} j^n f_n^Q \left[\hat{u}_z k_R^Q J_n'(k_R^Q a_Q) e^{jn\phi_Q} - \hat{u}_\phi k_R^Q J_n(k_R^Q a_Q) e^{jn\phi_Q}\right] \\
&-a_L^Q \frac{1}{k_0} \sum_{n=-\infty}^{+\infty} j^n g_n^Q \left[\hat{u}_z k_L^Q J_n'(k_L^Q a_Q) e^{jn\phi_Q} + \hat{u}_\phi k_L^Q J_n(k_L^Q a_Q) e^{jn\phi_Q}\right] = 0
\end{aligned} \tag{3.42}$$

Equating $\hat{u}_\varphi$ terms from equation (3.42)

$$\begin{aligned}
&-\frac{c_n^Q k_0}{\omega\mu_0} \sum_{n=-\infty}^{+\infty} H_n^{(1)}(k_0 a_Q) - \frac{c_n^L k_0}{\omega\mu_0} \sum_{n=-\infty}^{+\infty} \sum_{m=-\infty}^{+\infty} J_m(k_0 a_Q) H_{m-n}^{(1)}(k_0 d_{QL}) e^{-j(m-n)\psi_{QL}} \\
&+ f_n^Q \frac{k_R^Q}{k_0} \sum_{n=-\infty}^{+\infty} J_n(k_R^Q a_Q) - g_n^Q \frac{a_L^Q k_L^Q}{k_0} \sum_{n=-\infty}^{+\infty} J_n(k_L^Q a_Q) = 0
\end{aligned} \tag{3.43}$$

Equating $\hat{u}_z$ terms from equation (3.42)

$$\begin{aligned}
&-\frac{k_0}{j\omega\mu_0} \sum_{n=-\infty}^{+\infty} b_n^Q H_n^{(1)'}(k_0 a_Q) - \frac{b_n^L k_0}{j\omega\mu_0} \sum_{n=-\infty}^{+\infty} \sum_{m=-\infty}^{+\infty} J_m'(k_0 a_Q) H_{m-n}^{(1)}(k_0 d_{QL}) e^{-j(m-n)\psi_{QL}} \\
&- f_n^Q \frac{k_R^Q}{k_0} \sum_{n=-\infty}^{+\infty} J_n'(k_R^Q a_Q) - g_n^Q \frac{a_L^Q k_L^Q}{k_0} \sum_{n=-\infty}^{+\infty} J_n'(k_L^Q a_Q) = -\frac{k_0 e^{jk_0 d_Q \cos(\psi_Q+\alpha)}}{j\omega\mu_0} \sum_{n=-\infty}^{+\infty} J_n'(k_0 a_Q) e^{jn\alpha}
\end{aligned} \tag{3.44}$$

These eight linear equations obtained from the boundary conditions (3.22-3.25) can be written in the following matrix form to solve the unknown expansion coefficients $\left(b_n^L, c_n^L, b_n^Q, c_n^Q, g_n^L, f_n^L, g_n^Q, \text{and } f_n^Q\right)$ numerically.

$$[A]\,[a] = [I] \tag{3.45}$$

where the matrix [A] represents the elements of the unknown expansion coefficients, matrix [a] stands for unknown expansion coefficients which to be find out, and matrix [I] contains the elements without the unknown expansion coefficients.

## 3.4 Far Scattered Fields

The total scattered electric field ($\vec{E}^s$) can be determined after evaluating all unknown scattering expansion coefficients. The total scattered field can be expressed as

$$\vec{E}^s_{total} = \vec{E}^s_L + \vec{E}^s_Q \tag{3.46}$$

The expression of (3.46) can be expanded using equation (3.6) as

$$\vec{E}^s_{total} = -\frac{1}{k_0}\sum_{n=-\infty}^{+\infty} j^n \begin{bmatrix} b_n^L \vec{N}_n^3(k_0\rho_L) + b_n^Q \vec{N}_n^3(k_0\rho_Q) \\ + j\left\{c_n^L \vec{M}_n^3(k_0\rho_L) + c_n^Q \vec{M}_n^3(k_0\rho_Q)\right\} \end{bmatrix} \tag{3.47}$$

The total scattered field carries both co- and cross-polarized fields. The co-polarized scattered field can be written as

$$\vec{E}^s_{co} = -\frac{1}{k_0}\sum_{n=-\infty}^{+\infty} j^n\left[b_n^L \vec{N}_n^3(k_0\rho_L) + b_n^Q \vec{N}_n^3(k_0\rho_Q)\right]$$

$$\Rightarrow \vec{E}^s_{co} = -\hat{u}_z \sum_{n=-\infty}^{+\infty} j^n\left[b_n^L H_n^1(k_0\rho_L)e^{jn\phi_L} + b_n^Q H_n^1(k_0\rho_Q)e^{jn\phi_Q}\right] \tag{3.48}$$

The cross-polarized scattered field can be written as

$$\vec{E}^{s}_{cross} = -\frac{j}{k_0}\sum_{n=-\infty}^{+\infty} j^n\left[c_n^L \vec{M}_n^3(k_0\rho_L) + c_n^Q \vec{M}_n^3(k_0\rho_Q)\right]$$

$$\Rightarrow E^{s}_{cross} = \hat{u}_\phi\, j\sum_{n=-\infty}^{+\infty} j^n\left[c_n^L H_n^{(1)'}(k_0\rho_L)e^{jn\phi_L} + c_n^Q H_n^{(1)'}(k_0\rho_Q)e^{jn\phi_Q}\right] \tag{3.49}$$

The asymptotic expansion for the Hankel function for large arguments is applied here to achieve the far scattered fields. In the far field region ( $k_0\rho >> 1$ ), the Hankel function can be approximated [30] by

$$H_n^{(1)}(k_0\rho) \underset{k_0\rho\to\infty}{\cong} \sqrt{\frac{2}{j\pi k_0\rho}}\, j^{-n} e^{jk_0\rho} \tag{3.50}$$

The distances from cylinders to observation point can also be approximated for the far field region ( $k_0\rho >> 1$ )

$$\rho_L = \rho - d_L\cos(\psi_L - \phi) \tag{3.51}$$

$$\rho_Q = \rho - d_Q\cos(\psi_Q - \phi) \tag{3.52}$$

$$\phi = \phi_L = \phi_Q \tag{3.53}$$

Hence the far scattered co-polarized field is given by

$$\vec{E}^{s}_{co} \overset{k_0\rho\to\infty}{\cong} -\hat{u}_z \sum_{n=-\infty}^{+\infty}\sqrt{\frac{2}{j\pi k_0\rho}}\, e^{jk_0\rho}\left[b_n^L e^{-jk_0 d_L\cos(\psi_L-\phi)} + b_n^Q e^{-jk_0 d_Q\cos(\psi_Q-\phi)}\right]e^{jn\phi} \tag{3.54}$$

Similarly the far scattered cross-polarized field is given by

$$\vec{E}^{s}_{cross} \overset{k_0\rho\to\infty}{\cong} -\vec{u}_{\phi}\sum_{n=-\infty}^{+\infty}\sqrt{\frac{2}{j\pi k_0\rho}}\, e^{jk_0\rho}\left[c_n^{L}\, e^{-jk_0 d_L\cos(\psi_L-\phi)} + c_n^{Q} e^{-jk_0 d_Q\cos(\psi_Q-\phi)}\right] e^{jn\phi} \tag{3.55}$$

## 3.5 Echo Width

In this thesis, the main intention is to analysis the echo width from two chiral circular cylinders. The echo width is a far field parameter which is used to characterize the scattering properties of a target. The echo width can be obtained by knowing the scattered field in the far zone.

The co- and cross-polarized echo widths [30] can be expressed for the TM polarization as

$$\sigma_{co}^{TM} = \lim_{\rho\to\infty} 2\pi\rho \frac{\left|\vec{E}^{s}_{co}\right|^2}{\left|\vec{E}^{inc}\right|^2} \tag{3.56}$$

$$\sigma_{cross}^{TM} = \lim_{\rho\to\infty} 2\pi\rho \frac{\left|\vec{E}^{s}_{cross}\right|^2}{\left|\vec{E}^{inc}\right|^2} \tag{3.57}$$

The co-polarized echo width (3.56) can be written as

$$\sigma_{co}^{TM} = \frac{4}{k_0}\left|\sum_{n=-\infty}^{+\infty}\left[b_n^{L}\, e^{-jk_0 d_L\cos(\psi_L-\phi)} + b_n^{Q}\, e^{-jk_0 d_Q\cos(\psi_Q-\phi)}\right] e^{jn\phi}\right|^2 \tag{3.58}$$

The cross-polarized echo width (3.57) can be written as

$$\sigma_{cross}^{TM} = \frac{4}{k_0}\left|\sum_{n=-\infty}^{+\infty}\left[c_n^{L}\, e^{-jk_0 d_L\cos(\psi_L-\phi)} + c_n^{Q}\, e^{-jk_0 d_Q\cos(\psi_Q-\phi)}\right] e^{jn\phi}\right|^2 \tag{3.59}$$

## 3.6 Numerical Results

Numerical results are presented for the TM polarized incident wave using the formulation described in the earlier section. At first numerical results are validated with existing published results for special and limiting cases. After that several numerical results are given to observe the effects on echo width patterns for selected geometries and parameters. Both co- and cross-polarized far scattered fields are taken into consideration for all numerical results. The scattered echo width $\frac{\sigma}{\lambda}$ is obtained for all cases in this part.

The unknown expansion coefficients are numerically solved by a proper truncation of the infinite sums into finite sums. In order to generate numerical results, a truncation number N is used and it depends upon the degree of accuracy required, the electrical size of the cylinders, and distance between cylinders. For a large value of $k_r a_r$, N should be $2k_r a_r+2$. When $k_r a_r \approx 1$ or less, N should be $2k_r a_r+5$ to $2k_r a_r+10$ for acceptable accuracy.

In order to verify the foregoing formulation, the bistatic echo width pattern is shown in Fig. 3.2 for the scattering by two identical dielectric circular cylinders. The validity of the results is confirmed by comparing the far scattered field with results obtained by Sebak [14] and Elsherbeni and Kishk [12].

In addition to check the validity and accuracy of the foregoing formulation, the results are compared with single chiral circular cylinder scattering of Fig. 2.3 as shown in Fig. 3.3. In this special case, the electrical properties ($\varepsilon_L = 1$, $\mu_L = 1$, and $\gamma_L = 0$) of one cylinder set in such way that it looks like a free space for incident wave. The result is also in excellent agreement with the results obtained by Rojas [5].

Fig. 3.4 shows the co- and cross- polarized echo widths from two identical chiral circular cylinders. For comparison, the numerical result for the echo width pattern for two achiral cylinders is also given. As shown in the figure, backscattering echo width decreases and forward scattering echo width increases for two chiral cylinders compare to the two achiral cylinders.

Fig. 3.5 shows the co- and cross-polarized echo widths from two chiral circular cylinders for two different radii $a_r = 0.08\lambda$ and $a_r = 0.20\lambda$, respectively. The results illustrate that both echo widths are dependent upon the size of the cylinders and both echo width patterns increase with size for electrically large cylinder.

Fig. 3.6 shows the co- and cross-polarized echo widths from two chiral circular cylinders for two different chiral parameters $k_0\gamma = 0.10$ and $k_0\gamma = 0.20$, respectively. It is seen that backscattering echo widths reduce for large chirality parameter while forward scattering echo widths decrease for small chirality parameter. This result illustrates that the chirality parameter gives an extra degree of freedom to control the scattering properties because it has the capability to enhance or reduce the echo width.

Fig. 3.7 shows the co- and cross-polarized echo widths from two chiral circular cylinders for two different angles of incidence $\alpha = 0^0$ and $\alpha = -90^0$, respectively. From the numerical results, it can be seen that both echo widths also depend upon the incident angle of the plane wave.

Fig. 3.8 shows the co- and cross-polarized echo widths from two chiral circular cylinders for two different separation distances d = 0.80λ and d = 1.60λ, respectively. The results illustrate that both echo widths are dependent upon the separation distance between two cylinders. It is seen that co-polarized echo width for two different separation distances are equal when the observation angles are $90^0$ and $270^0$.

Fig. 3.9 shows the co- and cross-polarized echo widths from two chiral circular cylinders for two different frequencies 300 MHz and 600 MHz, respectively. Both echo width patterns vary with changing the frequency of operation. The results illustrate that backscattering echo widths reduce for lower frequency and forward scattering echo widths reduce for higher frequency.

Fig. 3.10 shows the co- and cross-polarized backscattering $(\phi = 270^0)$ echo widths versus the separation distance d for two identical chiral circular cylinders with $a_r = 0.16\lambda$, $\varepsilon_r = 4$, $\mu_r = 2$, $\psi_r = 0$, $\psi_{LQ} = \pi$, $\psi_{QL} = 0$, $d_L = d$, $d_Q = 0$, $k_0\gamma = 0.15$, and $f = 300\,\text{MHz}$, and $\alpha = -90^0$. It can be shown from the figure that the oscillation decay with increasing the separation distance between the cylinders. For comparison, the numerical result for the backscattering echo width for two achiral cylinders as a function of separation distance is also given. The magnitude of the co-polarized backscattering echo widths for two chiral cylinders are significantly reduced compare to the two achiral cylinders. Another point is noted here that the oscillations decaying rate for two chiral cylinders is different from two achiral cylinders.

Fig. 3.11 shows the co- and cross-polarized backscattering $(\phi = 180^0)$ echo widths versus the separation distance d for two identical chiral circular cylinders with $a_r = 0.16\lambda$, $\varepsilon_r = 4$, $\mu_r = 2$, $\psi_r = 0$, $\psi_{LQ} = \pi$, $\psi_{QL} = 0$, $d_L = d$, $d_Q = 0$, $k_0\gamma = 0.15$, and $f = 300\text{MHz}$, and $\alpha = 0^0$. As shown in the figure, the amplitude of the oscillations for co- and cross-polarized echo widths decay with increasing the separation distance between the two cylinders. For reference, the numerical result for the backscattering echo width for two achiral cylinders as a function of separation distance is also shown. It is seen that the magnitude of the backscattering echo widths for two chiral cylinders is reduced compare to the two achiral cylinders.

Fig. 3.12 shows the co- and cross-polarized forward scattering $(\phi = 90^0)$ echo widths versus the separation distance d for two identical chiral circular cylinders with $a_r = 0.16\lambda$, $\varepsilon_r = 4$, $\mu_r = 2$, $\psi_r = 0$, $\psi_{LQ} = \pi$, $\psi_{QL} = 0$, $d_L = d$, $d_Q = 0$, $k_0\gamma = 0.15$, and $f = 300\text{MHz}$, and $\alpha = -90^0$. It can be shown from the figure that the oscillation decay with increasing the separation distance between the two cylinders. The forward scattering echo width for two achiral cylinders as a function of separation distance is also given to compare the results. It is seen that the forward scattering echo width for two chiral cylinders is relatively lower than the two achiral cylinders.

Fig. 3.13 shows the co- and cross-polarized forward scattering $(\phi = 0^0)$ echo widths versus the separation distance d for two identical chiral circular cylinders with $a_r = 0.16\lambda$, $\varepsilon_r = 4$, $\mu_r = 2$, $\psi_r = 0$, $\psi_{LQ} = \pi$, $\psi_{QL} = 0$, $d_L = d$, $d_Q = 0$, $k_0\gamma = 0.15$, and

$f = 300\,\text{MHz}$, and $\alpha = 0^0$. The forward scattering echo width for two achiral cylinders as a function of separation distance is also given to compare the results. It can be shown from the results that the amplitude of the oscillations of each is almost constant and independent of separation distance. The magnitude of the forward scattering echo width for two chiral cylinders is significantly reduced compare to the two achiral cylinders.

Fig. 3.14 shows the dependence of the co- and cross-polarized backscattering echo widths as a function of the incident angle for two identical chiral circular cylinders with $a_r = 0.16\lambda$, $\varepsilon_r = 4$, $\mu_r = 2$, $d = d_L = 3\lambda$, $d_Q = 0$, $\psi_r = 0$, $\psi_{LQ} = \pi$, $\psi_{QL} = 0$, $k_0\gamma = 0.15$, and $f = 300\,\text{MHz}$. Also shown is the numerical result for the backscattering echo width for two achiral cylinders as a function of the angle of incidence. The magnitude of the backscattering echo width for two chiral cylinders reduces compare to the two achiral cylinders.

Fig. 3.15 shows the dependence of the co- and cross-polarized forward scattering echo widths as a function of the incident angle for two identical chiral circular cylinders with $a_r = 0.16\lambda$, $\varepsilon_r = 4$, $\mu_r = 2$, $d = d_L = 3\lambda$, $d_Q = 0$, $\psi_r = 0$, $\psi_{LQ} = \pi$, $\psi_{QL} = 0$, $k_0\gamma = 0.15$, and $f = 300\,\text{MHz}$. The forward scattering echo width for two achiral cylinders as a function of angle of incidence is also given to compare the results. The magnitude of the forward scattering echo width for two chiral cylinders is significantly reduced compare to the achiral cylinders.

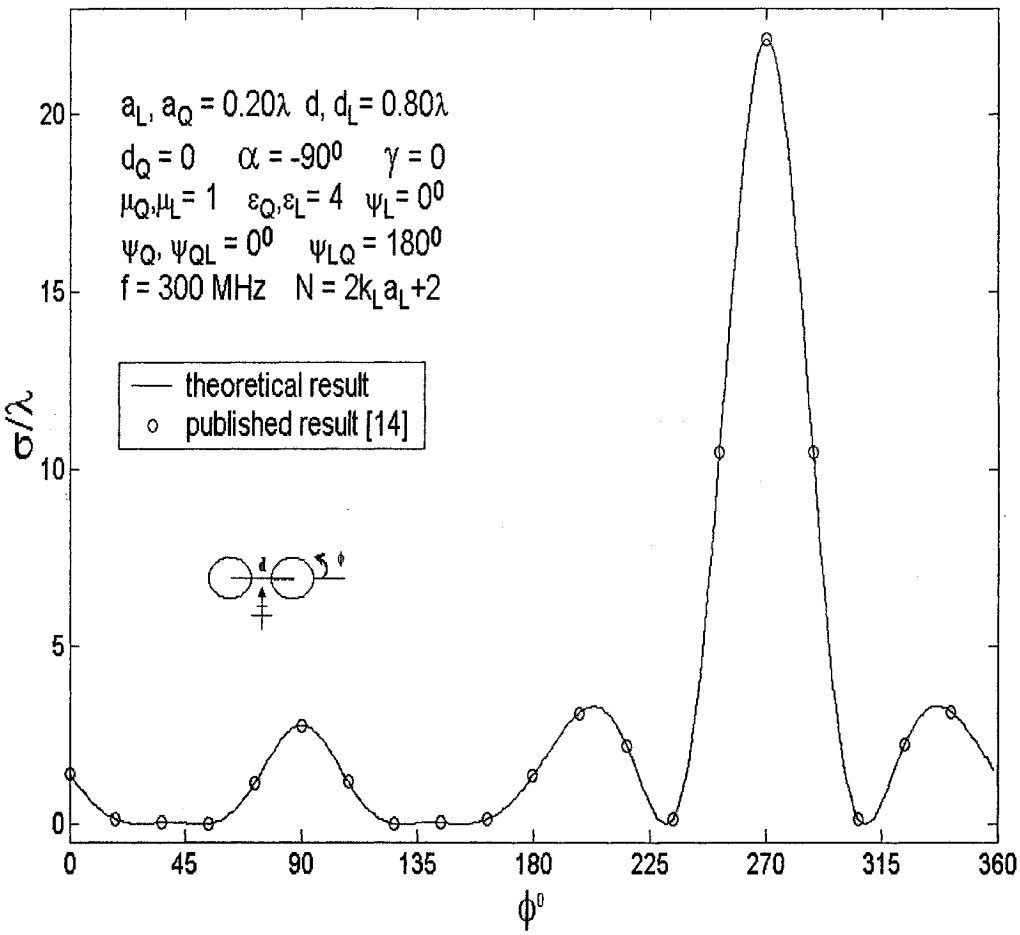


Fig. 3.2: The echo width pattern for two dielectric circular cylinders, TM case.

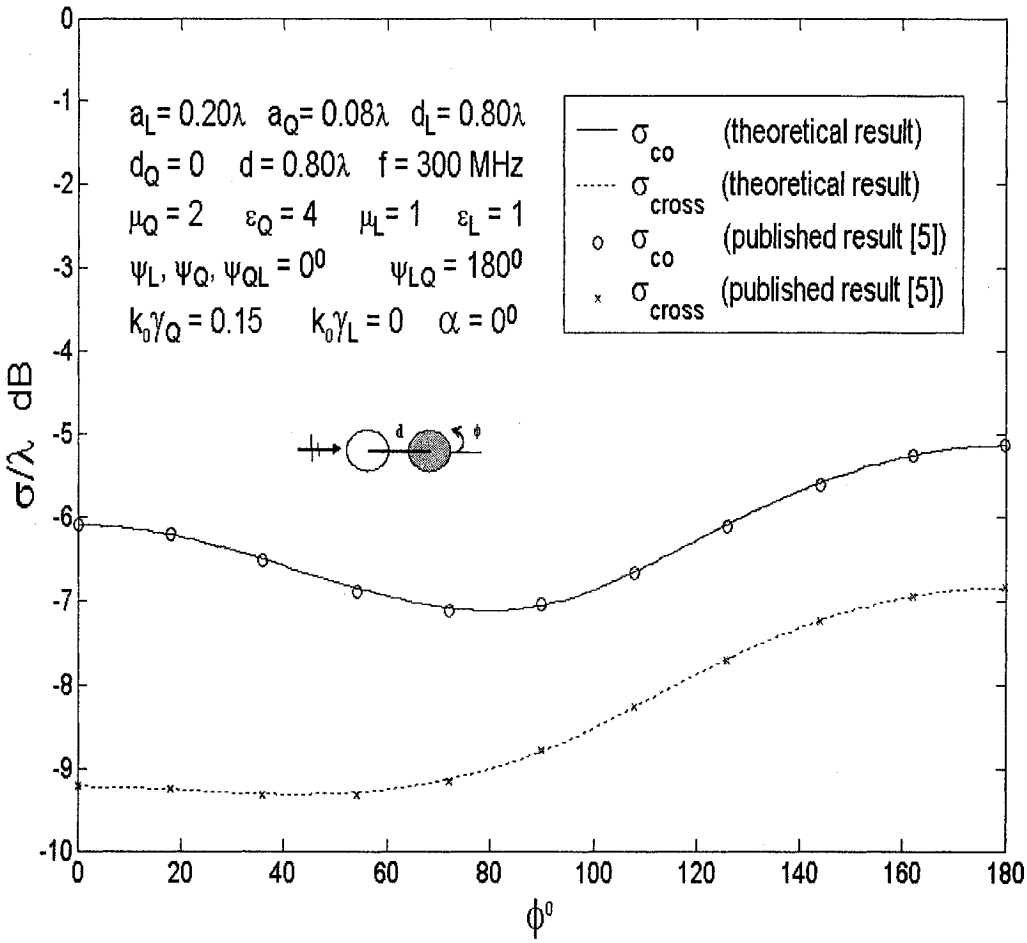


Fig. 3.3: The co- and cross-polarized echo width patterns for single chiral circular cylinder, TM case.

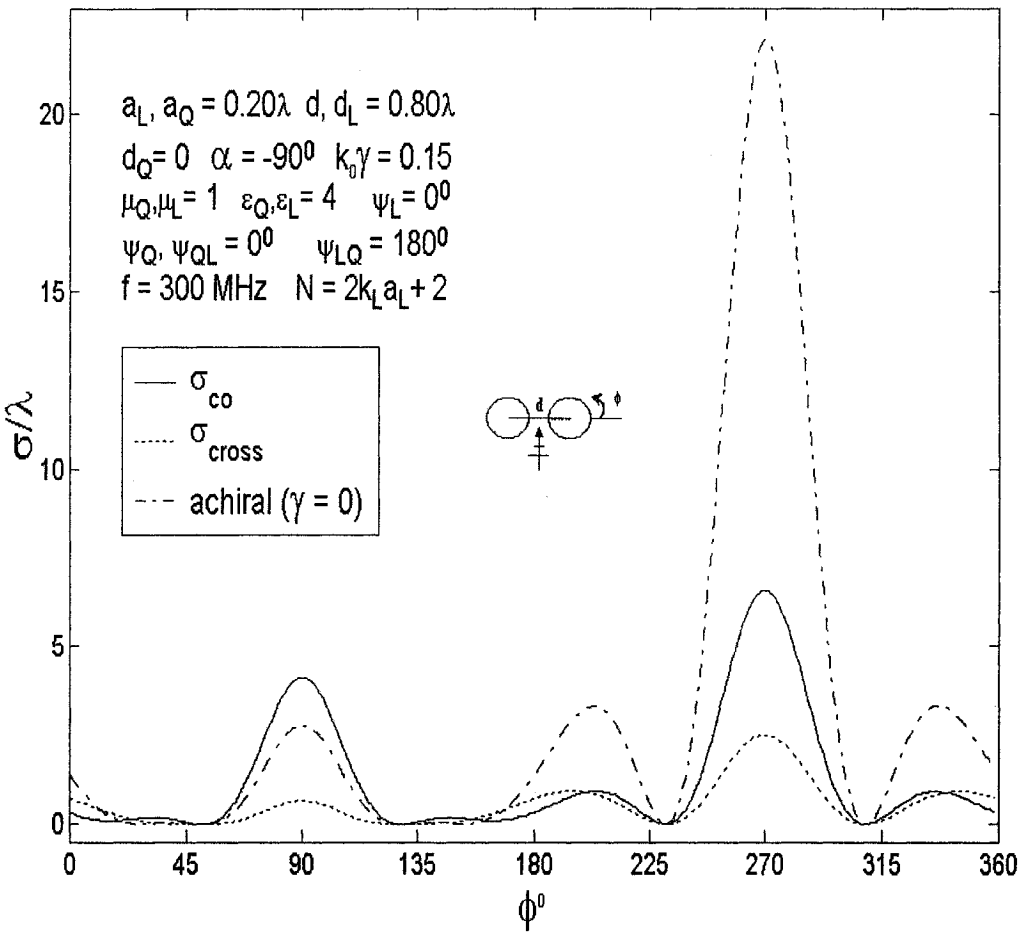


Fig. 3.4: The co- and cross-polarized echo width patterns for two chiral circular cylinders, TM case.

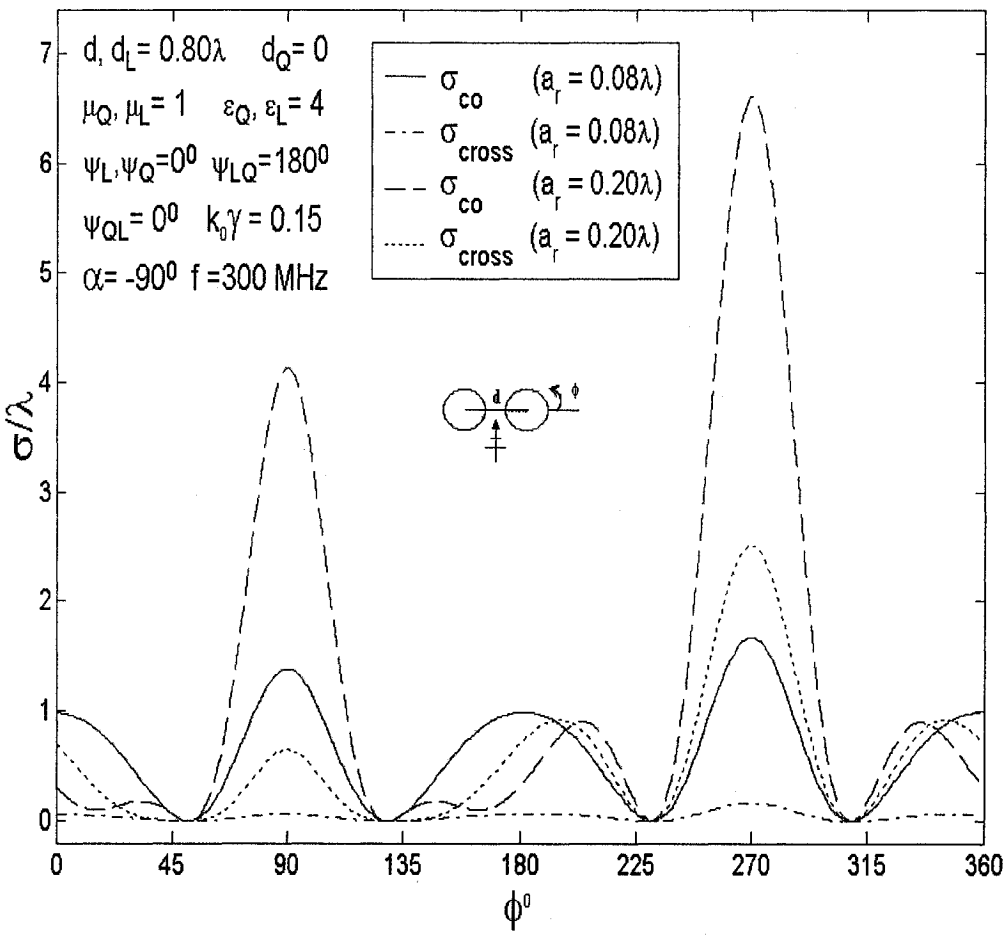


Fig. 3.5: The co- and cross-polarized echo width patterns from two chiral circular cylinders for two different radii, TM case.

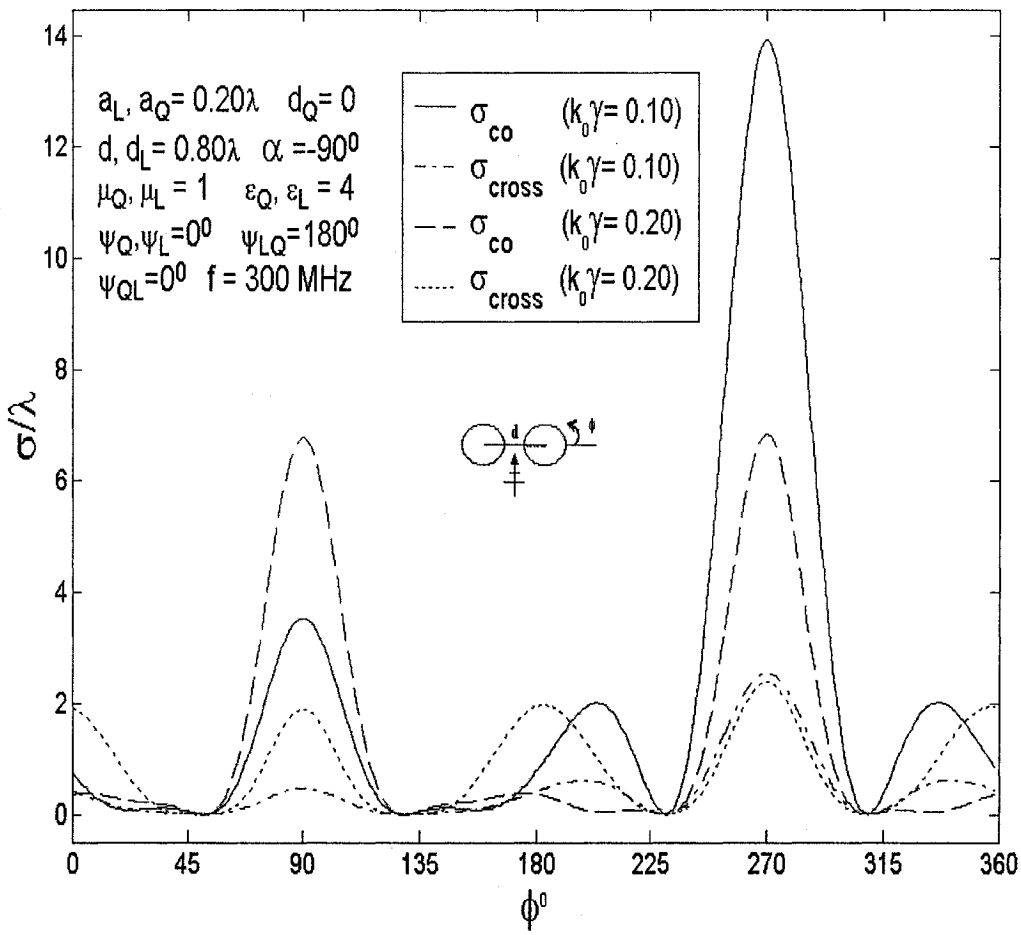


Fig. 3.6: The co- and cross-polarized echo width patterns from two chiral circular cylinders for two different chiral parameters, TM case.

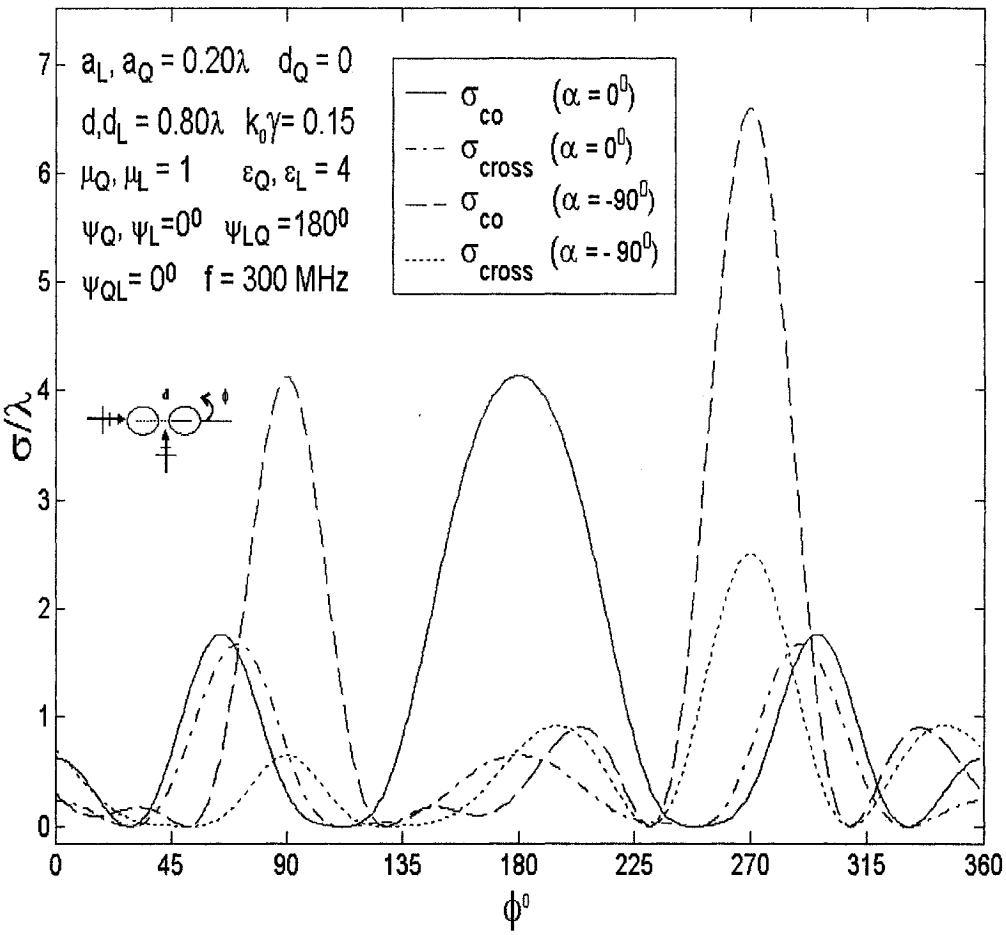


Fig. 3.7: The co- and cross-polarized echo width patterns from two chiral circular cylinders for two different angles of incidence, TM case.

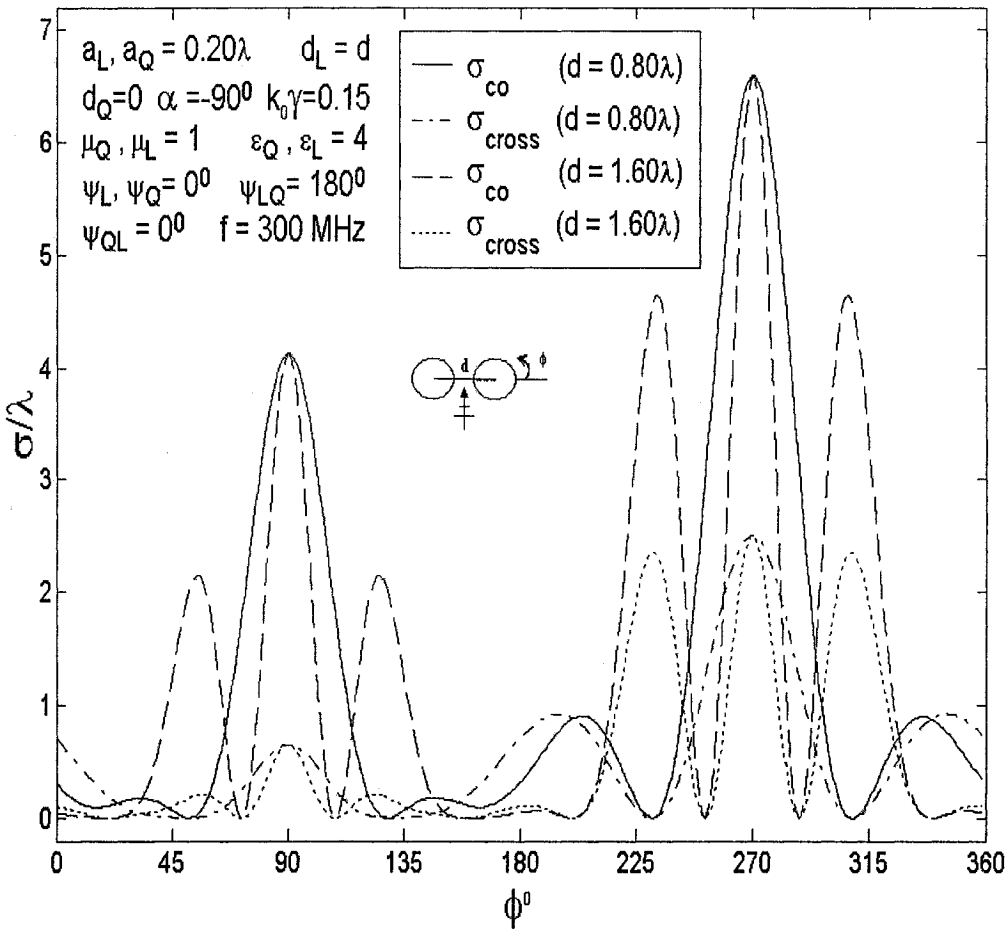


Fig. 3.8: The co- and cross-polarized echo width patterns from two chiral circular cylinders for two different separation distances, TM case.

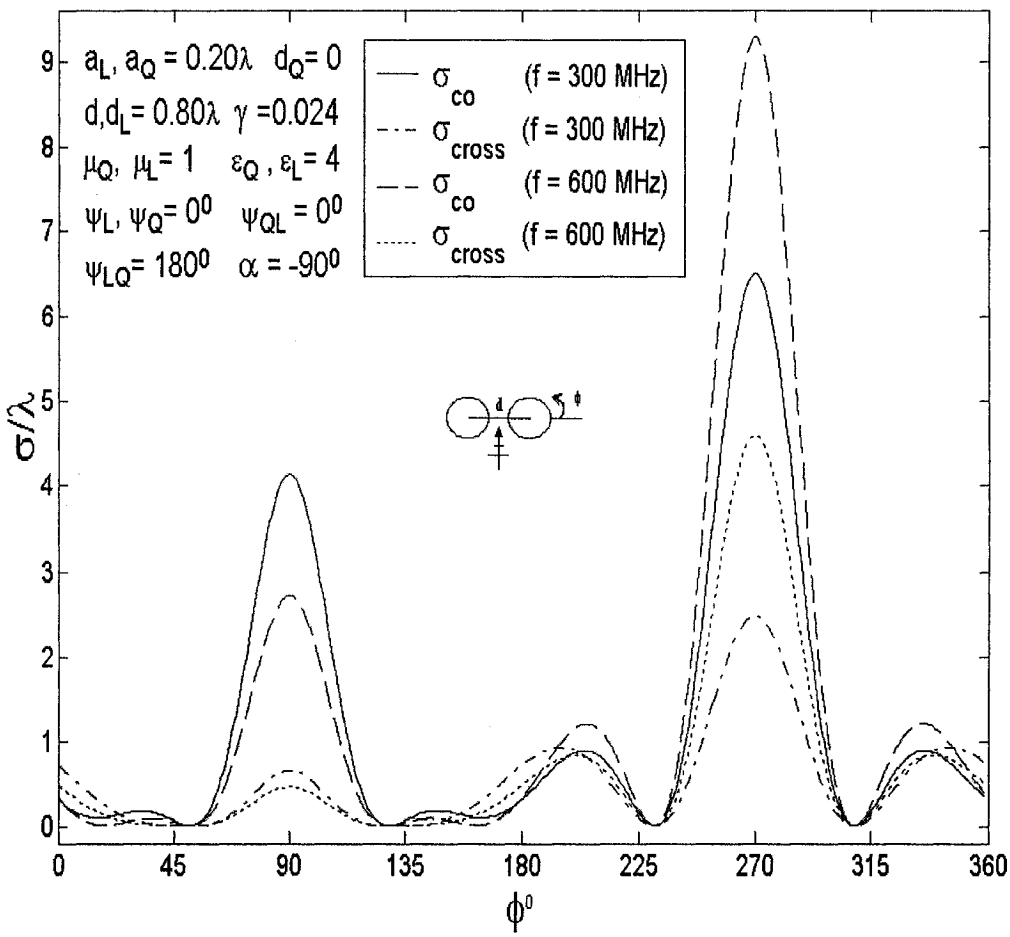


Fig. 3.9: The co- and cross-polarized echo width patterns from two chiral circular cylinders for two different frequencies, TM case.

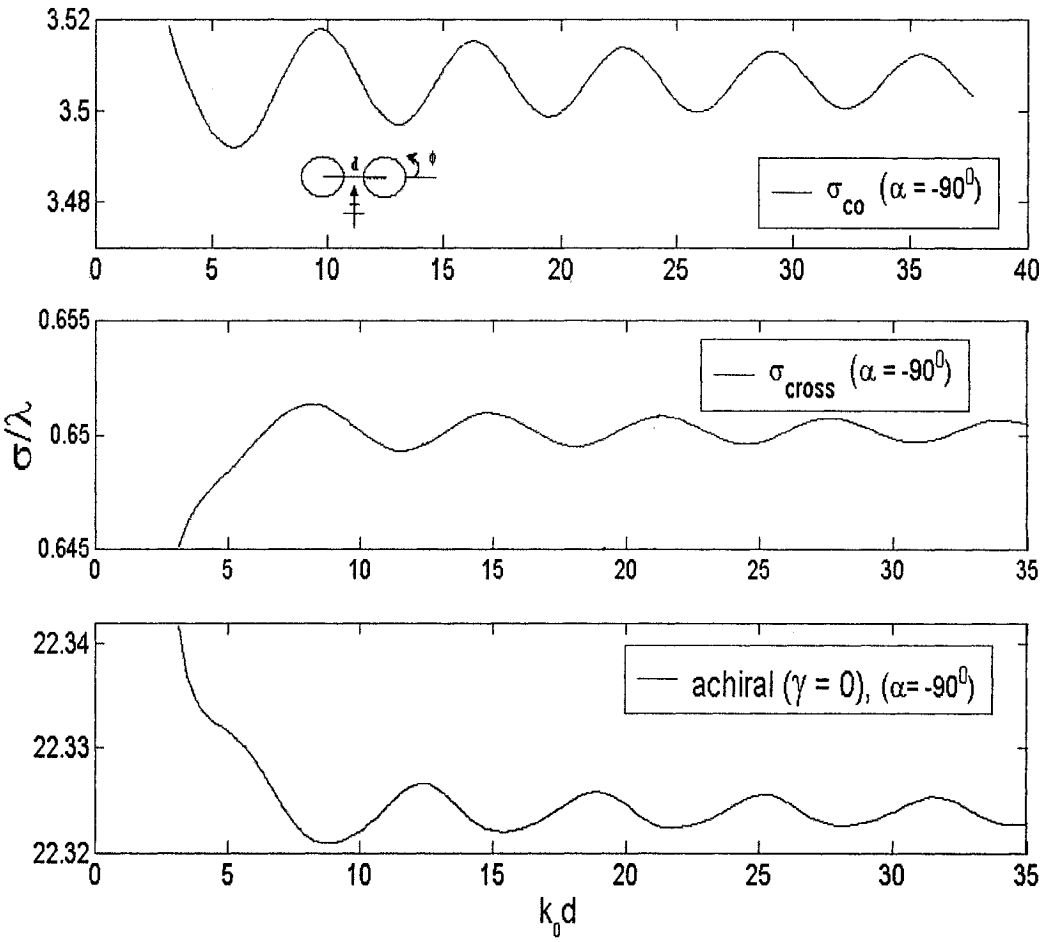


Fig. 3.10: The co- and cross-polarized backscattering echo widths versus the separation distance for two identical chiral circular cylinders with $\alpha = -90^0$, TM case.

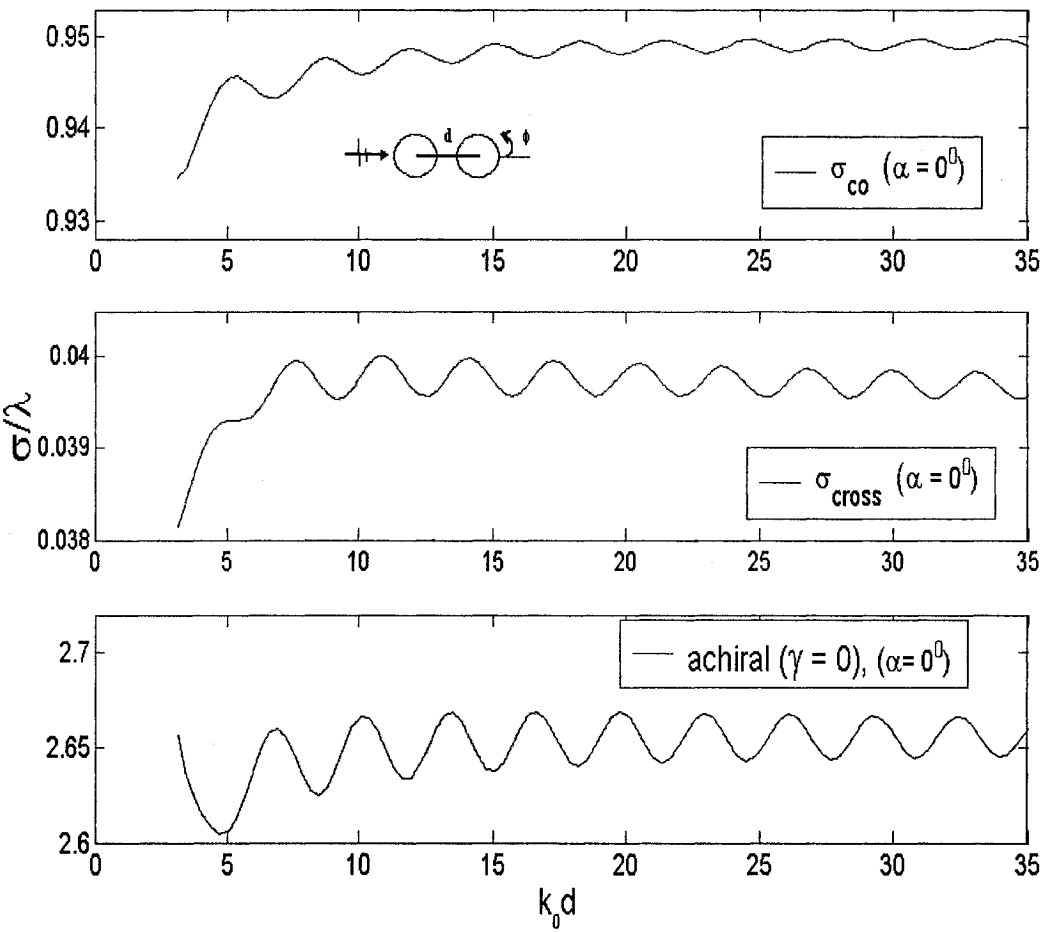


Fig. 3.11: The co- and cross-polarized backscattering echo widths versus the separation distance for two identical chiral circular cylinders with $\alpha = 0^0$, TM case.

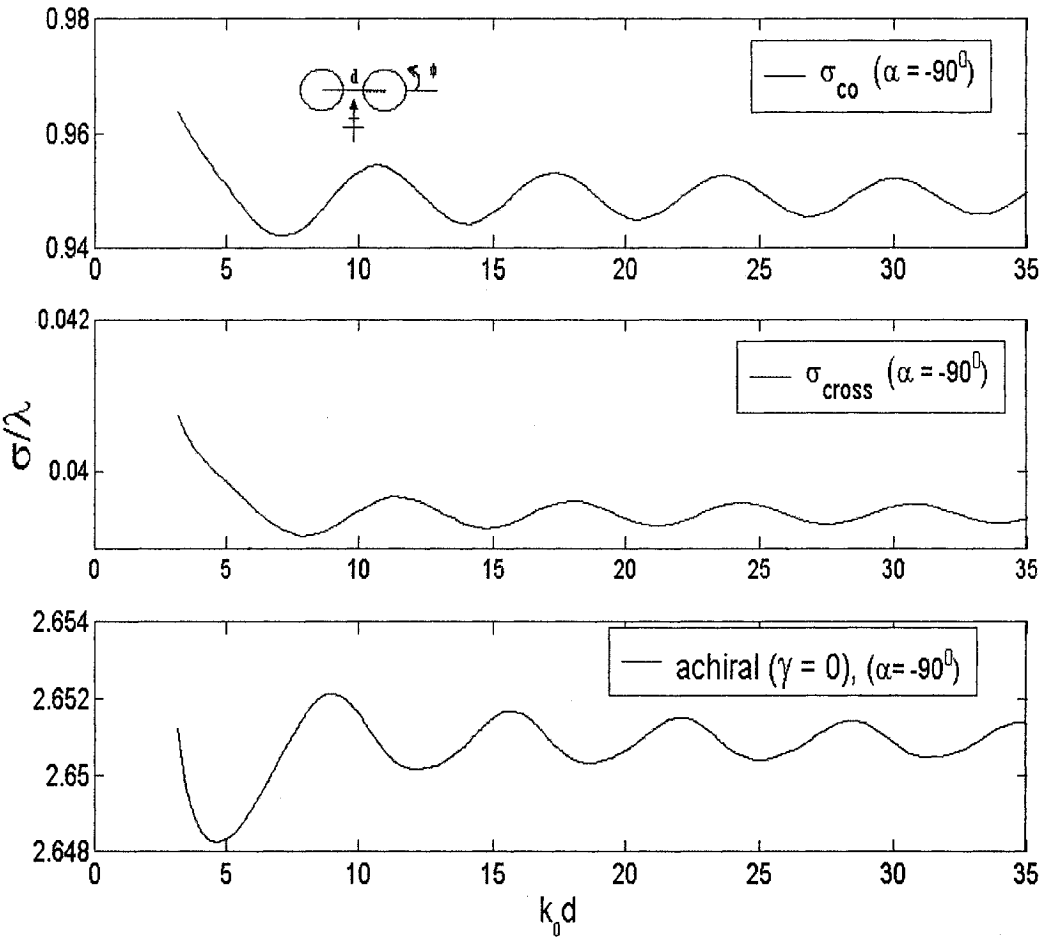


Fig. 3.12: The co- and cross-polarized forward scattering echo widths versus the separation distance for two identical chiral circular cylinders with $\alpha = -90^{\circ}$, TM case.

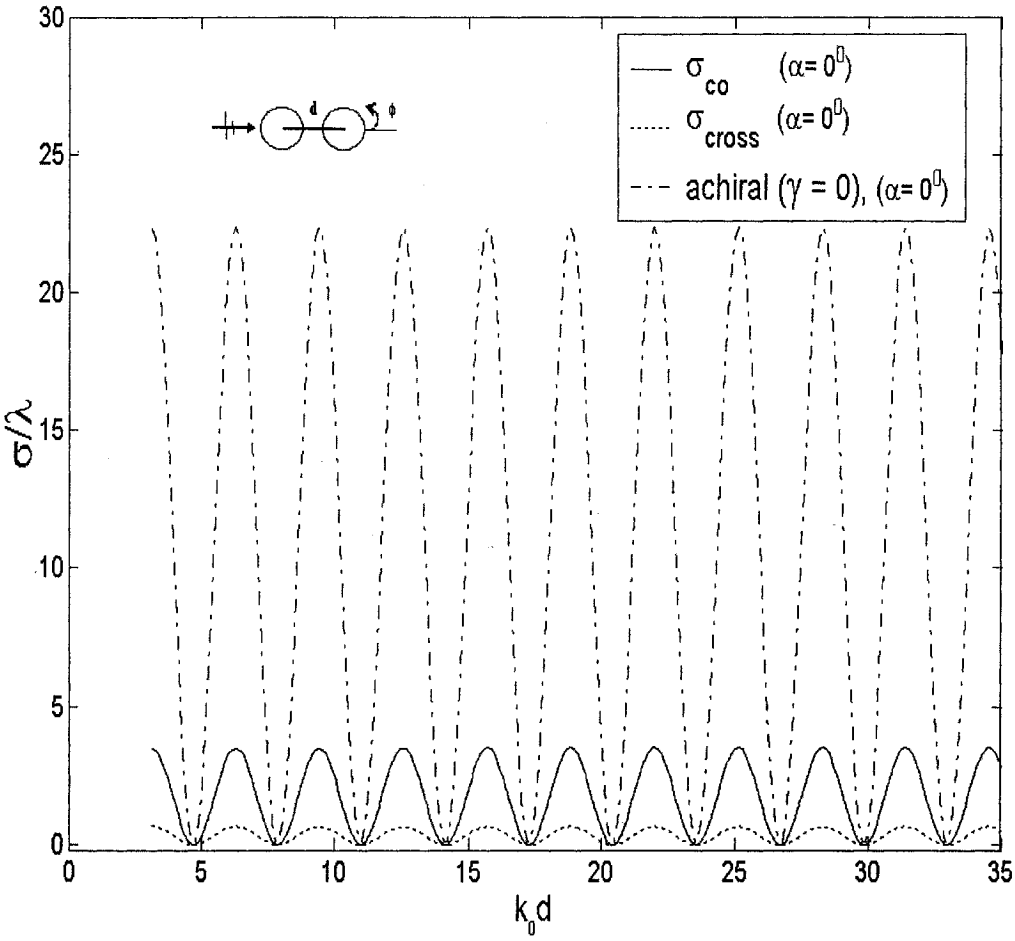


Fig. 3.13: The co- and cross-polarized forward scattering echo widths versus the separation distance for two identical chiral circular cylinders with $\alpha = 0^{o}$, TM case.

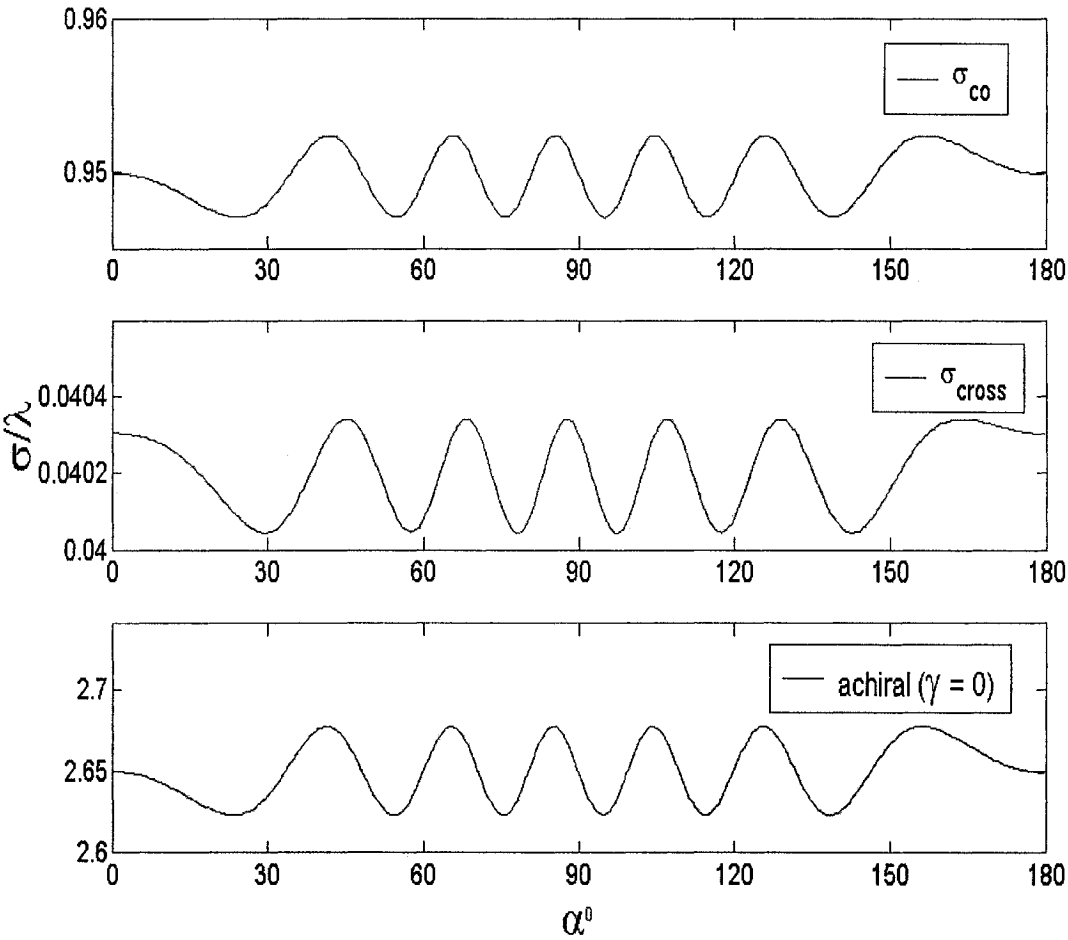


Fig. 3.14: The co- and cross-polarized backscattering echo widths versus the angle of incidence $\alpha$ for two identical chiral circular cylinders, TM case.

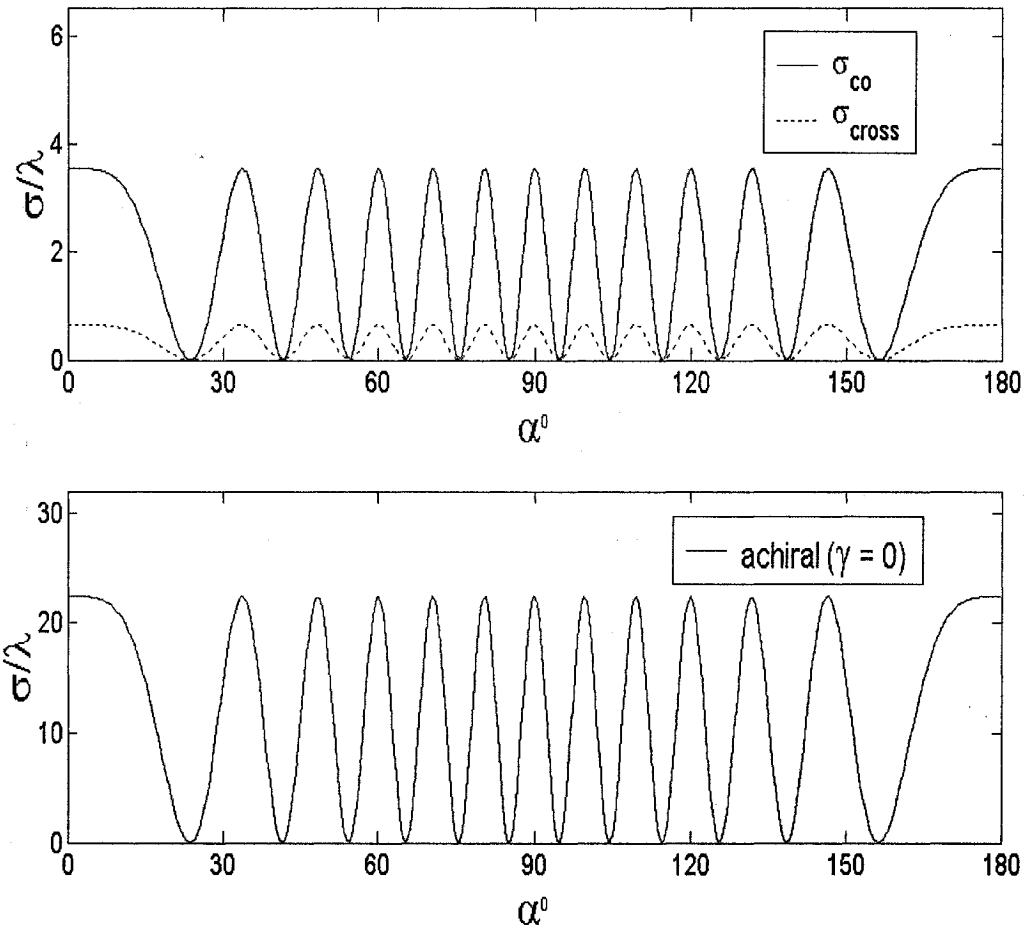


Fig. 3.15: The co- and cross-polarized forward scattering echo widths versus the angle of incidence $\alpha$ for two identical chiral circular cylinders, TM case.

# Chapter 4

# Scattering by Two Chiral Cylinders, TE case

## 4.1 Description of the Problem

The geometry of the scattering problem is shown in Fig. 4.1. Consider both cylinders are excited by a transverse electric (TE) wave. In a TE polarized incident plane wave, the incident magnetic field vector is parallel to the z axis. The physical dimensions and parameters for both cylinders are considered exactly identical to the scattering problem for TM case in Chapter 3. We consider TE polarized incident wave incident upon the cylindrical structures at an angle α with respect to the x axis.

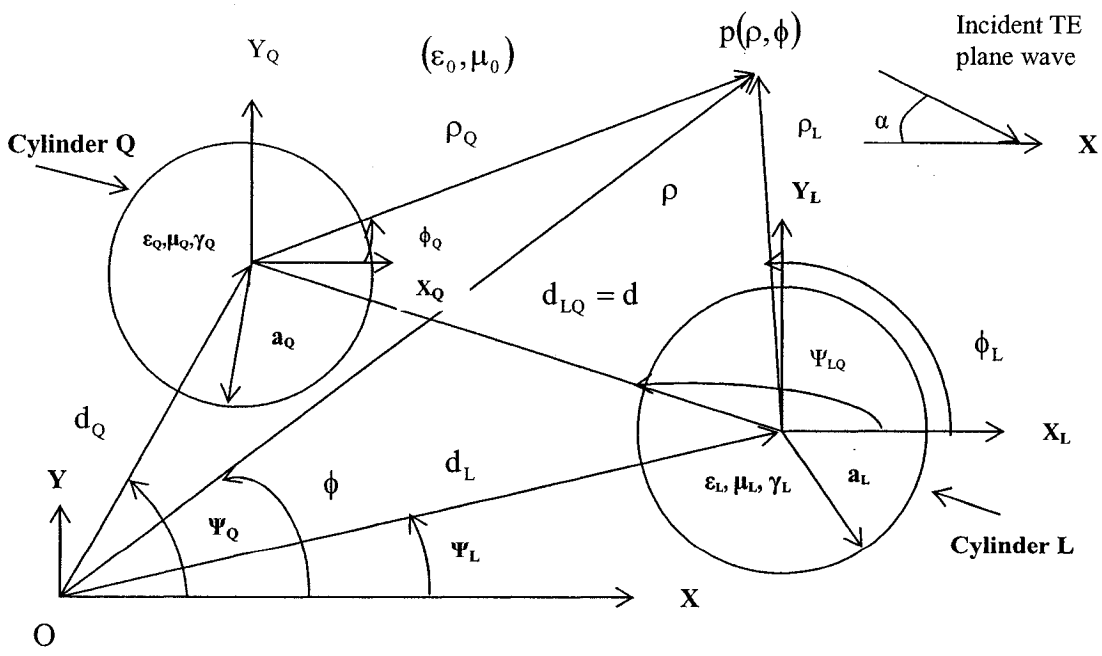


Fig. 4.1: The scattering geometry of two chiral circular cylinders, TE case

## 4.2 Expressions for Electromagnetic fields

### 4.2.1 Expressions for Incident Fields

The incident magnetic field can be expressed with respect to the co-ordinate system of the $r^{th}$ cylinder as

$$\vec{H}_r^{inc} = e^{jk_0 d_r \cos(\psi_r+\alpha)} \frac{1}{\omega\mu_0} \sum_{n=-\infty}^{+\infty} j^n \vec{N}_n^1(k_0\rho_r) \tag{4.1}$$

In an isotropic, homogeneous, and linear media with time dependence $e^{-j\omega t}$, the electric field can be written as

$$\vec{E} = \frac{j\omega\mu}{k^2}(\nabla \times \vec{H}) \tag{4.2}$$

Therefore, the corresponding incident electric field of the $r^{th}$ cylinder can be expressed as

$$\vec{E}_r^{inc} = e^{jk_0 d_r \cos(\psi_r+\alpha)} \frac{j}{k_0} \sum_{n=-\infty}^{+\infty} j^n \vec{M}_n^1(k_0\rho_r) \tag{4.3}$$

where $\vec{N}_n^1(k_0\rho_r)$ and $\vec{M}_n^1(k_0\rho_r)$ are the cylindrical vector wave functions, can be defined by

$$\vec{N}_n^1(k_0\rho_r) = \hat{u}_z k_0 J_n(k_0\rho_r) e^{jn(\phi_r+\alpha)} \tag{4.4}$$

$$\vec{M}_n^1(k_0\rho_r) = \hat{u}_\rho \frac{jn}{\rho_r} J_n(k_0\rho_r) e^{jn(\phi_r+\alpha)} - \hat{u}_\phi k_0 J_n'(k_0\rho_r) e^{jn(\phi_r+\alpha)} \tag{4.5}$$

### 4.2.2 Expressions for Scattered Fields

The scattered field of the chiral cylinder embraces both TM and TE fields since chiral scatterers generate both co- and cross- polarized scattered fields.

The scattered electric field of the $r^{th}$ cylinder can be written in terms of vector wave functions as

$$\vec{E}_r^s = -\frac{1}{k_0}\sum_{n=-\infty}^{+\infty} j^n\left[B_n^r\vec{N}_n^3(k_0\rho_r) + jC_n^r\vec{M}_n^3(k_0\rho_r)\right] \tag{4.6}$$

where $B_n^r$ and $C_n^r$ are the unknown scattering expansion coefficients of the $r^{th}$ cylinder.

The corresponding scattered magnetic field of the $r^{th}$ cylinder can be expressed as

$$\vec{H}_r^s = -\frac{1}{j\omega\mu_0}\sum_{n=-\infty}^{+\infty} j^n\left[B_n^r\vec{M}_n^3(k_0\rho_r) + jC_n^r\vec{N}_n^3(k_0\rho_r)\right] \tag{4.7}$$

where $\vec{N}_n^3(k_0\rho_r)$ and $\vec{M}_n^3(k_0\rho_r)$ are the cylindrical vector wave functions, can be written as

$$\vec{N}_n^3(k_0\rho_r) = \hat{u}_z k_0 H_n^{(1)}(k_0\rho_r)e^{jn\phi_r} \tag{4.8}$$

$$\vec{M}_n^3(k_0\rho_r) = \hat{u}_\rho \frac{jn}{\rho_r} H_n^{(1)}(k_0\rho_r)e^{jn\phi_r} - \hat{u}_\phi k_0 H_n^{(1)'}(k_0\rho_r)e^{jn\phi_r} \tag{4.9}$$

### 4.2.3 Expressions for Internal Fields

Generally two types of internal fields (LCP and RCP) exist in a chiral medium. These fields propagate with two different wave numbers. Bohren transformation is used here to express the LCP and RCP fields inside the chiral circular cylinders.

The internal LCP field $\left(\vec{Q}_L^r\right)$ and RCP field $\left(\vec{Q}_R^r\right)$ of the $r^{th}$ cylinder can be expressed as

$$\vec{Q}_L^r = \frac{1}{k_0}\sum_{n=-\infty}^{+\infty} j^n G_n^r\left[\vec{M}_n^1(k_L^r\rho_r) + \vec{N}_n^1(k_L^r\rho_r)\right] \tag{4.10}$$

$$\vec{Q}_R^r = \frac{1}{k_0}\sum_{n=-\infty}^{+\infty} j^n F_n^r\left[\vec{M}_n^1\left(k_R^r\rho_r\right) - \vec{N}_n^1\left(k_R^r\rho_r\right)\right] \tag{4.11}$$

where $G_n^r$ and $F_n^r$ are the unknown expansion coefficients of the internal fields of the $r^{th}$ cylinder. $k_L^r$ and $k_R^r$ are the LCP and RCP wave numbers of the $r^{th}$ cylinder, respectively, can be expressed as

$$K_L^r = \frac{k_r}{1-\gamma_r k_r} \qquad K_R^r = \frac{k_r}{1+\gamma_r k_r} \tag{4.12}$$

where $k_r = \omega\sqrt{\mu_0\mu_r\varepsilon_0\varepsilon_r}$, the wave number and $\gamma_r$ is the chirality parameter of the $r^{th}$ chiral cylinder.

Electric and magnetic fields inside the $r^{th}$ chiral cylinder are written by following relations in terms of left and right circularly polarized fields

$$\vec{E}_r^c = \vec{Q}_L^r + a_R^r\vec{Q}_R^r \tag{4.13}$$

$$\vec{H}_r^c = \vec{Q}_R^r + a_L^r\vec{Q}_L^r \tag{4.14}$$

where $a_R^r$ and $a_L^r$ have the unit of an impedance and an admittance of the $r^{th}$ chiral cylinder and can be denoted by

$$a_R^r = -i\sqrt{\frac{\mu_0\mu_r}{\varepsilon_0\varepsilon_r}} \qquad a_L^r = -i\sqrt{\frac{\varepsilon_0\varepsilon_r}{\mu_0\mu_r}} \tag{4.15}$$

The expression of the internal electric field (4.13) can be expanded as

$$\vec{E}_r^c = \frac{1}{k_0}\sum_{n=-\infty}^{+\infty} j^n G_n^r\left[\vec{M}_n^1\left(k_L^r\rho_r\right) + \vec{N}_n^1\left(k_L^r\rho_r\right)\right] + a_R^r\frac{1}{k_0}\sum_{n=-\infty}^{+\infty} j^n F_n^r\left[\vec{M}_n^1\left(k_R^r\rho_r\right) - \vec{N}_n^1\left(k_R^r\rho_r\right)\right] \tag{4.16}$$

The expression of the internal magnetic field (4.14) can be expanded as

$$\vec{H}_r^c = \frac{1}{k_0}\sum_{n=-\infty}^{+\infty} j^n F_n^r\left[\vec{M}_n^1\left(k_R^r\rho_r\right) - \vec{N}_n^1\left(k_R^r\rho_r\right)\right] + a_L^r\frac{1}{k_0}\sum_{n=-\infty}^{+\infty} j^n G_n^r\left[\vec{M}_n^1\left(k_L^r\rho_r\right) + \vec{N}_n^1\left(k_L^r\rho_r\right)\right] \tag{4.17}$$

## 4.3 Evaluation of the Unknown Expansion Coefficients

The unknown expansion coefficients can be determined by enforcing the boundary conditions in conjunction with the addition theorem for Hankel functions [18] on the surface of each cylinder. The boundary conditions of the electromagnetic scattering state that the tangential components of the electric and magnetic fields must be continuous across the boundary.

The boundary conditions on the surface of the $L^{th}$ cylinder i.e., $\rho_L = a_L$, are given by

$$\left(\vec{E}_L^{inc} + \vec{E}_L^s + \vec{E}_{QQ\to L}^s - \vec{E}_L^c\right)\times\hat{u}_\rho = 0 \tag{4.18}$$

$$\left(\vec{H}_L^{inc} + \vec{H}_L^s + \vec{H}_{QQ\to L}^s - \vec{H}_L^c\right)\times\hat{u}_\rho = 0 \tag{4.19}$$

where $\hat{u}_\rho$ is the outward unit vector normal to the cylinder surface. $\vec{E}_{QQ\to L}^s$ is the transform of the $Q^{th}$ cylinder scattered electric field as incident field for the $L^{th}$ cylinder and $\vec{H}_{QQ\to L}^s$ is the transform of the $Q^{th}$ cylinder scattered magnetic field as incident field for the $L^{th}$ cylinder

The boundary conditions on the surface of the $Q^{th}$ cylinder i.e., $\rho_Q = a_Q$, are given by

$$\left(\vec{E}_Q^{inc} + \vec{E}_Q^s + \vec{E}_{LL\to Q}^s - \vec{E}_Q^c\right)\times\hat{u}_\rho = 0 \tag{4.20}$$

$$\left(\vec{H}_Q^{inc} + \vec{H}_Q^s + \vec{H}_{LL\to Q}^s - \vec{H}_Q^c\right)\times \hat{u}_\rho = 0 \tag{4.21}$$

where $\vec{E}_{LL\to Q}^s$ is the transform of the $L^{th}$ cylinder scattered electric field as incident field for the $Q^{th}$ cylinder and $\vec{H}_{LL\to Q}^s$ is the transform of the $L^{th}$ cylinder scattered magnetic field as incident field for the $Q^{th}$ cylinder.

In order to solve the boundary conditions (4.18) to (4.21), the expressions of $\vec{E}_{QQ\to L}^s$, $\vec{E}_{LL\to Q}^s$, $\vec{H}_{QQ\to L}^s$, and $\vec{H}_{LL\to Q}^s$ can be expanded using the addition theorem of Hankel functions as

$$\vec{E}_{QQ\to L}^s \times \hat{u}_\rho = -\sum_{n=-\infty}^{+\infty} j^n \left[\begin{array}{l} \hat{u}_\phi B_n^Q \sum_{m=-\infty}^{+\infty} J_m(k_0\rho_L) H_{m-n}^{(1)}(k_0 d_{LQ}) e^{jm\phi_L} e^{-j(m-n)\psi_{LQ}} \\ + \hat{u}_z jC_n^Q \sum_{m=-\infty}^{+\infty} J_m'(k_0\rho_L) H_{m-n}^{(1)}(k_0 d_{LQ}) e^{jm\phi_L} e^{-j(m-n)\psi_{LQ}} \end{array}\right] \tag{4.22}$$

$$\vec{E}_{LL\to Q}^s \times \hat{u}_\rho = -\sum_{n=-\infty}^{+\infty} j^n \left[\begin{array}{l} \hat{u}_\phi B_n^L \sum_{m=-\infty}^{+\infty} J_m(k_0\rho_Q) H_{m-n}^{(1)}(k_0 d_{QL}) e^{jm\phi_Q} e^{-j(m-n)\psi_{QL}} \\ + \hat{u}_z jC_n^L \sum_{m=-\infty}^{+\infty} J_m'(k_0\rho_Q) H_{m-n}^{(1)}(k_0 d_{QL}) e^{jm\phi_Q} e^{-j(m-n)\psi_{QL}} \end{array}\right] \tag{4.23}$$

$$\vec{H}_{QQ\to L}^s \times \hat{u}_\rho = -\frac{k_0}{j\omega\mu_0} \sum_{n=-\infty}^{+\infty} j^n \left[\begin{array}{l} \hat{u}_z B_n^Q \sum_{m=-\infty}^{+\infty} J_m'(k_0\rho_L) H_{m-n}^{(1)}(k_0 d_{LQ}) e^{jm\phi_L} e^{-j(m-n)\psi_{LQ}} \\ + \hat{u}_\phi C_n^Q \sum_{m=-\infty}^{+\infty} J_m(k_0\rho_L) H_{m-n}^{(1)}(k_0 d_{LQ}) e^{jm\phi_L} e^{-j(m-n)\psi_{LQ}} \end{array}\right] \tag{4.24}$$

$$\vec{H}^{s}_{L_{L\to Q}} \times \hat{u}_{\rho} = -\frac{k_0}{j\omega\mu_0} \sum_{n=-\infty}^{+\infty} j^n \left[ \begin{array}{l} \hat{u}_z B_n^L \sum\limits_{m=-\infty}^{+\infty} J_m'(k_0\rho_Q) H_{m-n}^{(1)}(k_0 d_{QL}) e^{jm\phi_Q} e^{-j(m-n)\psi_{QL}} \\ + \hat{u}_\phi j C_n^L \sum\limits_{m=-\infty}^{+\infty} J_m(k_0\rho_Q) H_{m-n}^{(1)}(k_0 d_{QL}) e^{jm\phi_Q} e^{-j(m-n)\psi_{QL}} \end{array} \right] \tag{4.25}$$

where $(B_n^L, C_n^L)$ and $(B_n^Q, C_n^Q)$ are the unknown scattering expansion coefficients of the $L^{th}$ and $Q^{th}$ cylinders, respectively.

The boundary condition (4.18) can be written using equation (4.3), (4.6), (4.16), and (4.23) as

$$\begin{aligned} &\hat{u}_z e^{jk_0 d_L \cos(\psi_L+\alpha)} \sum_{n=-\infty}^{+\infty} j^n \, j\times J_n'(k_0 a_L) e^{jn(\phi_L+\alpha)} \\ &-\frac{1}{k_0} \sum_{n=-\infty}^{+\infty} j^n \left[ \hat{u}_\phi B_n^L k_0 H_n^{(1)}(k_0 a_L) e^{jn\phi_L} + \hat{u}_z j C_n^L k_0 H_n^{(1)'}(k_0 a_L) e^{jn\phi_L} \right] \\ &-\sum_{n=-\infty}^{+\infty} j^n \left[ \begin{array}{l} \hat{u}_\phi B_n^Q \sum\limits_{m=-\infty}^{+\infty} J_m(k_0 a_L) H_{m-n}^{(1)}(k_0 d_{LQ}) e^{jm\phi_L} e^{-j(m-n)\psi_{LQ}} \\ + \hat{u}_z j C_n^Q \sum\limits_{m=-\infty}^{+\infty} J_m'(k_0 a_L) H_{m-n}^{(1)}(k_0 d_{LQ}) e^{jm\phi_L} e^{-j(m-n)\psi_{LQ}} \end{array} \right] \\ &-\frac{1}{k_0} \sum_{n=-\infty}^{+\infty} j^n G_n^L \left[ \hat{u}_z k_L^L J_n'(k_L^L a_L) e^{jn\phi_L} + \hat{u}_\phi k_L^L J_n(k_L^L a_L) e^{jn\phi_L} \right] \\ &-\frac{a_R^L}{k_0} \sum_{n=-\infty}^{+\infty} j^n F_n^L \left[ \hat{u}_z k_R^L J_n'(k_R^L a_L) e^{jn\phi_L} - \hat{u}_\phi k_R^L J_n(k_R^L a_L) e^{jn\phi_L} \right] = 0 \end{aligned} \tag{4.26}$$

Equating $\hat{u}_\phi$ terms from equation (4.26)

$$\begin{aligned} &-B_n^L \sum_{n=-\infty}^{+\infty} H_n^{(1)}(k_0 a_L) - B_n^Q \sum_{n=-\infty}^{+\infty} \sum_{m=-\infty}^{+\infty} J_m(k_0 a_L) H_{m-n}^{(1)}(k_0 d_{LQ}) e^{-j(m-n)\psi_{LQ}} \\ &-G_n^L \frac{k_L^L}{k_0} \sum_{n=-\infty}^{+\infty} \left[ J_n(k_L^L a_L) \right] + F_n^L \frac{a_R^L k_R^L}{k_0} \sum_{n=-\infty}^{+\infty} \left[ J_n(k_R^L a_L) \right] = 0 \end{aligned} \tag{4.27}$$

Equating $\hat{u}_z$ terms from equation (4.26)

$$
\begin{aligned}
&-C_n^L \sum_{n=-\infty}^{+\infty} jH_n^{(1)'}(k_0 a_L) - C_n^Q \sum_{n=-\infty}^{+\infty} j \sum_{m=-\infty}^{+\infty} J_m'(k_0 a_L) H_{m-n}^{(1)}(k_0 d_{LQ})\, e^{-j(m-n)\psi_{LQ}} \\
&-G_n^L \frac{k_L^L}{k_0} \sum_{n=-\infty}^{+\infty} J_n'(k_L^L a_L) - F_n^L \frac{a_R^L k_R^L}{k_0} \sum_{n=-\infty}^{+\infty} J_n'(k_R^L a_L) = -je^{jk_0 d_L \cos(\psi_L+\alpha)} \sum_{n=-\infty}^{+\infty} J_n'(k_0 a_L) e^{jn\alpha}
\end{aligned}
\tag{4.28}
$$

The boundary condition (4.20) can be written using equations (4.3), (4.6), (4.16), and (4.24) as

$$
\begin{aligned}
&\hat{u}_z e^{jk_0 d_Q \cos(\psi_Q+\alpha)} \sum_{n=-\infty}^{+\infty} j^n\, j \times J_n'(k_0 a_Q)\, e^{jn(\phi_Q+\alpha)} \\
&-\frac{1}{k_0} \sum_{n=-\infty}^{+\infty} j^n \left[ \hat{u}_\phi B_n^Q k_0 H_n^{(1)}(k_0 a_Q) e^{jn\phi_Q} + \hat{u}_z jC_n^Q k_0 H_n^{(1)'}(k_0 a_Q) e^{jn\phi_Q} \right] \\
&-\sum_{n=-\infty}^{+\infty} j^n \left[ \begin{array}{l} \hat{u}_\phi B_n^L \sum_{m=-\infty}^{+\infty} J_m(k_0 \rho_Q) H_{m-n}^{(1)}(k_0 d_{QL}) e^{jm\phi_Q} e^{-j(m-n)\psi_{QL}} \\ + \hat{u}_z jC_n^L \sum_{m=-\infty}^{+\infty} J_m'(k_0 \rho_Q) H_{m-n}^{(1)}(k_0 d_{QL})\, e^{jm\phi_Q} e^{-j(m-n)\psi_{QL}} \end{array} \right] \\
&-\frac{1}{k_0} \sum_{n=-\infty}^{+\infty} j^n G_n^Q \left[ \hat{u}_z k_L^Q J_n'(k_L^Q a_Q) e^{jn\phi_L} + \hat{u}_\phi k_L^Q J_n(k_L^Q a_Q) e^{jn\phi_Q} \right] \\
&-\frac{a_R^Q}{k_0} \sum_{n=-\infty}^{+\infty} j^n F_n^Q \left[ \hat{u}_z k_R^Q J_n'(k_R^Q a_Q) e^{jn\phi_Q} - \hat{u}_\phi k_R^Q J_n(k_R^Q a_Q) e^{jn\phi_Q} \right] = 0
\end{aligned}
\tag{4.29}
$$

Equating $\hat{u}_\phi$ terms from equation (4.29)

$$
\begin{aligned}
&-B_n^Q \sum_{n=-\infty}^{+\infty} H_n^{(1)}(k_0 a_Q) - B_n^L \sum_{n=-\infty}^{+\infty} \sum_{m=-\infty}^{+\infty} J_m(k_0 a_Q) H_{m-n}^{(1)}(k_0 d_{QL})\, e^{-j(m-n)\psi_{QL}} \\
&-G_n^Q \frac{k_L^Q}{k_0} \sum_{n=-\infty}^{+\infty} J_n(k_L^Q a_Q) + F_n^Q \frac{a_R^Q k_R^Q}{k_0} \sum_{n=-\infty}^{+\infty} J_n(k_R^Q a_Q) = 0
\end{aligned}
\tag{4.30}
$$

Equating $\hat{u}_z$ terms from equation (4.29)

$$
\begin{aligned}
&-C_n^Q \sum_{n=-\infty}^{+\infty} jH_n^{(1)'}(k_0 a_Q) - C_n^L \sum_{n=-\infty}^{+\infty} j \sum_{m=-\infty}^{+\infty} J_m'(k_0 a_Q) H_{m-n}^{(1)}(k_0 d_{QL})\, e^{-j(m-n)\psi_{QL}} \\
&-G_n^Q \frac{k_L^Q}{k_0} \sum_{n=-\infty}^{+\infty} J_n'(k_L^Q a_Q) - F_n^Q \frac{a_R^Q k_R^Q}{k_0} \sum_{n=-\infty}^{+\infty} J_n'(k_R^Q a_Q) = -je^{jk_0 d_Q \cos(\psi_Q+\alpha)} \sum_{n=-\infty}^{+\infty} J_n'(k_0 a_Q) e^{jn\alpha}
\end{aligned}
\tag{4.31}
$$

The boundary condition (4.19) can be written using equations (4.1), (4.7), (4.17), and (4.25) as

$$
\begin{aligned}
&\hat{u}_\phi \frac{k_0}{\omega\mu_0} e^{jk_0 d_L \cos(\psi_L+\alpha)} \sum_{n=-\infty}^{+\infty} j^n J_n(k_0 a_L) e^{jn(\phi_L+\alpha)} \\
&-\frac{k_0}{j\omega\mu_0} \sum_{n=-\infty}^{+\infty} j^n \left[\hat{u}_z B_n^L H_n^{l'}(k_0 a_L) e^{jn\phi_L} + \hat{u}_\phi j C_n^L H_n^{(1)}(k_0 a_L) e^{jn\phi_L}\right] \\
&-\frac{k_0}{j\omega\mu_0} \sum_{n=-\infty}^{+\infty} j^n \left[\begin{array}{l} \hat{u}_z B_n^Q \sum_{m=-\infty}^{+\infty} J_m'(k_0\rho_L) H_{m-n}^{(1)}(k_0 d_{LQ}) e^{jm\phi_L} e^{-j(m-n)\psi_{LQ}} \\ +\hat{u}_\phi j C_n^Q \sum_{m=-\infty}^{+\infty} J_m(k_0 a_L) H_{m-n}^{(1)}(k_0 d_{LQ}) e^{jm\phi_L} e^{-j(m-n)\psi_{LQ}} \end{array}\right] \\
&-\frac{1}{k_0} \sum_{n=-\infty}^{+\infty} j^n F_n^L \left[\hat{u}_z k_R^L J_n'(k_R^L a_L) e^{jn\phi_L} - \hat{u}_\varphi k_R^L J_n(k_R^L a_L) e^{jn\phi_L}\right] \\
&-a_L^L \frac{1}{k_0} \sum_{n=-\infty}^{+\infty} j^n G_n^L \left[\hat{u}_z k_L^L J_n'(k_L^L a_L) e^{jn\phi_L} + \hat{u}_\phi k_L^L J_n(k_L^L a_L) e^{jn\phi_L}\right] = 0
\end{aligned}
\tag{4.32}
$$

Equating $\hat{u}_\phi$ terms from equation (4.32)

$$
\begin{aligned}
&-\frac{C_n^L k_0}{\omega\mu_0} \sum_{n=-\infty}^{+\infty} H_n^{(1)}(k_0 a_L) - \frac{C_n^Q k_0}{\omega\mu_0} \sum_{n=-\infty}^{+\infty} \sum_{m=-\infty}^{+\infty} J_m(k_0 a_L) H_{m-n}^{(1)}(k_0 d_{LQ})\, e^{-j(m-n)\psi_{LQ}} \\
&+F_n^L \frac{k_R^L}{k_0} \sum_{n=-\infty}^{+\infty} J_n(k_R^L a_L) - G_n^L \frac{a_L^L k_L^L}{k_0} \sum_{n=-\infty}^{+\infty} J_n(k_L^L a_L) = -\frac{k_0 e^{jk_0 d_L \cos(\psi_L+\alpha)}}{\omega\mu_0} \sum_{n=-\infty}^{+\infty} J_n(k_0 a_L) e^{jn\alpha}
\end{aligned}
\tag{4.33}
$$

Equating $\hat{u}_z$ terms from equation (4.32)

$$-\frac{B_n^L k_0}{j\omega\mu_0}\sum_{n=-\infty}^{+\infty} H_n^{(1)'}(k_0 a_L) - \frac{B_n^Q k_0}{j\omega\mu_0}\sum_{n=-\infty}^{+\infty}\sum_{m=-\infty}^{+\infty} J_m'(k_0 a_L) H_{m-n}^{(1)}(k_0 d_{LQ})\, e^{-j(m-n)\psi_{LQ}}$$
$$-F_n^L \frac{k_R^L}{k_0}\sum_{n=-\infty}^{+\infty} J_n'(k_R^L a_L) - G_n^L \frac{a_L^L k_L^L}{k_0}\sum_{n=-\infty}^{+\infty} J_n'(k_L^L a_L) = 0 \qquad (4.34)$$

The boundary condition (4.21) can be written using equations (4.1), (4.7), (4.17), and (4.26) as

$$\hat{u}_z \frac{k_0}{\omega\mu_0} e^{jk_0 d_Q \cos(\psi_Q+\alpha)} \sum_{n=-\infty}^{+\infty} j^n J_n'(k_0 a_Q)\, e^{jn(\phi_Q+\alpha)}$$
$$-\frac{k_0}{j\omega\mu_0}\sum_{n=-\infty}^{+\infty} j^n\left[\hat{u}_z B_n^Q H_n^{(1)'}(k_0 a_Q) e^{jn\phi_Q} + \hat{u}_\phi j C_n^Q H_n^{(1)}(k_0 a_Q) e^{jn\varphi_Q}\right]$$
$$-\frac{k_0}{j\omega\mu_0}\sum_{n=-\infty}^{+\infty} j^n\left[\begin{array}{l}\hat{u}_z B_n^L \sum_{m=-\infty}^{+\infty} J_m'(k_0 a_Q) H_{m-n}^{(1)}(k_0 d_{QL}) e^{jm\phi_Q} e^{-j(m-n)\psi_{QL}} \\ + \hat{u}_\phi j C_n^L \sum_{m=-\infty}^{+\infty} J_0(k_0 a_Q) H_{m-n}^{(1)}(k_0 d_{QL}) e^{jm\phi_Q} e^{-j(m-n)\psi_{QL}}\end{array}\right] \qquad (4.35)$$
$$-\frac{1}{k_0}\sum_{n=-\infty}^{+\infty} j^n F_n^Q\left[\hat{u}_z k_R^Q J_n'(k_R^Q a_Q) e^{jn\phi_Q} - \hat{u}_\phi k_R^Q J_n(k_R^Q a_Q) e^{jn\phi_Q}\right]$$
$$-a_L^Q \frac{1}{k_0}\sum_{n=-\infty}^{+\infty} j^n G_n^Q\left[\hat{u}_z k_L^Q J_n'(k_L^Q a_Q) e^{jn\phi_Q} + \hat{u}_\phi k_L^Q J_n(k_L^Q a_Q) e^{jn\phi_Q}\right]$$

Equating $\hat{u}_\phi$ terms from equation (4.35)

$$-\frac{C_n^Q k_0}{\omega\mu_0}\sum_{n=-\infty}^{+\infty} H_n^{(1)}(k_0 a_Q) - \frac{C_n^L k_0}{\omega\mu_0}\sum_{n=-\infty}^{+\infty}\sum_{m=-\infty}^{+\infty} J_m(k_0 a_Q) H_{m-n}^{(1)}(k_0 d_{QL})\, e^{-j(m-n)\psi_{QL}}$$
$$+F_n^Q \frac{k_R^Q}{k_0}\sum_{n=-\infty}^{+\infty} J_n(k_R^Q a_Q) - G_n^Q \frac{a_L^Q k_L^Q}{k_0}\sum_{n=-\infty}^{+\infty} J_n(k_L^Q a_Q) = -\frac{k_0 e^{jk_0 d_Q \cos(\psi_Q+\alpha)}}{\omega\mu_0}\sum_{n=-\infty}^{+\infty} J_n(k_0 a_Q) e^{jn\alpha} \qquad (4.36)$$

Equating $\hat{u}_z$ terms from equation (4.35)

$$-\frac{B_n^Q k_0}{j\omega\mu_0}\sum_{n=-\infty}^{+\infty} H_n^{(1)'}(k_0 a_Q)-\frac{B_n^L k_0}{j\omega\mu_0}\sum_{n=-\infty}^{+\infty}\sum_{m=-\infty}^{+\infty} J_m'(k_0 a_Q)H_{m-n}^{(1)}(k_0 d_{QL})\, e^{-j(m-n)\psi_{QL}}$$
$$-F_n^Q\frac{k_R^Q}{k_0}\sum_{n=-\infty}^{+\infty} J_n'(k_R^Q a_Q)-G_n^Q\frac{a_L^Q k_L^Q}{k_0}\sum_{n=-\infty}^{+\infty} J_n'(k_L^Q a_Q)=0 \tag{4.37}$$

These eight linear equations obtained from the boundary conditions (4.18-4.21) can be written in the following matrix form to solve the unknown expansion coefficients $\left(B_n^L, C_n^L, B_n^Q, C_n^Q, G_n^L, F_n^L, G_n^Q, \text{and } F_n^Q\right)$ numerically.

$$[A]\,[a] = [I] \tag{4.38}$$

where the matrix [A] represents the elements of the unknown expansion coefficients, matrix [a] stands for unknown expansion coefficients which to be find out, and matrix [I] contains the elements without the unknown expansion coefficients.

## 4.4 Far Scattered Fields

The total scattered field can be determined after evaluating all scattering expansion coefficients from two chiral circular cylinders. The total scattered magnetic field can be written as

$$\vec{H}_{total}^s = \vec{H}_L^s + \vec{H}_Q^s \tag{4.39}$$

The expression of (4.39) can be expanded using equation (4.6) as

$$\vec{H}_{total}^s = -\frac{1}{j\omega\mu_0}\sum_{n=-\infty}^{+\infty} j^n\begin{bmatrix} B_n^L\,\vec{M}_n^3(k_0\rho_L)+B_n^Q\,\vec{M}_n^3(k_0\rho_Q) \\ +j\left\{C_n^L\,\vec{N}_n^3(k_0\rho_L)+\ C_n^Q\,\vec{N}_n^3(k_0\rho_Q)\right\}\end{bmatrix} \tag{4.40}$$

The total scattered field has both co- and cross-polarized fields. The co-polarized scattered field can be written as

$$\vec{H}^s_{co} = -\frac{1}{\omega\mu_0}\sum_{n=-\infty}^{+\infty} j^n\left[C_n^L \vec{N}_n^3(k_0\rho_L) + C_n^Q \vec{N}_n^3(k_0\rho_Q)\right]$$

$$\Rightarrow \vec{H}^s_{co} = -\hat{u}_z\frac{1}{\eta_0}\sum_{n=-\infty}^{+\infty} j^n\left[C_n^L H_n^{(1)}(k_0\rho_L)e^{jn\phi_L} + C_n^Q H_n^{(1)}(k_0\rho_Q)e^{jn\phi_Q}\right] \quad (4.41)$$

where $\eta_0 = \sqrt{\frac{\mu_0}{\varepsilon_0}}$, is the intrinsic impedance of the region surrounding the cylinders.

The cross-polarized scattered field can be written as

$$\vec{H}^s_{cross} = -\frac{1}{j\omega\mu_0}\sum_{n=-\infty}^{+\infty} j^n\left[B_n^L \vec{M}_n^3(k_0\rho_L) + B_n^Q \vec{M}_n^3(k_0\rho_Q)\right]$$

$$\Rightarrow \vec{H}^s_{cross} = \hat{u}_\phi\frac{1}{j\eta_0}\sum_{n=-\infty}^{+\infty} j^n\left[B_n^L H_n^{(1)'}(k_0\rho_L)e^{jn\phi_L} + B_n^Q H_n^{(1)'}(k_0\rho_Q)e^{jn\phi_Q}\right] \quad (4.42)$$

The asymptotic expansion for the Hankel function for large arguments is applied here to obtain the far scattered fields. In the far field region ($k_0\rho >> 1$), the Hankel function can be approximated by

$$H_n^1(k_0\rho) \underset{k_0\rho\to\infty}{\cong} \sqrt{\frac{2}{j\pi k_0\rho}}\, j^{-n} e^{jk_0\rho} \quad (4.43)$$

The distances from cylinders to observation point can also be approximated for the far field region ($k_0\rho >> 1$)

$$\rho_L = \rho - d_L\cos(\psi_L - \phi) \quad (4.44)$$

$$\rho_Q = \rho - d_Q \cos(\psi_Q - \phi) \tag{4.45}$$

$$\phi = \phi_L = \phi_Q \tag{4.46}$$

Hence the far scattered co-polarized field is given by

$$\vec{H}_{co}^{s} \overset{k_0\rho\to\infty}{\cong} -\hat{u}_z \frac{e^{jk_0\rho}}{\eta_0}\sqrt{\frac{2}{j\pi k_0\rho}} \sum_{n=-\infty}^{+\infty}\left[C_n^L e^{-jk_0 d_L \cos(\psi_L-\phi)} + C_n^Q e^{-jk_0 d_Q \cos(\psi_Q-\phi)}\right] e^{jn\phi} \tag{4.47}$$

Similarly the far scattered cross-polarized field is given by

$$\vec{H}_{cross}^{s} \overset{k_0\rho\to\infty}{\cong} \hat{u}_\phi \frac{e^{jk_0\rho}}{\eta_0}\sqrt{\frac{2}{j\pi k_0\rho}} \sum_{n=-\infty}^{+\infty}\left[B_n^L e^{-jk_0 d_L \cos(\psi_L-\phi)} + B_n^Q e^{-jk_0 d_Q \cos(\psi_Q-\phi)}\right] e^{jn\phi} \tag{4.48}$$

## 4.5 Echo Width

The echo width can be obtained by knowing the scattered field in the far zone. The co- and cross-polarized echo widths [30] can be expressed for the TE polarization as

$$\sigma_{co}^{TE} = \lim_{\rho\to\infty} 2\pi\rho \frac{\left|\vec{H}_{co}^{s}\right|^2}{\left|\vec{H}^{inc}\right|^2} \tag{4.49}$$

$$\sigma_{cross}^{TE} = \lim_{\rho\to\infty} 2\pi\rho \frac{\left|\vec{H}_{cross}^{s}\right|^2}{\left|\vec{H}^{inc}\right|^2} \tag{4.50}$$

The co-polarized echo width (4.49) can be written as

$$\sigma_{co}^{TE} = \frac{4}{k_0}\left|\sum_{n=-\infty}^{+\infty}\left[C_n^L e^{-jk_0 d_L \cos(\psi_L-\phi)} + C_n^Q e^{-jk_0 d_Q \cos(\psi_Q-\phi)}\right] e^{jn\phi}\right|^2 \tag{4.51}$$

The cross-polarized echo width (4.50) can be written as

$$\sigma_{cross}^{TE} = \frac{4}{k_0}\left| \sum_{n=-\infty}^{+\infty}\left[B_n^L e^{-jk_0 d_L \cos(\psi_L-\phi)} + B_n^Q e^{-jk_0 d_Q \cos(\psi_Q-\phi)}\right] e^{jn\phi} \right|^2 \tag{4.52}$$

## 4.6 Numerical Results

Numerical results are presented for the TE polarized incident wave using the formulation described in the earlier section. At first numerical results are validated with existing published results for special and limiting cases. After that several numerical results are given to observe the effects on echo width patterns for selected geometries and parameters. Both co- and cross-polarized far scattered fields are taken into consideration for all numerical results. The scattered echo width $\frac{\sigma}{\lambda}$ is obtained for all cases in this part. The unknown expansion coefficients are numerically solved by a proper truncation of the infinite sums into finite sums. In order to generate numerical results, a truncation number N is used and it depends upon the degree of accuracy required, the electrical size of the cylinders, and distance between cylinders. For a large value of $k_r a_r$, N should be $2k_r a_r+2$. When $k_r a_r \approx 1$ or less, N should be $2k_r a_r+5$ to $2k_r a_r+10$ for acceptable accuracy.

In order to verify the foregoing formulation, the echo width pattern is shown in Fig. 4.2 for the scattering by two dielectric circular cylinders. The validity of the results is confirmed by comparing the far scattered field with results obtained by Elsherbeni and Kishk [12].

In addition to check the validity and accuracy of the foregoing formulation, the results are compared with single chiral circular cylinder scattering of Fig. 2.8 as shown in Fig. 4.3. In this special case, the electrical properties ($\varepsilon_L = 1$, $\mu_L = 1$, and $\gamma_L = 0$) of one cylinder set in such way that it looks like a free space for incident wave. The results are also in excellent agreement with the results obtained by Rojas [5].

Fig. 4.4 shows the co- and cross-polarized echo widths from two identical chiral circular cylinders. For comparison, the numerical result for the echo width pattern for two achiral cylinders is also given. It is seen from the figure that back and forward scattering echo widths decrease for two chiral cylinders compare to the two achiral cylinders.

Fig. 4.5 shows the co- and cross-polarized echo widths from two chiral circular cylinders for two different radii $a_r = 0.20\lambda$ and $a_r = 0.30\lambda$, respectively. The results illustrate that both echo widths are dependent upon the size of the cylinders and backscattering echo width increases with size for electrically large cylinders.

Fig. 4.6 shows the co- and cross-polarized echo widths from two chiral circular cylinders for two different chiral parameters $k_0\gamma = 0.15$ and $k_0\gamma = 0.30$, respectively. The results illustrate that backscattering echo widths reduce for large chirality parameter while forward scattering echo widths decrease for small chirality parameter.

Fig. 4.7 shows the co- and cross-polarized echo widths from two chiral circular cylinders for two different angles of incidence $\alpha = 0^0$ and $\alpha = -90^0$, respectively. It can be shown that echo widths also depend upon the incident angle.

Fig. 4.8 shows the co- and cross-polarized echo widths from two chiral circular cylinders for two different separation distances d = 0.80λ and d = 1.60λ, respectively. The results illustrate that both echo widths are dependent upon the separation distance between two cylinders. It is seen that co-polarized echo width for two different separation distances are same when the observation angles are $90^0$ and $270^0$.

Fig. 4.9 shows the co- and cross-polarized echo widths from two chiral circular cylinders for two different frequencies 300 MHz and 600 MHz, respectively. The results illustrate that both echo width patterns vary with changing the frequency of operation. The results illustrate that both back and forward scattering echo widths reduce with increasing the frequency of operation.

Fig. 4.10 shows the co- and cross-polarized backscattering $\left(\phi = 270^0\right)$ echo widths versus the separation distance d for two identical chiral circular cylinders with $a_r = 0.16\lambda$, $\varepsilon_r = 4$, $\mu_r = 2$, $\psi_r = 0$, $\psi_{LQ} = \pi$, $\psi_{QL} = 0$, $d_L = d$, $d_Q = 0$, $k_0\gamma = 0.15$, and $f = 300\,\text{MHz}$, and $\alpha = -90^0$. It can be shown from the figure that the oscillation decays with increasing the separation distance between the cylinders. For comparison, the numerical result for the backscattering echo width for two achiral cylinders as a function of separation distance is also given. The magnitude of the co-polarized backscattering echo width for two chiral cylinders is significantly reduced compare to the two achiral cylinders.

Fig. 4.11 shows the co- and cross-polarized backscattering $(\phi = 180^0)$ echo widths versus the separation distance d for two identical chiral circular cylinders with $a_r = 0.16\lambda$, $\varepsilon_r = 4$, $\mu_r = 2$, $\psi_r = 0$, $\psi_{LQ} = \pi$, $\psi_{QL} = 0$, $d_L = d$, $d_Q = 0$, $k_0\gamma = 0.15$, and $f = 300\,\text{MHz}$, and $\alpha = 0^0$. It can be shown from the figure that the oscillation decays slowly with increasing the separation distance between the two cylinders. The back-scattering echo width for two achiral cylinders as a function of separation distance is also given to compare the results. It can be shown that the magnitude of the backscattering echo width for two chiral cylinders is significantly reduced compare to the two achiral cylinders.

Fig. 4.12 shows the co- and cross-polarized forward scattering $(\phi = 90^0)$ echo widths versus the separation distance d for two identical chiral circular cylinders with $a_r = 0.16\lambda$, $\varepsilon_r = 4$, $\mu_r = 2$, $\psi_r = 0$, $\psi_{LQ} = \pi$, $\psi_{QL} = 0$, $d_L = d$, $d_Q = 0$, $k_0\gamma = 0.15$, and $f = 300\,\text{MHz}$, and $\alpha = -90^0$. It can be shown from the figure that the oscillation decay with increasing the separation distance between the two cylinders. The forward scattering echo width for two achiral cylinders as a function of separation distance is also given to compare the results. It is seen that the forward scattering echo width for two chiral cylinders is lower than the two achiral cylinders.

Fig. 4.13 shows the co- and cross-polarized forward scattering $(\phi = 0^0)$ echo widths versus the separation distance d for two identical chiral circular cylinders with $a_r = 0.16\lambda$, $\varepsilon_r = 4$, $\mu_r = 2$, $\psi_r = 0$, $\psi_{LQ} = \pi$, $\psi_{QL} = 0$, $d_L = d$, $d_Q = 0$, $k_0\gamma = 0.15$, and

$f = 300\,\text{MHz}$, and $\alpha = 0^0$. The forward scattering echo width pattern for two achiral cylinders as a function of separation distance is also shown to compare the results. It can be shown from the results that the amplitude of the oscillations of each is almost constant and independent of separation distance. The magnitude of the forward scattering echo width for two chiral cylinders is significantly reduced compare to the achiral cylinders.

Fig. 4.14 shows the dependence of the co- and cross-polarized backscattering echo widths as a function of incident angle for two identical chiral circular cylinders with $a_r = 0.16\lambda$, $\varepsilon_r = 4$, $\mu_r = 2$, $d = d_L = 3\lambda$, $d_Q = 0$, $\psi_r = 0$, $\psi_{LQ} = \pi$, $\psi_{QL} = 0$, $k_0\gamma = 0.15$, and $f = 300\,\text{MHz}$. For reference, the numerical result for the backscattering echo width for two achiral cylinders as a function of the incident angle is also shown. The magnitude of the backscattering echo width of two chiral cylinders is significantly reduced compare to the two achiral cylinders.

Fig. 4.15 shows the dependence of the co- and cross-polarized forward scattering echo widths as a function of the incident angle for two identical chiral circular cylinders with $a_r = 0.16\lambda$, $\varepsilon_r = 4$, $\mu_r = 2$, $d = d_L = 3\lambda$, $d_Q = 0$, $\psi_r = 0$, $\psi_{LQ} = \pi$, $\psi_{QL} = 0$, $k_0\gamma = 0.15$, and $f = 300\,\text{MHz}$. For comparison, the numerical result for the forward scattering echo width for two achiral cylinders as a function of the incident angle is also given. The magnitude of the forward scattering of two chiral cylinders echo width is significantly reduced compare to the achiral cylinders.

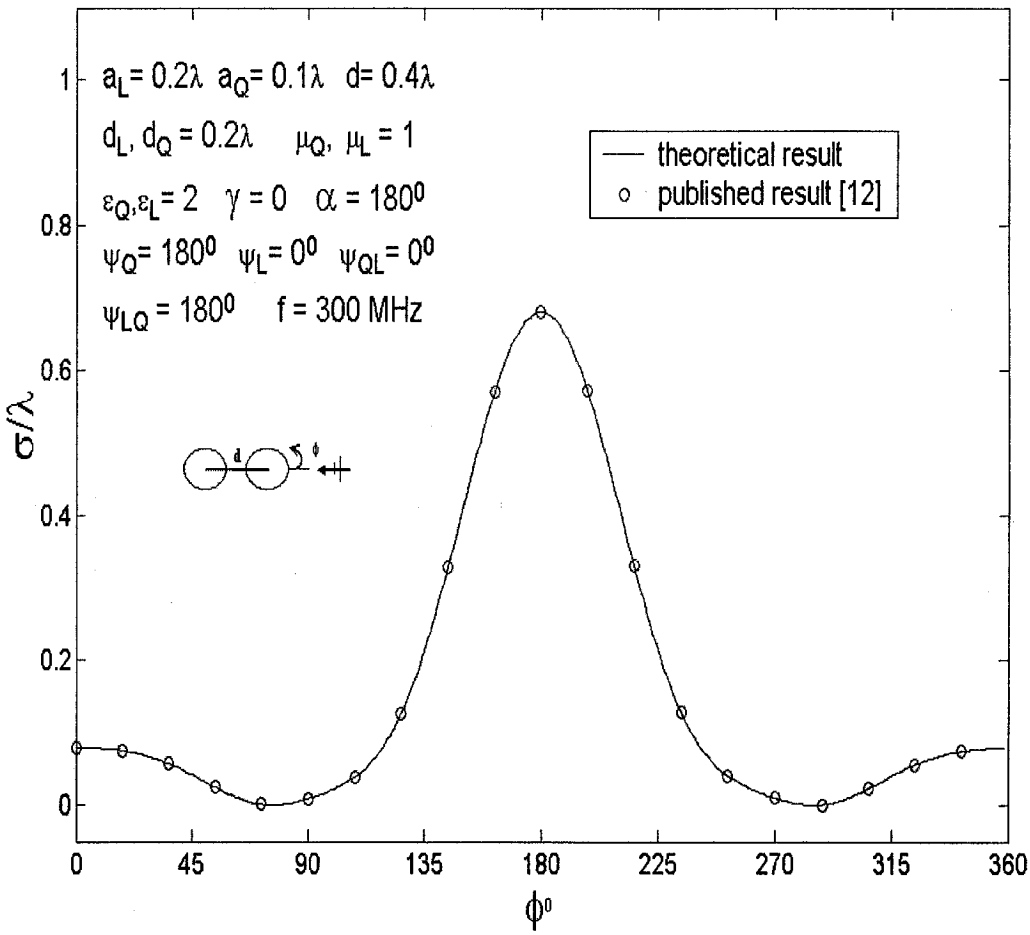


Fig. 4.2: The echo width pattern for two dielectric circular cylinders, TE case.

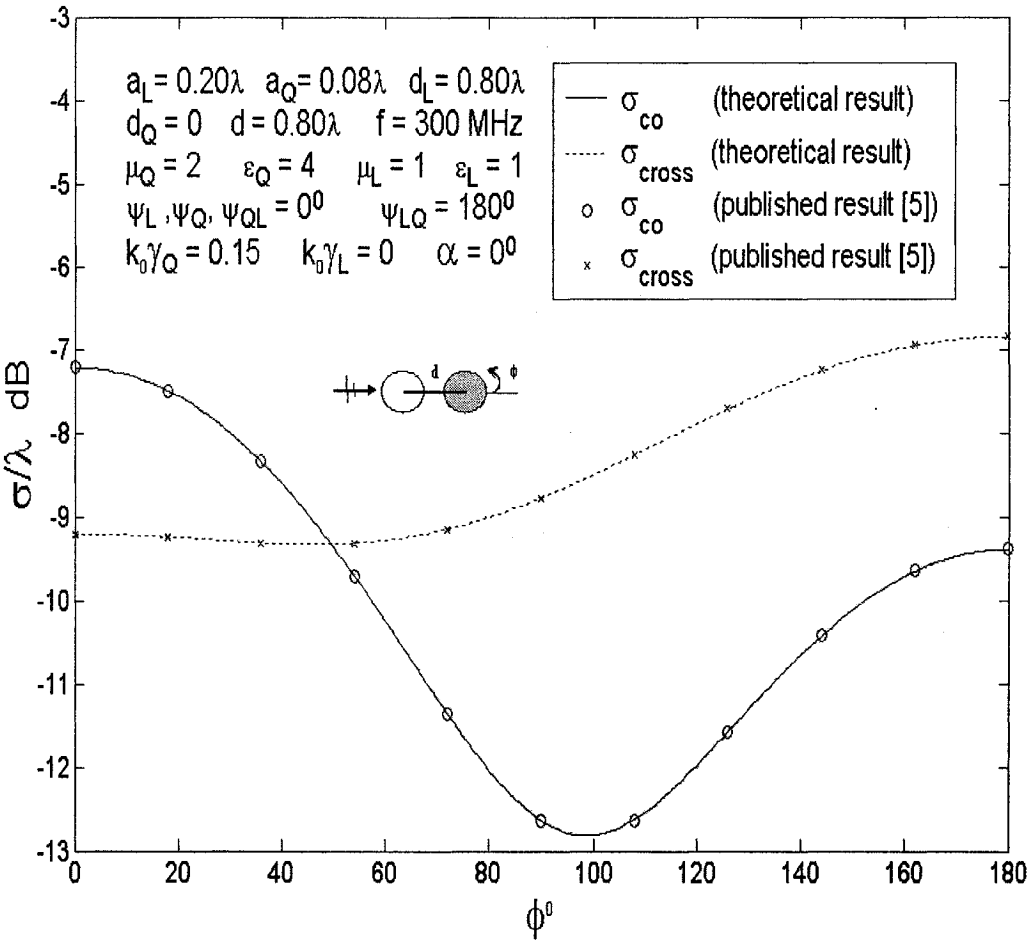


Fig. 4.3: The co-polarized and cross-polarized echo width patterns for single chiral circular cylinder, TE case.

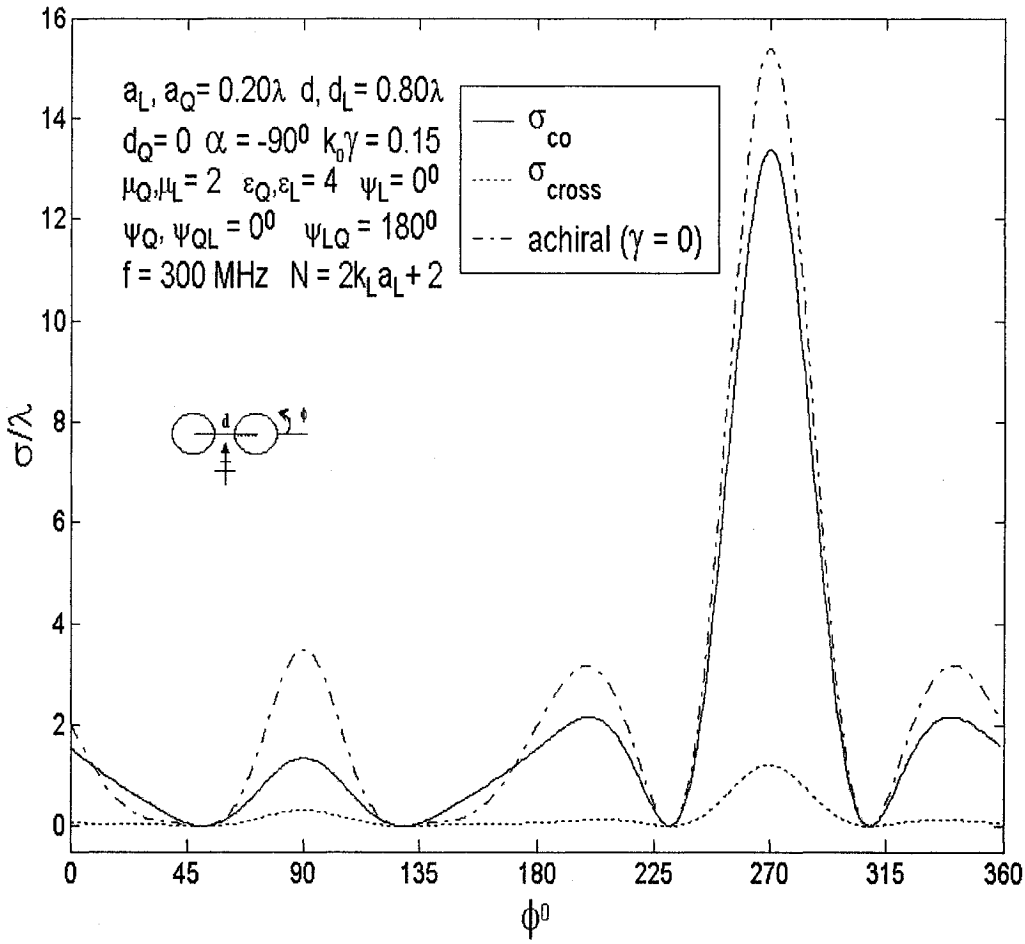


Fig. 4.4: The co- and cross-polarized echo width patterns for two chiral circular cylinders, TE case.

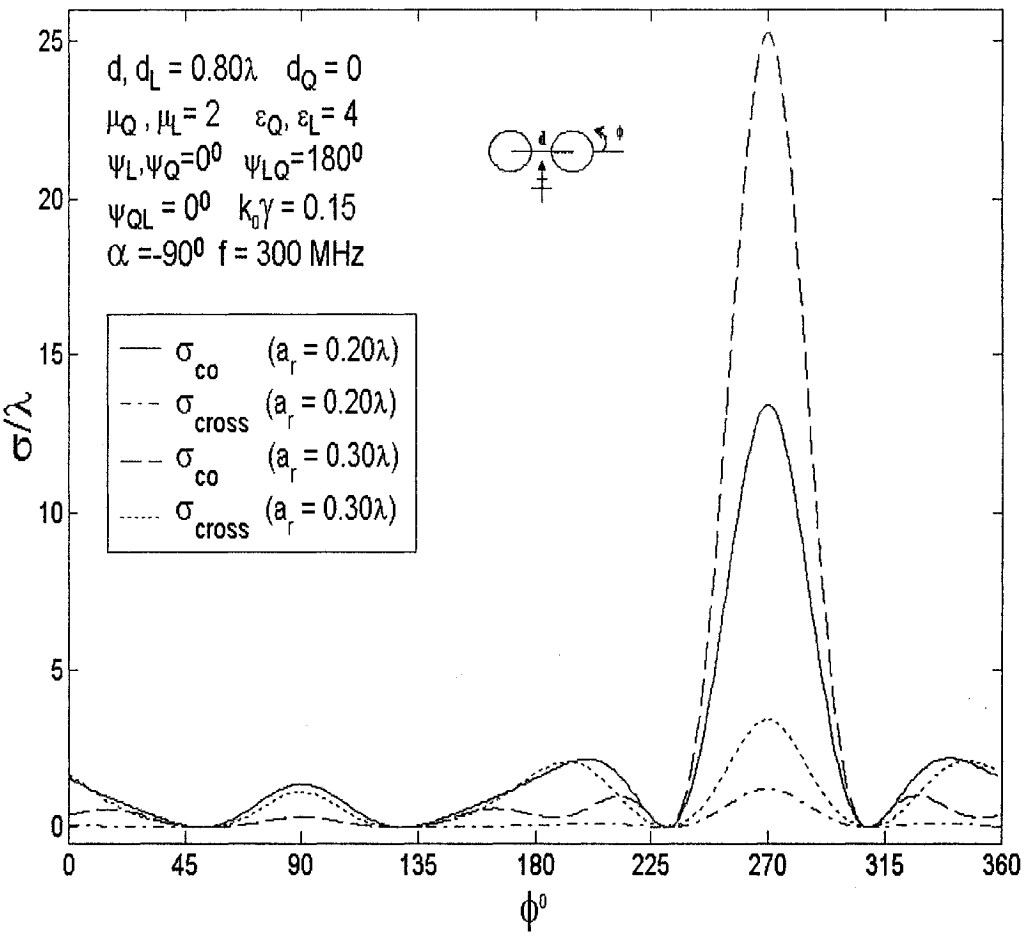


Fig. 4.5: The co- and cross- polarized echo width patterns from two chiral circular cylinders for two different radii, TE case.

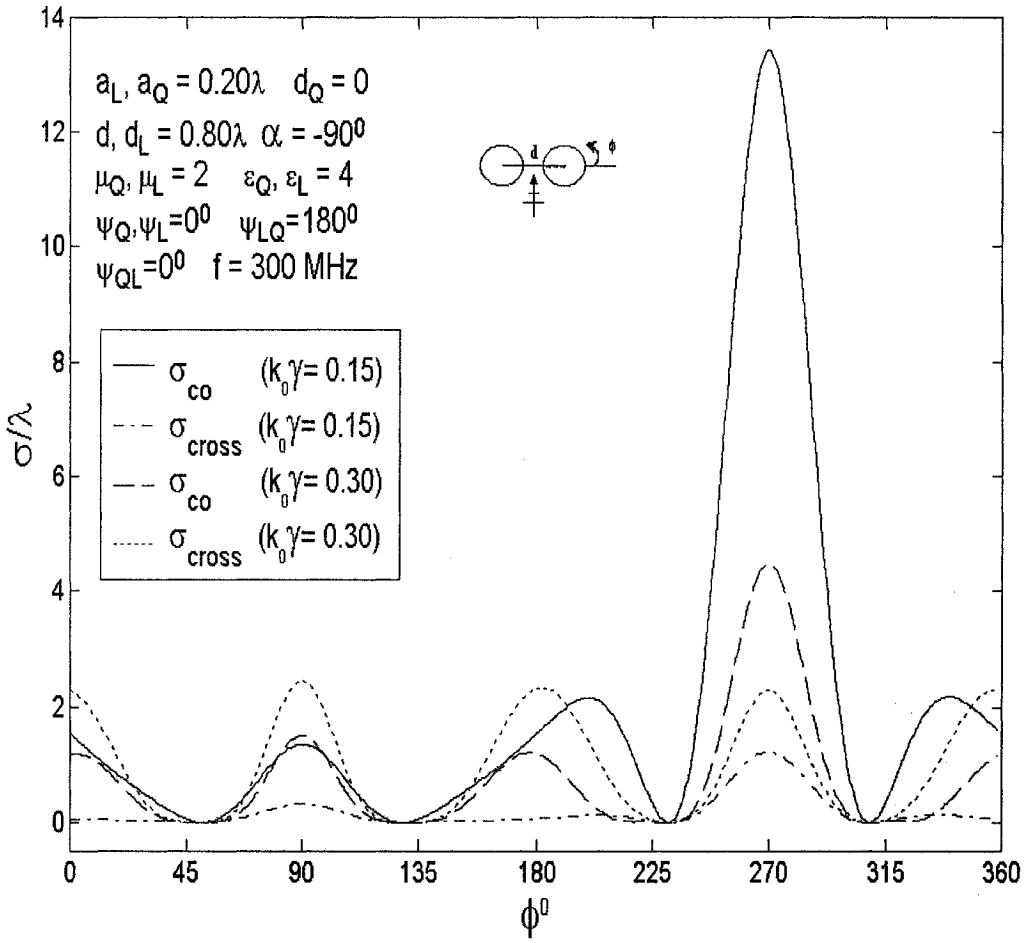


Fig. 4.6: The co- and cross-polarized echo width patterns from two chiral circular cylinders for two different chiral parameters, TE case.

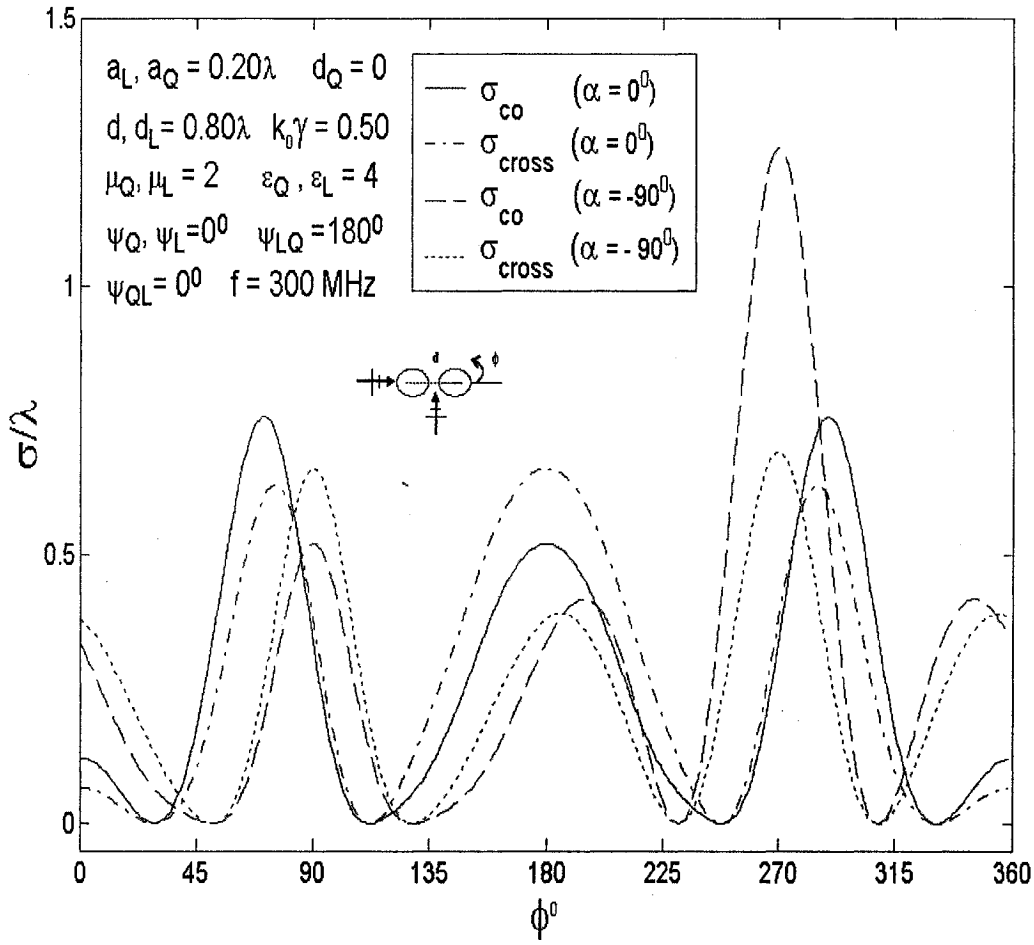


Fig. 4.7: The co- and cross-polarized echo width patterns from two chiral circular cylinders for two different angles of incidence, TE case.

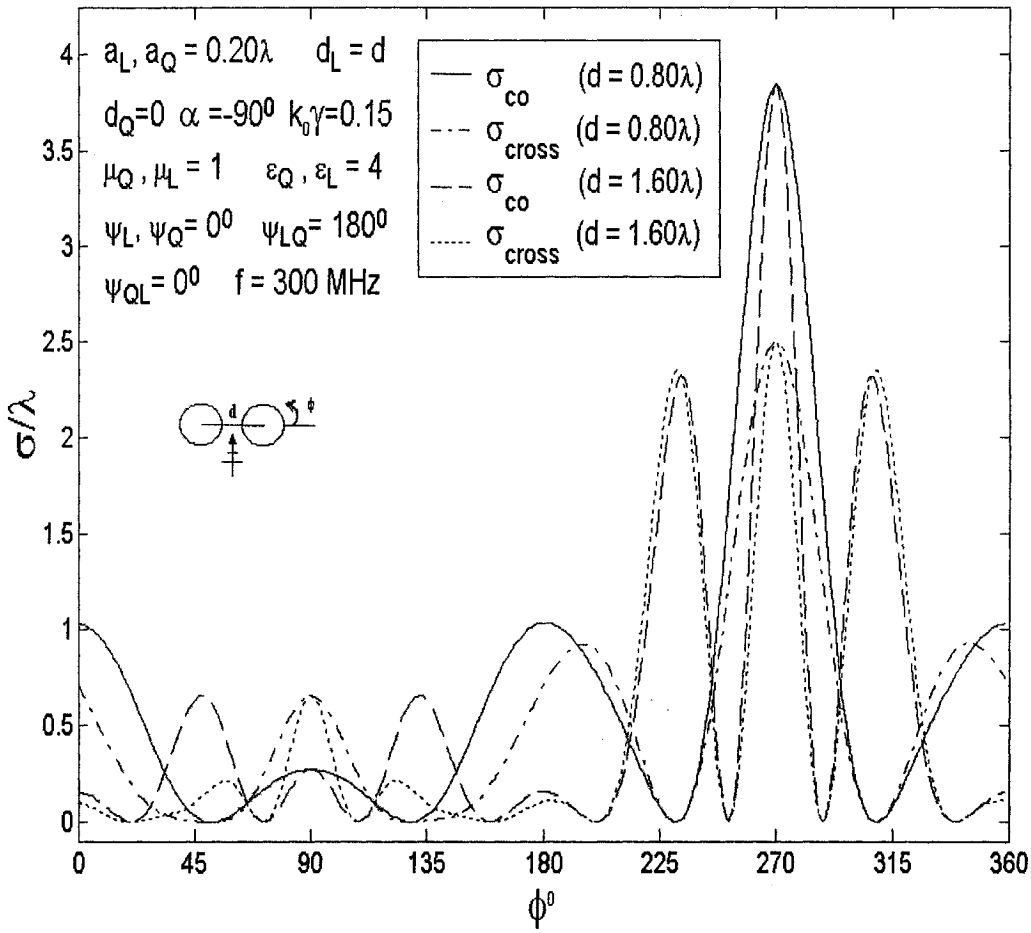


Fig. 4.8: The co- and cross-polarized echo width patterns from two chiral cylinders for two different separation distances, TE case.

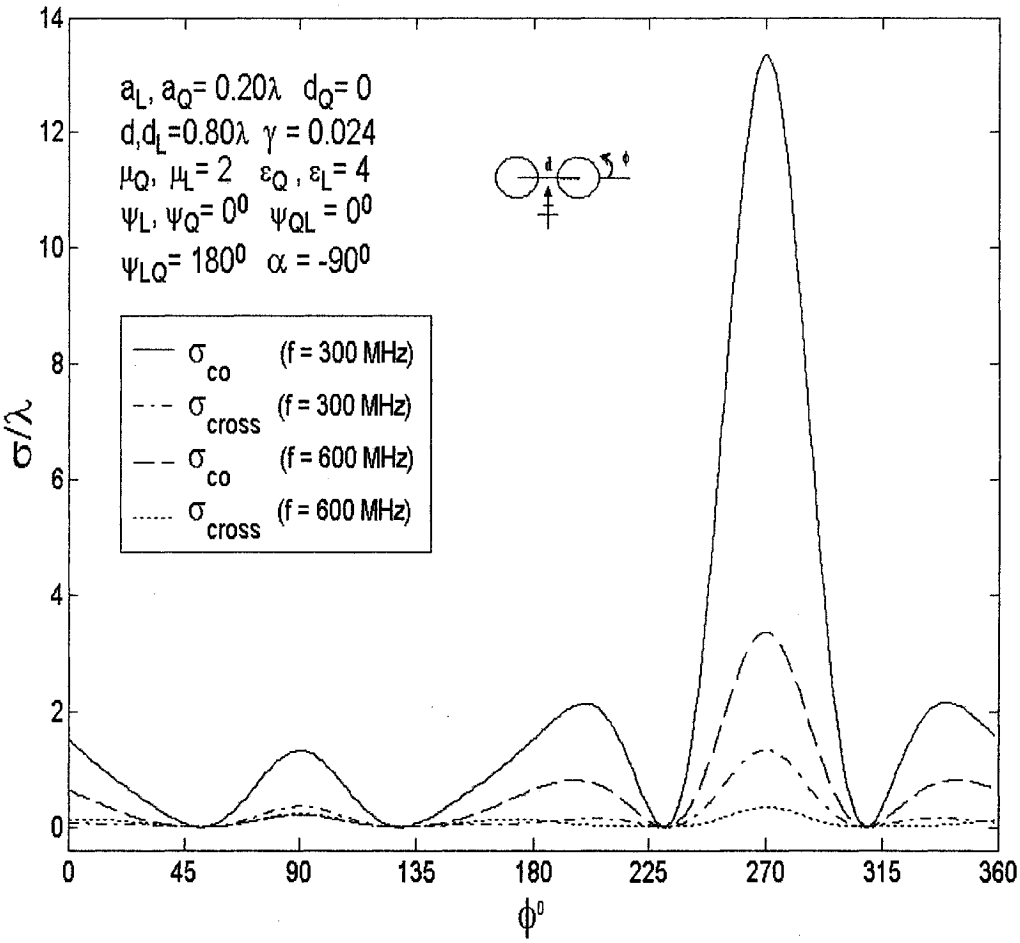


Fig. 4.9: The co- and cross-polarized echo width patterns from two chiral circular cylinders for two different frequencies, TE case.

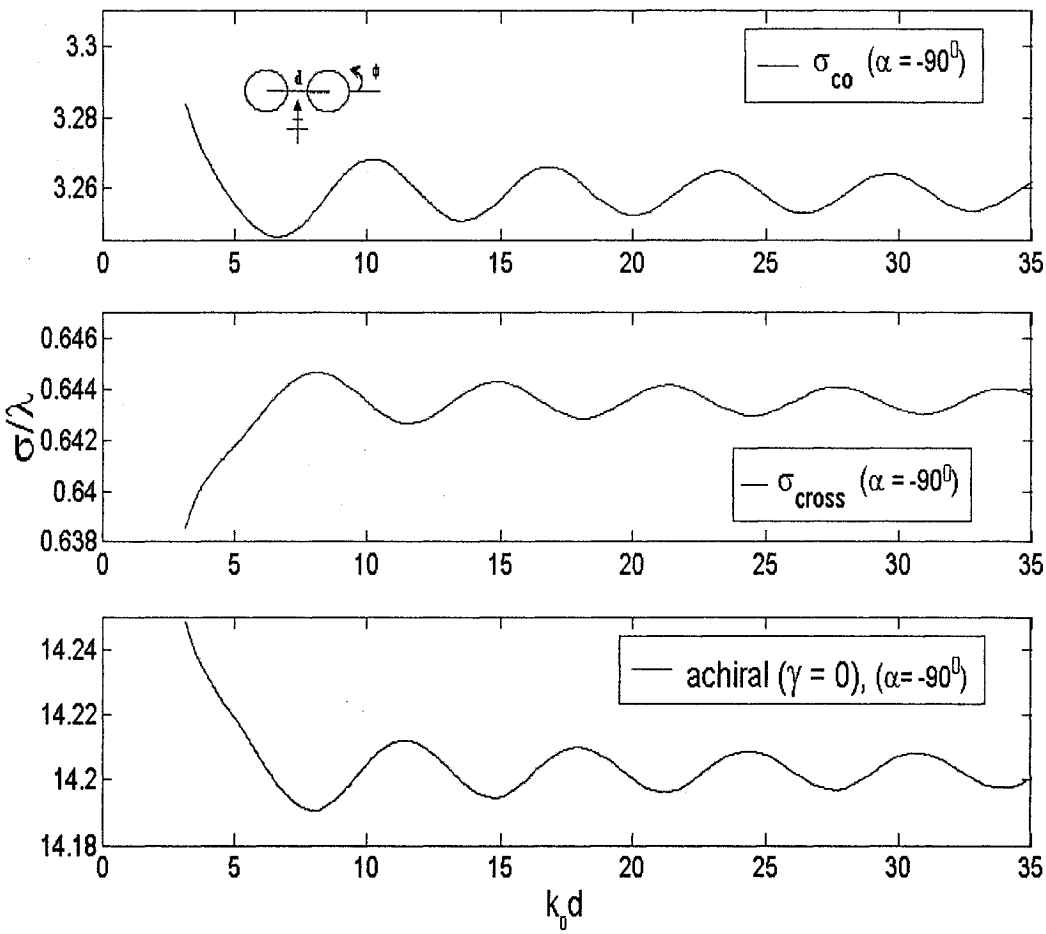


Fig. 4.10: The co- and cross-polarized backscattering echo widths versus the separation distance for two identical chiral circular cylinders with $\alpha = -90^0$, TE case.

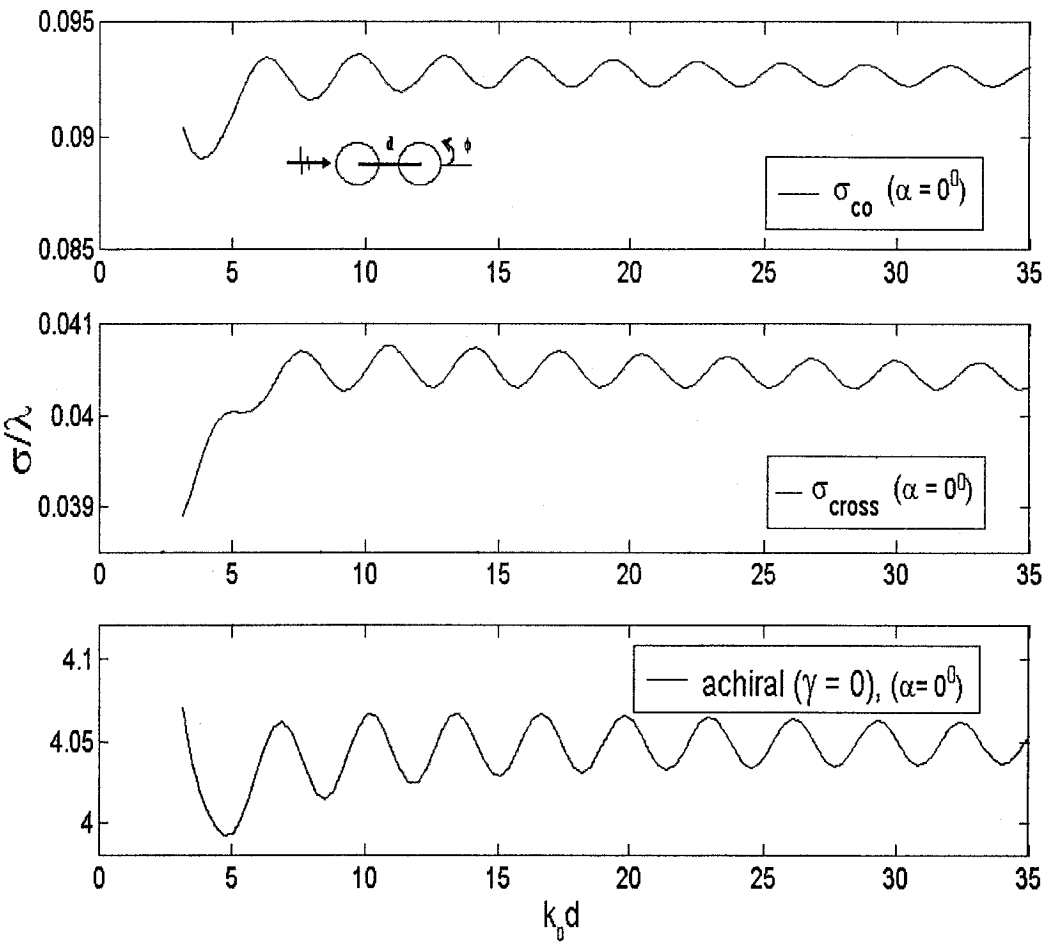


Fig. 4.11: The co- and cross-polarized backscattering echo widths versus the separation distance for two identical chiral circular cylinders with $\alpha = 0^0$, TE case.

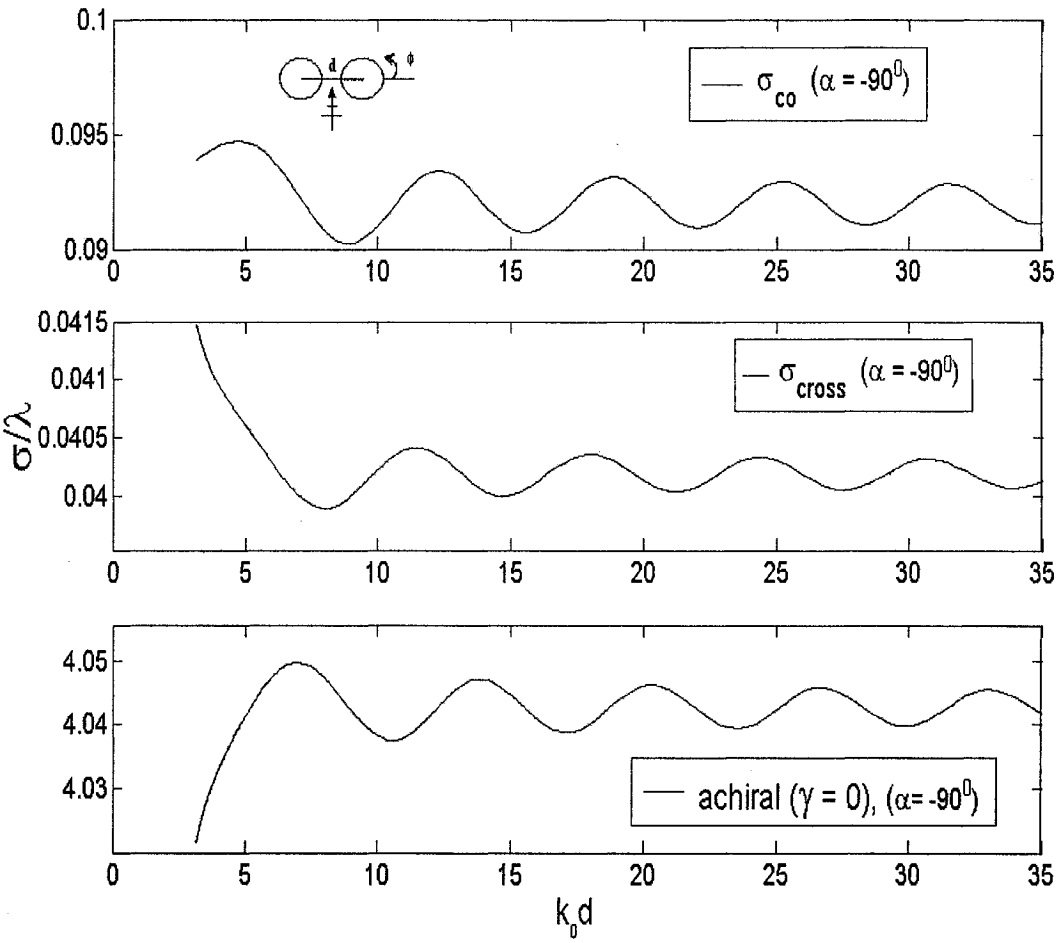


Fig. 4.12: The co- and cross-polarized forward scattering echo widths versus the separation distance for two identical chiral circular cylinders with $\alpha = -90^0$, TE case.

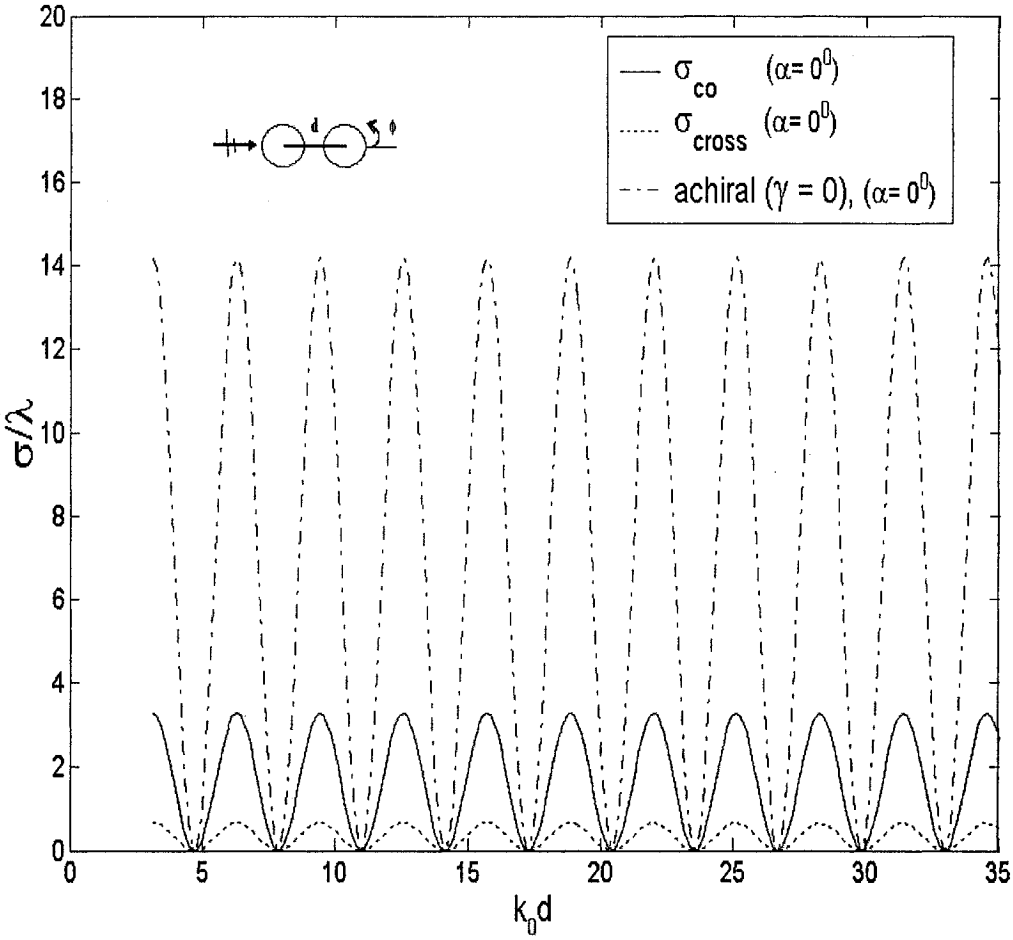


Fig. 4.13: The co- and cross-polarized forward scattering echo widths versus the separation distance for two identical chiral circular cylinders with $\alpha = 0^0$, TE case.

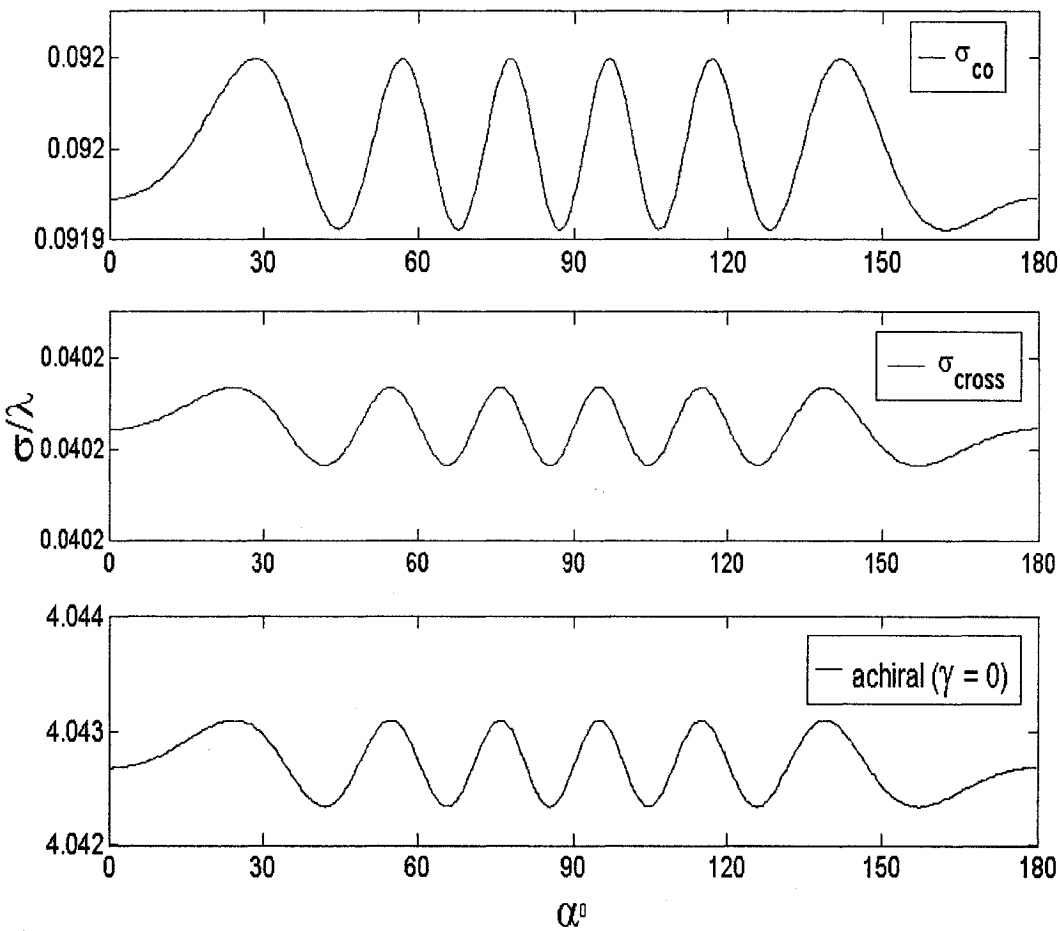


Fig. 4.14: The co- and cross-polarized backscattering echo widths versus the angle of incidence $\alpha$ for two identical chiral circular cylinders, TE case.

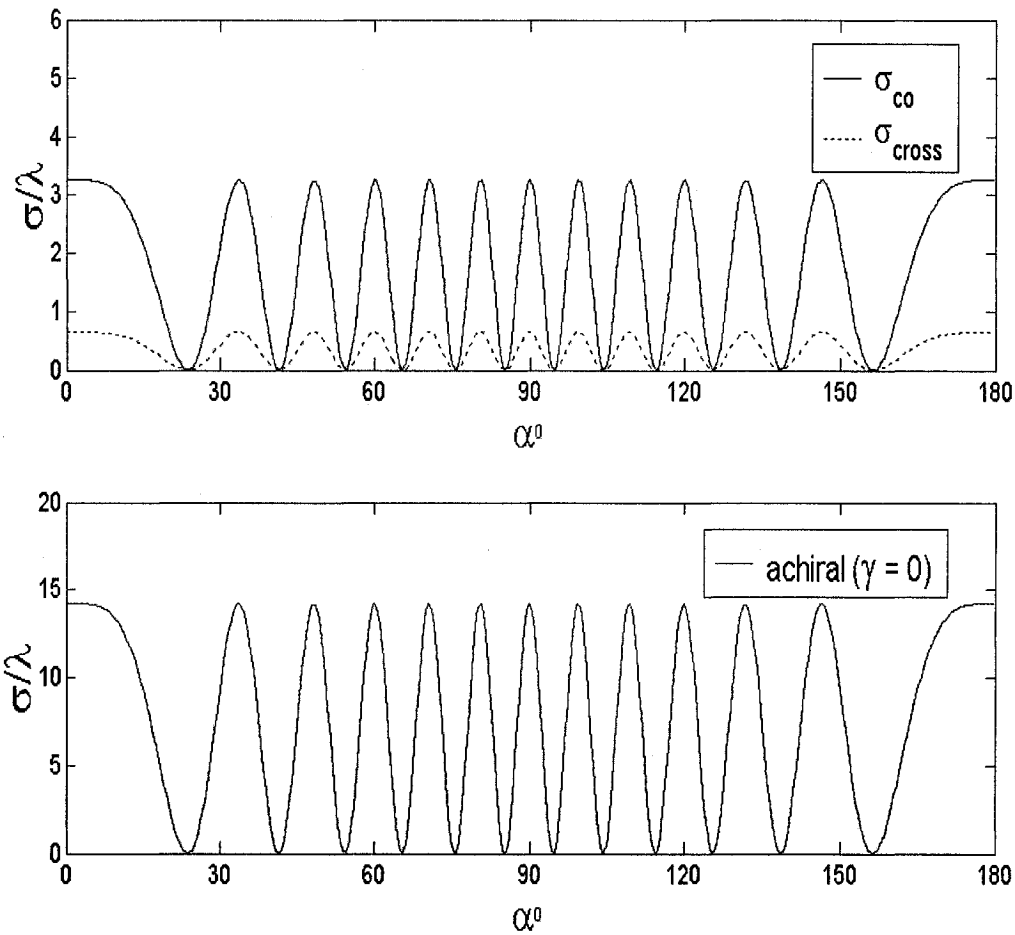


Fig. 4.15: The co- and cross-polarized forward scattering echo widths versus the angle of incidence $\alpha$ for two identical chiral circular cylinders, TE case.

# Chapter 5

# Conclusions

The problem of scattering of electromagnetic waves by two parallel chiral circular cylinders has been analyzed using a boundary value problem approach. The analyzed results are computed for both transverse magnetic and transverse electric polarized electromagnetic waves. The scattering of electromagnetic waves by single chiral circular cylinder is also analyzed and computed for both the TM and TE polarizations.

In Chapter 2, TM and TE scattering of electromagnetic waves by single chiral circular cylinder are analyzed using a boundary value problem approach. Cylindrical vector wave functions are used to express the electromagnetic incident, scattered, and internal fields. DBF constitutive relations and the Bohren decomposition formulas are used to express the electromagnetic fields inside the chiral cylinder. The unknown expansion coefficients of the scattered and internal fields can be solved numerically by enforcing the boundary conditions on the surface of the cylinder. Several numerical results are given to show the co- and cross-polarized echo widths effect and compared well with existing published results. The several effects on echo width are given by varying the different chirality parameters and cylinder radii of the chiral cylinder. The numerical results are also generated to show the dependence of the back and forward scattering co- and cross-polarized echo widths as a function of cylinder radius. Numerical results illustrated that co- and cross-polarized echo widths are dependent upon the constitutive parameters and electrical size of the cylinder.

In Chapter 3 and 4, TM and TE scattering of electromagnetic waves by two parallel chiral circular cylinders are analyzed and computed using a boundary value problem approach. The separation of variable technique and proper transformation theorems are used to formulate the solution. The incident, scattered, and transmitted fields are expanded in terms of the cylindrical vector wave functions. DBF constitutive relations and the Bohren decomposition formula are used to express the electromagnetic fields inside the chiral cylinders. The scattered field from each cylinder is considered to be the incident field for the other cylinder. The boundary conditions are then imposed in conjunction with the addition theorem for Hankel functions on the boundary surface of each cylinder. The result is a system of linear equations for the unknown expansion coefficients which is numerically solved by a proper truncation of the infinite sums into finite sums.

The total scattered field can be determined after evaluating all unknown scattering expansion coefficients. The echo width is a far field parameter which is used to characterize the scattering properties of a target. The echo width from two chiral circular cylinders can be obtained by knowing the scattered fields in the far zone. The asymptotic expansion for the Hankel function for large arguments is applied to obtain the far-zone scattered fields. Both co- and cross-polarized far scattered fields are taken into consideration for all numerical results. Several numerical results are presented to show the effects on the echo width with respect to different chirality parameters, frequencies, radii, separation distances between two cylinders, and incident angles. The effects on the back and forward scattering co- and cross-polarized echo widths are also given with respect to the separation distance between two cylinders and angle of incidence. The

validity and accuracy of the results are compared with the published results for the special cases of two dielectric circular cylinders and single chiral circular cylinder.

From all numerical results, it can be observed that both co- and cross-polarized echo widths are controlled by changing the angle of incidence, the angle of observation, the frequency of operation, the location of two cylinders, the radius of the cylinders, and the constitutive parameters of chiral circular cylinders. Furthermore the results illustrate that the echo width patterns are greatly influenced by chirality parameter which may enhance or reduce the echo width. It provides designer an extra degree of freedom to control the echo width of chiral scatterers.

In conclusion, the analysis of electromagnetic scattering by two chiral circular cylinders provides some idea about the far scattered field characteristics which can be used as a reference for modeling of complex structures and controlling of echo width of different objects in such a type of complex media.

Finally, the analysis of scattering of electromagnetic waves by two parallel chiral circular cylinders can be further studied for a number of chiral cylinders in reciprocal or nonreciprocal media.

# References

[1] C. F. Bohren, "Scattering of electromagnetic waves by an optically active cylinder," The Journal of Colloid and Interface Science, vol.66, no.1, Aug. 1978, pp.105–109.

[2] C. F. Bohren, "Light scattering by an optically active sphere," Chem. Phys. Lett., vol.29, Dec. 1974, pp. 458-462.

[3] C. F. Bohren, "Scattering of electromagnetic waves by an optically active spherical shell," The Journal of Chemical Physics, vol.62, no.4, Feb. 1975, pp. 1566–1571.

[4] M. S. Kluskens and E. H. Newman, "Scattering by a chiral cylinder of arbitrary cross section," IEEE Transactions on Antennas and Propagation, vol.38, no.9, Sep. 1990, pp. 1448-1455.

[5] R. G. Rojas, "Integral equations for EM scattering by homogeneous/inhomogeneous two-dimensional chiral bodies," IEE Proc.- Microwave Antennas Propagation, vol.141, no.5, Oct. 1994, pp. 385-392.

[6] M. A. Al-Kanhal and E. Arvas, "Electromagnetic scattering from a chiral cylinder of arbitrary cross section," IEEE Transactions on Antennas and Propagation, vol.44, no.7, July 1996, pp. 1041-1048.

[7] M. S. Kluskens and E. H. Newman, "Scattering by a multilayer chiral cylinder," IEEE Transactions on Antennas and Propagation, vol.39, no.1, Jan. 1991, pp. 91-96.

[8] V. Twersky, "Multiple scattering of radiation by an arbitrary configuration of parallel cylinders," The Journal of the Acoustical Society of America, vol.24, no.1, Jan. 1952, pp.42-46.

[9] G. O. Olaofe, "Scattering by two cylinders," Radio Science, vol.5, no.11, Nov. 1970, pp.1351-1360.

[10] J. W. Young and J. C. Bertrand, "Multiple scattering by two cylinders," The Journal of the Acoustical society of America, vol.58, no.6, Dec. 1975, pp.1191-1195.

[11] H. A. Ragheb and M. Hamid, "Scattering by N parallel conducting circular cylinders," Int. Journal Electronics, vol.59, no.4, Oct. 1985, pp. 407-421.

[12] A. Z. Elsherbeni and A. A. Kishk, "Modeling of cylindrical objects by circular dielectric and conducting cylinders," IEEE Transactions on Antennas and Propagation, vol.40, no.1, Jan. 1992, pp. 96-99.

[13] A. R. Sebak and Y. Antar, "Multiple scattering by parallel conducting elliptic cylinders: TE case," IEE Proc.- Microwave Antennas Propagation, vol.142, no.2 April 1995, pp. 178-182.

[14] A. R. Sebak, "Electromagnetic scattering by two parallel dielectric elliptic cylinders," IEEE Transactions on Antennas and Propagation, vol.42, no.11, Nov. 1994, pp. 1521–1527.

[15] M. A. Sharkawy, A. Z. Elsherbeni, and S. F. Mahmoud, "Electromagnetic scattering from parallel chiral cylinders of circular cross-sections using an iterative procedure," Progress in Electromagnetics Research, PIER 47, 2004, pp. 87-110.

[16] W. Y. Yin, L. W. Li, and M. S. Leong, "Scattering from multiple bianisotropic cylinders and their modeling of cylindrical objects of arbitrary cross-section," Progress in Electromagnetics Research, PIER 27, 2000, pp. 159-184.

[17] I. V. Lindell, A. H. Sihvola, S. A. Tretyakov, and A. J. Viitanen, "Electromagnetic Waves in Chiral and Bi-isotropic Media," (Artech house, Boston. London), 1994.

[18] J. A. Stratton, "Electromagnetic Theory," (McGraw-Hill, New York), 1941.

[19] F. Mariotte, S. A. Tretyakov, and B. Sauviac, "Modeling effective properties of chiral composites," IEEE Antennas and Propagation Magazine, vol.38, no.2, April 1996, pp. 22-32.

[20] A. Lakhtakia, V. K. Varadan, and V. V. Varadan, "Time-Harmonic Electromagnetic fields in chiral media," (Springer-Verlag), 1989.

[21] S. Uckun and T. Ege, "On the incompatibility of chirality parameter $\alpha$ and chirality admittance $\xi$ of chiral media," Antennas and Propagation Society, IEEE International Symposium, vol.3, July 1999, pp.1974 - 1977.

[22] D. L. Jaggard, X. Sun, and N. Engheta "Canonical sources and duality in chiral media," IEEE Transactions on Antennas and Propagation, vol.36, no.7, July 1988, pp. 1007-1013.

[23] S. F. Mahmood, "Characteristics of a chiral-coated slotted cylindrical antenna," IEEE Transactions on Antennas and Propagation, vol.44, no.7, July 1996, pp. 814-821.

[24] D. M. Pozar, "Microstrip antennas and arrays on chiral substrate," IEEE Transactions on Antennas and Propagation, vol.40, no.10, 1992, pp. 1260-1263.

[25] P. Pelet and N. Engheta, "The theory of chirowaveguides," IEEE Transactions on Antennas and Propagation, vol.38, no.1, Jan. 1990, pp. 90-98.

[26] D. L. Jaggard and N. Engheta, "Chirosorb as an invisible medium," Electronics Letters, vol.25, no.3, Feb. 1989, pp. 173-174.

[27] Z. X. Shen, "Electromagnetic scattering by an impedance cylinder coated eccentrically with a chiroplasma cylinder," IEE Proc.- Microwave Antennas Propagation, vol. 141, no.4 Aug. 1994, pp. 279-284.

[28] H. Cory and I. Rosenhouse, "Minimization of reflection coefficient at feed of radomes-covered reflector antenna by chiral device," Electronics Letters, vol.27, no.25, pp. 2345-2347.

[29] R. F. Harrington, "Time Harmonic Electromagnetic fields," (McGraw-Hill, New York), 1961.

[30] C. A. Bananis, "Advanced Engineering Electromagnetics," (John Wiley & Sons, Inc., New York), 1989.